British Geological Survey
NATURAL ENVIRONMENT RESEARCH COUNCIL

Microbial effects on transport processes (BioTran). Experimental Methodologies and Results

(April 2007 – March 2008)

Environment and Health Programme

Research Report OR/08/057

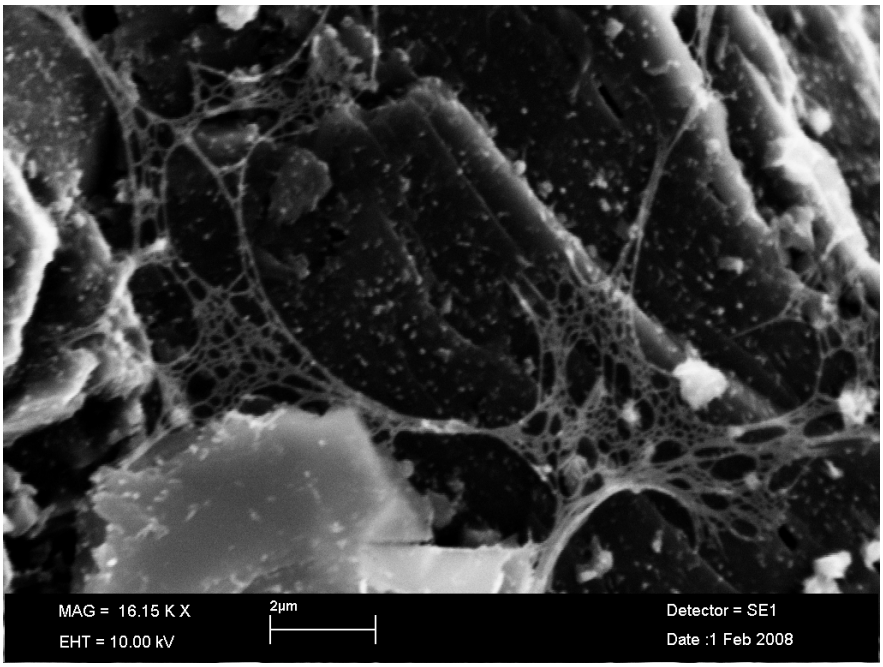

BRITISH GEOLOGICAL SURVEY

ENVIRONMENT AND HEALTH

OPEN REPORT OR/08/057

Microbial effects on transport processes (BioTran). Experimental Methodologies and Results (April 2007 – March 2008)

J M West (editor), K Bateman, P Coombs, H M Harrison, J Harrington, A M Lacinska, A E Milodowski, D J Noy, G H Turner, D Wagner

Keywords

microbiology, experiment, biofilm, mineralogy, porosity, permeability, pore fabric.

Front cover

Web-like biofilm comprising a mesh of biofilaments coating mineral grains recovered from BioTran column 2 experiment.

Bibliographical reference

WEST, J.M., BATEMAN, K., COOMBS, P., HARRISON, H.M., HARRINGTON, J., LACINSKA, A.M., MILODOWSKI, A.E., NOY, D.J., TURNER, G.H. AND WAGNER, D. 2008. Microbial effects on transport process (BioTran). Experimental Results (April 2007 – March 2008). *British Geological Survey Research Report*, OR/08/057. pp.

Keyworth, Nottingham British Geological Survey 2008

BRITISH GEOLOGICAL SURVEY

The full range of our publications is available from BGS shops at Nottingham, Edinburgh, London and Cardiff (Welsh publications only) see contact details below or shop online at www.geologyshop.com

The London Information Office also maintains a reference collection of BGS publications, including maps, for consultation.

We publish an annual catalogue of our maps and other publications; this catalogue is available online or from any of the BGS shops.

The British Geological Survey carries out the geological survey of Great Britain and Northern Ireland (the latter as an agency service for the government of Northern Ireland), and of the surrounding continental shelf, as well as basic research projects. It also undertakes programmes of technical aid in geology in developing countries.

The British Geological Survey is a component body of the Natural Environment Research Council.

British Geological Survey offices

BGS Central Enquiries Desk

Tel 0115 936 3143 Fax 0115 936 3276
email enquiries@bgs.ac.uk

Kingsley Dunham Centre, Keyworth, Nottingham NG12 5GG

Tel 0115 936 3241 Fax 0115 936 3488
email sales@bgs.ac.uk

Murchison House, West Mains Road, Edinburgh EH9 3LA

Tel 0131 667 1000 Fax 0131 668 2683
email scotsales@bgs.ac.uk

London Information Office at the Natural History Museum (Earth Galleries), Exhibition Road, South Kensington, London SW7 2DE

Tel 020 7589 4090 Fax 020 7584 8270
Tel 020 7942 5344/45 email
bgslondon@bgs.ac.uk

Columbus House, Greenmeadow Springs, Tongwynlais, Cardiff CF15 7NE

Tel 029 2052 1962 Fax 029 2052 1963

Forde House, Park Five Business Centre, Harrier Way, Sowton EX2 7HU

Tel 01392 445271 Fax 01392 445371

Maclean Building, Crowmarsh Gifford, Wallingford OX10 8BB

Tel 01491 838800 Fax 01491 692345

Geological Survey of Northern Ireland, Colby House, Stranmillis Court, Belfast BT9 5BF

Tel 028 9038 8462 Fax 028 9038 8461

www.bgs.ac.uk/gsni/

Parent Body

Natural Environment Research Council, Polaris House, North Star Avenue, Swindon SN2 1EU

Tel 01793 411500 Fax 01793 411501
www.nerc.ac.uk

Website www.bgs.ac.uk
Shop online at www.geologyshop.com

Foreword

As part of the Environment and Health Theme, the BioTran project is examining microbial effects on transport processes. This report details progress on the experimental programme, which aims to address some of the knowledge gaps relating to the influences of biofilms on transport of fluids through crushed rock materials.

Acknowledgements

The mineralogical analysis of the BioTran experimental materials was also supported with additional funding from the Geochemistry, Mineralogy and Hydrogeology "Maintenance of Capability ("MaDCap") Project". The authors are grateful to Mr Shaun Reeder (Head of Laboratory Operations) for his support in this research. We also thank Dr Joanna Wragg for helpful comments.

Contents

FIGURES

PLATES

TABLES

Summary

Risk assessments for landfills and geological repositories for radioactive waste are primarily based on the precepts of contaminant transport; and are concerned with understanding the movement of gas, wastes and solutes through engineered barriers and natural groundwater systems, within the concept of 'Source', 'Pathway', and 'Receptor'. The emphasis on solute migration for landfill investigations is reflected in the theoretical development used during numerical simulation. However, microbes living in such environments can have an impact on transport processes (Bateman *et al.,* 2006; Chapelle 2000; Cunningham *et al.*,1997; Fredrickson *et al.*, 1989; Keith-Loach and Livens 2002; West and Chilton 1997). Microbial activity in any environment is generally located on chemical or physical interfaces, usually within biofilms, and the impacts can be both physical (e.g. altering porosity) and/or chemical (e.g. changing pH, redox conditions) and may result in intracellular or extracellular mineral formation or degradation (Beveridge *et al.*, 1997; Ehrlich 1999; Konhauser *et al.*, 1998; Milodowski *et al.*, 1990; Tuck *et al.*, 2006). These processes could all impact on fluid flow through fractures and porous media by, for example, blocking of constrictions in fracture flow pathways and pore throats.

The BioTran project was initiated to examine the effects of microbes on transport processes, especially in the context of contaminant properties of host rocks. An understanding of these microbial processes will also be relevant to other areas such as bioremediation of contaminated land, borehole and reservoir clogging and enhanced oil recovery. More broadly, these processes impinge on aquifer recharge, pathogen survival, and ultimately on groundwater protection. To

date, the project has comprehensively reviewed the available literature and developed methodologies for experimental studies to provide information and data for existing transport models (Bateman *et al.*, 2006; Coombs *et al.*, 2008; Wagner *et al.*, 2007).

The experimental work in BioTran project has focussed on materials from the Äspö Underground Research Laboratory (URL) in the context of the geological containment of radioactive waste in hard rock (diorite) environments. The significance of microbiological processes in the containment of radioactive waste has long been recognised (West and McKinley, 2002) and, consequently, detailed evaluations of the biofilms present on the walls of the URL and on the significance of indigenous microbial populations has been a key area of work (Pedersen 1999). An *in-situ* study at the URL examined the redox buffering of groundwater in vertical fracture-zones penetrated by recent, oxidising, meteoric water and showed that indigenous bacteria were capable of maintaining reducing conditions in the deep groundwaters (Banwart, 1995). Experimental work has also simulated the interactions of indigenous microbes with mineralogical surfaces associated with groundwater flow systems at Äspö (Hama *et al.*, 2001); and ascertained that these microbes can either concentrate relevant chemical species for mineral formation in localised microenvironments or accelerate clay formation, the implications of this being that local hydrological conditions can be changed by microbial activity (Tuck *et al.*, 2006). Also, biogenic mineral precipitates and trapped mineral matter are much more chemically and physically stable than a biofilm, persisting in the system long after the biofilm has decayed or been removed (Brydie *et al.*, 2005).

As a result of these studies, the BioTran project has undertaken pilot studies to examine the influences of biofilm growth, from the bacteria *Pseudomonas aeruginosa,* on groundwater flow though crushed diorite from the Äspö Hard Rock Laboratory, Sweden.

This report details these experimental methodologies and results from pilot studies.

The aims were to:

1. Develop methodologies to grow and observe biofilms in flow-through cells and columns:
2. Undertake a pilot study to quantitatively evaluate the effects of biofilms on fluid flow;
3. Evaluate the effect of a pH change and introduction of bacteriophage on these biofilms and on fluid flow.

The work described in this report has shown that:

- *P. aeruginosa* biofilms can be grown reliably using Äspö diorite and synthetic groundwater as a growth medium;
- *P. aeruginosa* biofilms can be grown in a variety of laboratory flowing systems;
- Biofilm growth and development can be imaged using a variety of techniques.

The pilot quantitative study evaluated the effects of biofilms on fluid flow through crushed Äspö diorite over a total period of 2141 hours. It showed that:

- Numbers of *P. aeruginosa* gradually increased suggesting that the bacteria were not only surviving, but were also growing in the flow systems;
- Biofilms developed in the two columns studied as evidenced by direct observations and by petrographic analysis of both columns at the end of the experiment;
- Quantitative results could be obtained using the methodologies described in this report, allowing calculation of hydraulic conductivity. The fluctuations in transport properties during the experiments demonstrate the complexity of systems which include a biological component. The results also show, indirectly, the effect of biofilm on transport properties which is particularly evident after 500 hours when flow in both columns dropped to very low rates. However, use of these data in existing and microbial

transport and clogging models is limited because few of them provide the option of coupling flow to microbial growth;

- Changes in pH do not appear to influence transport properties in the described flowing systems containing *P. aeruginosa* biofilms over the experimental exposure period. It is possible that column material and the biofilms may not have been exposed to the pH change because of the low flow rates which will need to be further investigated in future experiments;
- Introduction of phage E79 does not appear to influence transport properties in these flowing systems containing *P. aeruginosa* biofilms. However, it is possible that the phage were not active in these experiments;
- No observable fluid/solid interactions took place in either column.

Future work will concentrate on developing the quantitative methodologies further so that studies can be undertaken under anaerobic conditions. Further development work is also required to directly observe biofilm growth in columns, particularly for petrographic analysis. Consideration is also needed on how best to utilise the quantitative transport measurements as existing transport models are very limited in their ability to couple biological processes with flow calculations. Development of the BGS in-house model PRECIP model may be the most appropriate.

1 Introduction

1.1 BACKGROUND

Risk assessments for landfills and geological repositories for radioactive waste are primarily based on the precepts of contaminant transport; and are concerned with understanding the movement of gas, wastes and solutes through engineered barriers and natural groundwater systems, within the concept of 'Source', 'Pathway', and 'Receptor'. The emphasis on solute migration for landfill investigations is reflected in the theoretical development used during numerical simulation. However, microbes living in such environments can have an impact on transport processes (Bateman *et al.*, 2006; Chapelle 2000; Cunningham *et al.*,1997; Fredrickson *et al.*, 1989; Keith-Loach and Livens 2002; West and Chilton 1997). Microbial activity in any environment is generally located on chemical or physical interfaces, usually within biofilms, and the impacts can be both physical (e.g. altering porosity) and/or chemical (e.g. changing pH, redox conditions) and may result in intracellular or extracellular mineral formation or degradation (Beveridge *et al.*, 1997; Ehrlich 1999; Konhauser *et al.*, 1998; Milodowski *et al.*, 1990; Tuck *et al.*, 2006). These processes could all impact on fluid flow through fractures and porous media by, for example, blocking of constrictions in fracture flow pathways and pore throats.

The BioTran project was initiated to examine the effects of microbes on transport processes, especially in the context of contaminant properties of host rocks. An understanding of these microbial processes will also be relevant to other areas such as bioremediation of contaminated land, borehole and reservoir clogging and enhanced oil recovery. More broadly, these processes impinge on aquifer recharge, pathogen survival, and ultimately on groundwater protection. To date, the project has comprehensively reviewed the available literature and developed methodologies for experimental studies to provide information and data for existing transport models (Bateman *et al.*, 2006; Coombs *et al.*, 2008; Wagner *et al.*, 2007).

1.2 THE CONTEXT OF THE EXPERIMENTAL WORK

The experimental work in BioTran project has focussed on materials from the Äspö Underground Research Laboratory (URL) in the context of the geological containment of radioactive waste in hard rock (diorite) environments. The significance of microbiological processes in the containment of radioactive waste has long been recognised (West and McKinley, 2002) and, consequently, detailed evaluations of the biofilms present on the walls of the URL and on the significance of indigenous microbial populations has been a key area of work (Pedersen 1999). An *in-situ* study at the URL examined the redox buffering of groundwater in vertical fracture-zones penetrated by recent, oxidising, meteoric water and showed that indigenous bacteria were capable of maintaining reducing conditions in the deep groundwaters (Banwart, 1995). Experimental work has also simulated the interactions of indigenous microbes with mineralogical surfaces associated with groundwater flow systems at Äspö (Hama *et al.*, 2001); and ascertained that these microbes can either concentrate relevant chemical species for mineral formation in localised microenvironments or accelerate clay formation, the implications of this being that local hydrological conditions can be changed by microbial activity (Tuck *et al.*, 2006). Also, biogenic mineral precipitates and trapped mineral matter are much more chemically and physically stable than a biofilm, persisting in the system long after the biofilm has decayed or been removed (Brydie *et al.*, 2005).

As a result of these studies, the BioTran project has undertaken pilot studies to examine the influences of biofilm growth on groundwater flow though crushed diorite from the Äspö Hard Rock Laboratory, Sweden.

This report details these experimental methodologies and results from pilot studies.

The aims were to:

1. Develop methodologies to grow and observe biofilms in flow-through cells and columns:
2. Undertake a pilot study to quantitatively evaluate the effects of biofilms on fluid flow;
3. Evaluate the effect of a pH change and introduction of bacteriophage on these biofilms and on fluid flow.

Appendix 1 provides background information on biofilms; microbial transport studies at Äspö; and modelling of microbial influences on transport properties. A glossary is also appended.

2 Experimental methodologies

2.1 EQUIPMENT

Several laboratory experiments were undertaken and while each one had a different aim, much of the apparatus and test materials were common to all the experiments. Biofilm growth studies used PTFE tubing to connect a reservoir of synthetic groundwater to a flow cell packed with granitic sand via a peristaltic pump. Later work replaced the flow cell with packed borosilicate glass columns.

2.2 FLOWCELL APPARATUS

The flowcell was composed of Teflon with an acrylic lid as shown in Plate 1. A quartz window was later incorporated into the Perspex lid to allow for digital images to be captured under UV illumination. The flow cell was custom-made by the BGS workshops.

Plate 1 Custom-made flowcell apparatus

2.3 COLUMN APPARATUS

Fixed length Omnifit chromatography columns (25 mm I.D x 250 mm) capable of operating up to 150 psi (10 bar) were purchased from Kinesis (Part No. 006CC-25-25-ff). These columns were made from borosilicate glass, threaded at each end and supplied with fixed-length endpieces, Viton O-rings and 1/4-28 UNF endcaps. A 25 µm polyethylene frit in each endpiece allows even distribution of the diorite sand over the surface of the packing bed. PTFE tubing (1/16in. O.D) was supplied as part of the column kit and the ends of the columns were secured with M6 endcaps. An image of the type of column used in the experiments is shown in Plate 2.

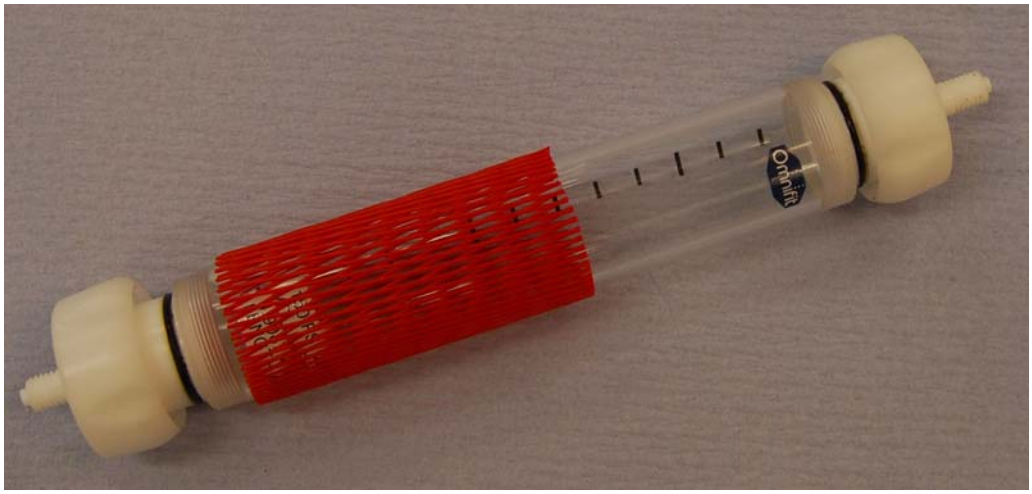

Plate 2 Image showing the type of Omnifit column used in the experiments

2.4 ÄSPÖ SYNTHETIC GROUNDWATER

A synthetic groundwater based on the composition of Äspö borehole water (ID KA1755A) (Hama *et al.*, 2001) was prepared and the pH adjusted to 7.2 with 0.1 M HCl as shown in Table 1. The synthetic groundwater was filter sterilised through a 0.2 µm VacuCap 90 filter unit, (Gelman Sciences Prod 4622).

2.5 ÄSPÖ DIORITE SAND

The diorite sand was prepared from whole rock. It was first crushed, then jaw-split by a manual rock-splitter equipped with hardened chromium steeljaws. The fragmented material was then passed twice through a laboratory jaw-crusher equipped with hardened chromium steel jaws to produce a material with particle sizes ranging from 250 to 500 µm but which was still representative of the whole rock. At each stage of the preparation, fines were formed due to the substantial differences in friability of the minerals within the diorite. Jaw crushing alone produced particles of differing size, some of which were already <150 µm. To reduce this effect, fine material was discarded after jaw crushing and a multi-stage milling regime was then carried out on the remaining broken rock fragments with each mill run lasting a minute or less. After jaw crushing, the fragments were milled in a hardened chrome steel Tema mill and sieved through mesh sieves. After each milling stage, the sample was sieved through 500 µm and 250 µm sieves. Material with a particle size of <250 µm was discarded while material coarser than 500 µm was re-milled. All the sieve fractions ranging from 250 µm to 500µm were then combined to produce the final material. This diorite sand was then packed into flowcell and columns and an example is shown in Plate 3. To ascertain if this fraction of material was representative of 'whole' diorite rock, the material was analysed by X-ray diffraction (XRD). Before use, the sand was sterilised by overnight exposure to UV radiation in a laminar flow cabinet. The material was spread thinly over several paper surfaces to enable the UV light to penetrate. The

columns were filled under gravity by the addition of small aliquots of diorite sand which was compacted by tapping the sides of the column.

Table 1 Composition of synthetic groundwater

Synthetic groundwater	(g l^{-1})
$NaH_2PO_4.2H_2O$	0.0002
$NaHCO_3$	0.028
KCl	0.023
$SrCl_2.6H_2O$	0.243
$MgSO_2.7H_2O$	0.508
$CaSO_4.2H_2O$	0.835
$CaCl_2.2H_2O$	15.245
NaCl	7.403
Concentration	(mg l^{-1})
Ca^{2+}	4351
Mg^{2+}	50
Na^{+}	2920
K^{+}	12
Cl^{-}	11919
Sr^{2+}	80
HPO_4^{-}	0.1
HCO_3^{-}	20
SO_4^{2-}	664
Total S	222

2.5.1 X-ray diffraction analysis of diorite sand

X-ray diffraction (XRD) was used to determine if the minerals present in the rock fractions differed from the whole rock. XRD was performed on samples of the <250 µm and 125 – 250 µm fractions and their peak intensities compared. For whole rock XRD analysis, a representative portion of the samples was hand-crushed by pestle and mortar. The crushed material was then tema-milled to <0.12 mm. In order to provide a finer and uniform particle-size, a c.3 g portion of the milled material was wet-micronised under acetone for 10 minutes, dried, disaggregated and back-loaded into a standard stainless steel sample holder for analysis.

XRD analysis was carried out using a PANalytical X'Pert Pro series diffractometer equipped with a cobalt-target tube, X'Celerator detector and operated at 45 kV and 40 mA. The samples were scanned from 4.5-85°2θ at 2.76°2θ min^{-1}. Diffraction data were initially analysed using 2004 PANalytical X'Pert Highscore Plus software coupled to the International Centre for Diffraction Data (ICDD) database.

XRD analysis of the diorite samples showed that both grain size fractions predominantly consist of quartz and albite with minor amounts of orthoclase, 'mica' (undifferentiated mica species including muscovite, biotite, illite) and chlorite and traces of hematite and calcite. By comparing

XRD peak intensities only minimal changes in the relative proportions of the minerals were noticed between the <250 µm and the 125-250 µm fraction. Thereby mainly the quartz content seems to vary with increased amounts in the <250 µm fractions whereas the albite and orthoclase content decreases slightly in this grain size fraction.

Figure 1 shows the overlain X-ray diffraction profiles for comparison of mineralogical differences between prepared diorite sand fractions of <250 µm (red) and 125-250 µm (black). Figure 2 for the extracted sample peaks (orange) and the identified mineral standard data. The key to X-ray diffraction traces are: Vertical axis - Intensity (counts per second) and Horizontal axis - °2θ Co-Kα

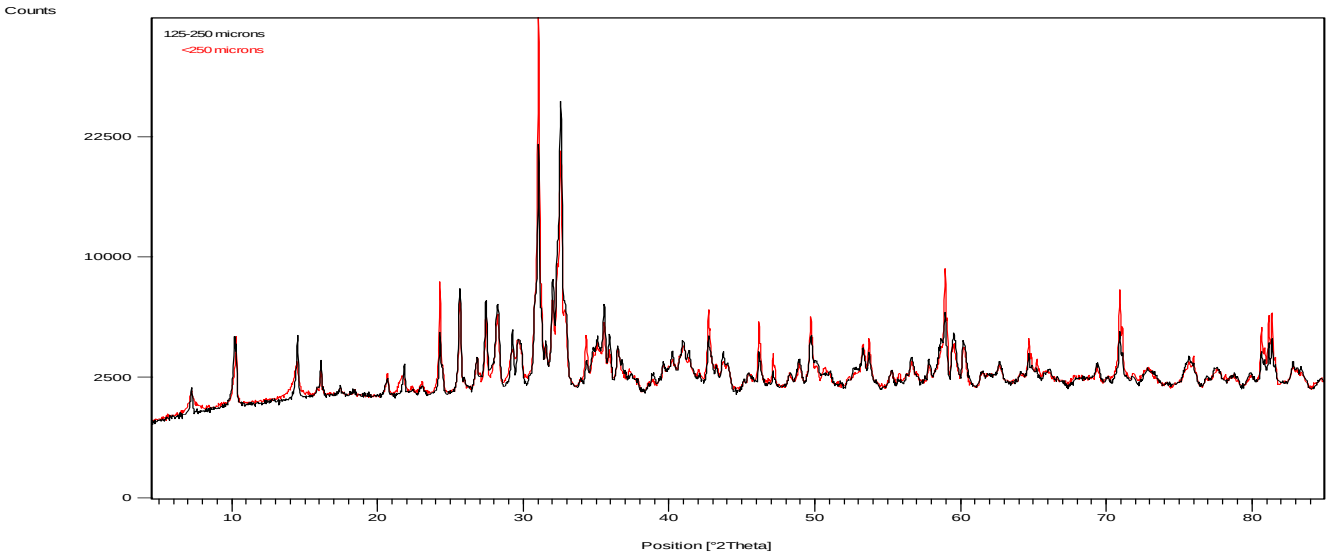

Figure 1 X-ray diffraction profile of <250 µm (red) and 125-250 µm (black) diorite fractions

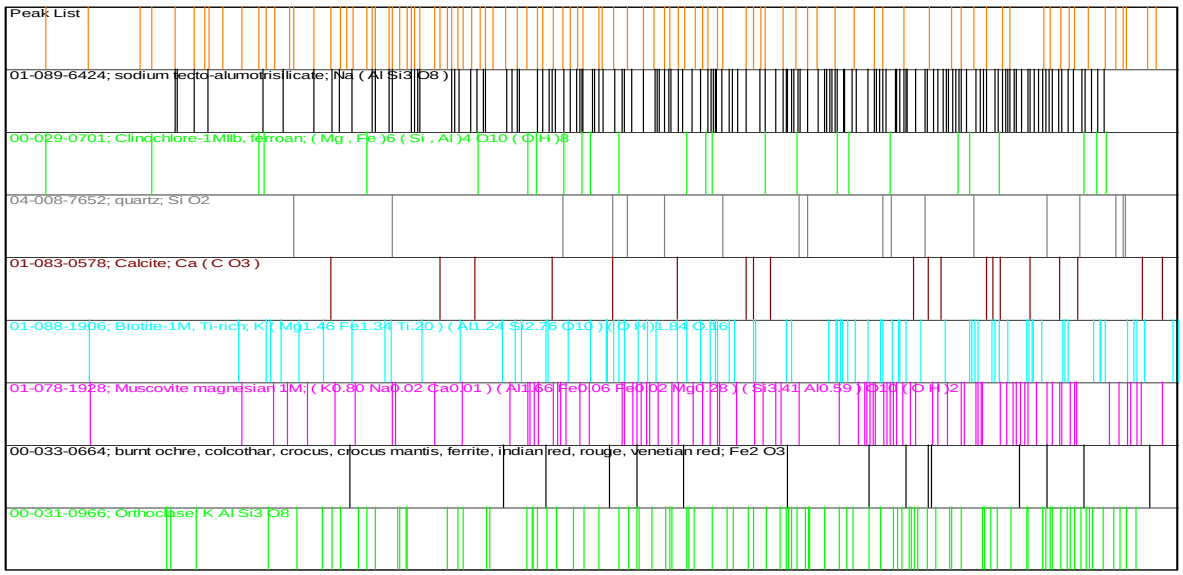

Figure 2 X-ray Diffraction Stick Pattern Data

Plate 3 Digital image taken at 10X magnification illustrating the heterogeneity of the diorite grains, the particles shown range between 250 µm and 500 µm in size

2.6 BACTERIAL CULTURE

Pseudomonas aeruginosa was selected for its biofilm (exopolysaccharide - EPS) forming properties (Vaughan *et al.*, 2001). It is a gram-negative rod, 0.5 to 0.8 µm wide by 1.5 to 3.0 µm in length and is a pathogen of humans. The matrix of the *P. aeruginosa* biofilm is composed of an alginate polymer of mannuronic and glucuronic acids. Its natural habitat is soil but it is also common to water and vegetation. Primarily aerobic, *P. aeruginosa* will grow anaerobically in the presence of nitrate which it can use as a respiratory electron acceptor; it is also resistant to high concentrations of salt. In this respect, it is a suitable strain for these experiments as the Äspö groundwater has a high sodium chloride content, negligible nitrate and experiments took place in an aerobic environment. *P. aeruginosa* is capable of producing two types of pigments when grown in aqueous media, one is the fluorescent pigment pyoverdin and the other, the blue pigment pyocyanin. Pyocyanin is known to be produced in low-iron content media, a characteristic which was observed during the culturing of the bacteria for these experiments. The siderophore, pyochelin, is a derivative of pyocyanin and is used by the bacterium to sequester iron from the environment.

2.6.1 Preparation of bacterial culture

P. aeruginosa (NCIMB 10548) was received in a freeze dried state and resuscitated by adding 0.5 ml of sterile Nutrient broth (OXOID). This suspension was then subcultured onto agar slopes (OXOID CM3) and into a 50 ml flask of sterile nutrient broth. The slopes were refrigerated to maintain a stock culture for future experiments. The flask was placed on an orbital shaker and incubated overnight at 36 ºC. After 24 hours the actively growing culture was then further inoculated into 500 ml flasks of sterile nutrient broth to achieve a large volume of bacteria. The culture was then transferred to 35 ml sterile tubes and centrifuged at 4600 rpm for 20 minutes. The supernatant was aseptically removed and the volume replaced with sterile artificial Äspö groundwater. The tubes were remixed and the centrifugation process repeated four times until traces of culture media were 'washed' from the bacteria. The concentrated culture, suspended in the groundwater, was then injected into the reservoir with a sterile syringe via the access port as shown in Plate 4.

Plate 4 Inoculation of the synthetic groundwater via the access port

2.7 BACTERIOPHAGE

Sutherland *et al.* (2004) suggested that when bacteriophage come into contact with biofilms interaction may occur depending upon the susceptibility of the biofilm bacteria. Alternatively coexistence between the phage and the host bacteria may develop. If cell lysis is effected by the bacteriophage the integrity of the biofilm may be destroyed and transport properties altered. In studies by Doolittle (1996) the bacteriophage E79 was shown to infect surface cells of a thick *P. aeruginosa* biofilm. It is also recognised that pH can affect the infectivity of phage by altering electrostatic forces influencing attachment mechanisms (Schulze-Makuch *et al.*, 2003). The bacteriophage E79 (accession number 10884, strain PA01) was obtained from NCIMB Ltd. This was received in a liquid form as cell-free lysate in a phage buffer in the range 1 x 10^8 to 1 x 10^{11} plaque forming units (PLU) ml^{-1}. The viability of the phage was checked using the phage assay method detailed in Section 2.7.1.

2.7.1 Phage Assay Method

A double-agar-layer method (Pepper *et al.*, 1995) was used to check the viability of the bacteriophage E79. Two drops of the bacteriophage E79 were added to a tube containing 3 ml of cooled sloppy nutrient agar (Tryptic Soy Broth + 6 g of Agar No.1 per litre). 0.2 ml of a fresh overnight culture of the host bacteria *P. aeruginosa* was added and this was mixed gently and poured onto a pre-dried plate containing 20 ml of solid medium (Tryptic Soy Broth + 10g of Agar No.1 per litre). The plate was then swirled to ensure even coverage across the surface. After the top agar layer congealed the plate was then covered, inverted and incubated for 48 hours at 37ºC. Duplicate plates were prepared in this way. The plates were then examined to determine areas of lysis, i.e. where areas of clearing (plaques) appear. The presence of these plaques indicated bacteriophage activity.

2.8 MICROSCOPIC METHODS

Three microscopic techniques were used in the experiments; epifluorescence, visible light and digital microscopy.

2.8.1 Epifluoresence Microscopy

Epifluorescence microscopy uses a short wavelength transmission source to fluoresce a sample stained with the nucleic acid selective cationic fluorochrome. In the experiments, the fluorescent stain, Acridine Orange, or N,N,N',N'-tetramethylacridine3,6-diamine ($C_{17}H_{19}N_3$), was used to determine total cell counts (Jass and Lappin-Scott, 1992); and to assess the extent of biofilm growth in the flowcell and columns. Acridine Orange is capable of permeating cells and interacts with DNA and RNA by intercalation or electrostatic attractions. When the fluorescent stain interacts with DNA, which is spectrally similar to fluorescein, the excitation maximum is at 502 nm and the emission maximum at 525 nm (green) while RNA interactions shift the excitation maximum to 460 nm (blue) and then emission maximum to 650 nm (red). Thus it is possible to determine if cells are metabolically active as they appear red; or inactive when they appear green.

2.8.1.1 PREPARATION OF GLUTERALDEHYDE FIXATIVE

Gluteraldehyde fixative was used prior to staining with Acridine Orange for epifluorescence microscopy. A solution of cacodylic acid was prepared by dissolving 8 g of acid in 500 ml of demineralised water and adjusting the pH to 7.4 if required. The solution was filter sterilised through a 0.45 µm Millipore filter. A 25% gluteraldehyde solution was diluted with the cacodylate buffer to make a 0.5% gluteraldehyde solution.

2.8.1.2 PREPARATION OF ACRIDINE ORANGE

Acridine Orange was dissolved in a mixed potassium monobasic/dibasic phosphate buffer. The potassium phosphate dibasic buffer solution was prepared by dissolving 4.35 g of K_2HPO_4 in 500 ml of demineralised water and sterilising through a 0.2 µm Millipore filter. The potassium phosphate monobasic buffer solution was prepared by dissolving 3.40 g of KH_2PO_4 in 500 ml of RO water and sterilising through a 0.2 µm Millipore filter. To prepare the Acridine Orange stain, 42 ml of potassium phosphate dibasic buffer solution was combined with 8 ml of potassium phosphate monobasic buffer solution, the pH was adjusted to pH to 7.5 with the monobasic solution and 5mg of Acridine Orange stain was added. The Acridine Orange stain was syringe filter sterilised through a 0.45 µm Millipore filter.

2.8.1.3 PROCEDURE FOR EPIFLUORESCENCE MICROSCOPY

Bacterial cells were fixed by pipetting 1 ml of the synthetic groundwater from the reservoir to 10 ml of gluteraldehyde fixative. A pre-wetted black Nucleopore membrane was transferred to the bottom of a Millipore filter apparatus with forceps, ensuring that the surface of the membrane was in contact with the filter base before clamping on the chimney and drawing vacuum. A 5 ml aliquot of sample of the fixed bacterial solution was pipetted into the chimney of the filter apparatus and vacuum drawn until the sample was filtered. The vacuum was then released. A one ml aliquot of the Acridine Orange stain was dispensed into the filter apparatus, with minimal disturbance of the bacteria on the filter and allowed to stain for two minutes before removing the staining solution under vacuum. Whilst maintaining the vacuum, 1.5 ml of isopropyl alcohol was then carefully added to ‘destain’ the sample. The vacuum was run for a short period to dry the filter before releasing the vacuum. The membrane was transferred using sterilised tweezers to a dry filter paper in a small petri dish and allowed to dry for at least 20 minutes. The dry stained membrane was then placed onto a glass microscope slide and a drop of immersion oil was placed onto the membrane before covering with a cover slip. The slides were counted on a Zeiss

microscope fitted with a fluorescence lamp (The excitation wavelength of Acridine Orange is between 450-490 nm). Using a gridded eyepiece and a 10x lens the filter membrane was brought into focus. The magnification was increased to a 100x oil immersion lens to count the numbers of bacteria per gridded area. Twenty fields of view were counted to give mean numbers of bacteria and standard deviations were calculated.

2.8.2 Visible Light Microscopy

Light microscopy was used to examine bacterial cells and biofilm stained with Congo Red; and their association with solid substrate in the flowcell. Congo Red is a secondary diazo dye ($C_{32}H_{22}N_6Na_2O_6S_2$) and is the sodium salt of benzidinediazo-bis-1-naphtylamine-4-sulphonic acid. Often used as a pH indicator, Congo Red has been shown to stain bacteria dark red and biofilm EPS an orange-pink colour (Allison and Sutherland, 1984). Cetyl pyridinium chloride (10 mM) is used initially to precipitate the polysaccharide material which is stained by a saturated aqueous solution of Congo Red. A 10% Tween 80 solution intensifies the colouration. The bacterial cells and biofilm are then stained with a 10% Ziehl carbol fuchsin solution was then used to stain the bacterial cells.

2.8.2.1 PROCEDURE FOR LIGHT MICROSCOPY

On completion of the biofilm growth experiments, diorite material was taken from the flowcell and carefully transferred to glass microscope slides which were flooded with 10 mM cetylpyridinium chloride. The slides were dried in air for 30 minutes, fixed by gently warming and then allowed to cool to room temperature. The EPS was stained for 15 minutes using a 2:1 mixture of Congo Red solution and Tween 80. The slides were rinsed and the bacterial cells were stained with the Ziehl carbol fuchsin stain before final rinsing and drying at 37 °C.

2.8.3 Digital Microscopy

Still and time-lapse video footage of the flowcell during biofilm growth experiments were captured using a 10X to 200X digital microscope and associated software. Time-lapse settings allowed for images to be captured at intervals of between 30 seconds and 30 minutes. The flowcell was monitored for 360 hours after inoculation of the bacterial culture.

2.9 FLUID CHEMISTRY ANALYTICAL METHODS

The fluid chemistry of samples were determined using Inductively Coupled Plasma Atomic Emission Spectrometry (ICP-AES), Ion Chromatography (IC) and Flow-Injection Visible Spectometry. The determination of major and trace cations in aqueous samples was performed on a Varian Vista ICP-AES using the procedure described in BGS Technical Procedure AGN 2.3.5 Issue 7.0. A Dionex DX-600 Ion Chromatograph was used to determine the anion concentration; this procedure is detailed in BGS Technical Procedure AGN 2.3.6 Issue 10.0. The determination of reduced iron (Fe^{2+}) was also considered to be important as the bacterium is known to sequester iron during growth. An automated flow-injection visible spectroscopic method was therefore used to determine Fe^{2+}; this method again used the Dionex DX-600 Ion Chromatograph according to BGS Technical Procedure AGN 2.3.11 Issue 4.0.

Samples were filtered thorough a 0.2 µm Millipore filter to remove the pathogenic bacteria. Each sample was then sub-divided into three separate aliquots. For ICP-AES analysis, the groundwater was preserved in 1% v/v of concentrated Aristar grade nitric acid. For reduced iron, vials containing 1.5 ml of 1% 2,2'–dipyridyl solution were made up to 15 ml with sterilised sample. No preservative was required for IC analysis. All samples were stored in a fridge below 5 °C prior to analysis.

2.10 MINERALOGICAL ANALYSIS (QUANTITATIVE STUDIES ONLY)

Petrographical analysis of the diorite used in the quantitative column experiments was examined by Scanning Electron Microscopy (SEM). SEM observations were made on: cryogenically-preserved subsamples (cryoSEM); Freeze-dried subsamples and subsamples prepared by solvent-displacement drying with diffusive impregnation with polystyrene cement. These different sample preparation methods are described in the following sections.

SEM analysis was performed using a LEO 435VP variable pressure digital scanning electron microscope. The SEM instrument was equipped with an Everhart-Thornley type detector for Secondary Electron Imaging (SEI) and a KE Developments four-quadrant (4 diode-type) solid-state detector for Backscattered Electron Imaging (BSEM). The instrument was also equipped with an Oxford Instruments CT1500 cryogenic sample handling and preparation unit directly interfaced to the SEM chamber, with a cryogenically-cooled SEM sample stage attachment. Phase/mineral identification was aided by qualitative observation of energy-dispersive X-ray spectra recorded simultaneously during SEM observation, using an Oxford Instruments INCA energy-dispersive X-ray microanalysis (EDXA) system.

2.10.1 Cryogenic SEM

CryoSEM was undertaken using the Oxford Instruments CT1500 cryogenic sample preparation and SEM sample transfer unit attached directly to the LEO435VP SEM instrument. Small cubic samples (~5-10 mm) were cut (using a scalpel blade) from selected positions along each column ("A" samples). The samples were then placed into a small liquid-nitrogen–chilled aluminium "cup" (Plate 5), which was then rapidly pre-frozen by immersing in melting liquid nitrogen-solid nitrogen slush. The purpose of rapid pre-freezing was to limit the formation of coarse ice crystals that might cause microstructural deformation within the sample. The frozen samples were then stored under liquid nitrogen until required for cryoSEM analysis.

To prepare SEM mounts for cryoSEM analysis, the frozen blocks were transferred into a bath of liquid nitrogen placed within a purpose-built environment glove box that interfaced with the CT1500 cryogenic preparation and sample transfer chamber (Plate 6). The box was constantly flushed with dry nitrogen gas to keep atmospheric moisture from forming hoar-frost on the surface of the sample. The frozen sample was then fractured under liquid nitrogen by chisel to produce a fresh surface for observation. Freshly-fractured chips of material were then mounted onto a cryogenic sample holder, and kept in place with the addition of a small droplet of water that instantly froze the sample to the surface of the gold-plated sample mount. This was then transferred to the cryogenically-cooled sample stage (at -170 °C) in the SEM via the CT1500 cryogenic sample preparation and transfer unit (Plate 6).

Once inside the SEM, the sample stage was slowly warmed to between -60 to -80 °C to slowly ablate the frozen interstitial porewater under vacuum.This process allowed the intergranular pore fabrics to be revealed. The rate of ablation was controlled by constant observation under the SEM so as to just reveal the delicate intergranular and grain-coating features and not cause or minimise any collapse of the fabric. When the desired "development" of the sample surface was achieved, the stage was rapidly re-cooled to -170 °C to stop further ablation of ice from the sample. The samples were then observed under the SEM using BSEM imaging under variable pressure/low vacuum (0.4 torr). This allowed the frozen samples to be observed in the SEM without the need for coating with an electrically-conductive material such as gold or carbon (required for conventional high vacuum SEM analysis).

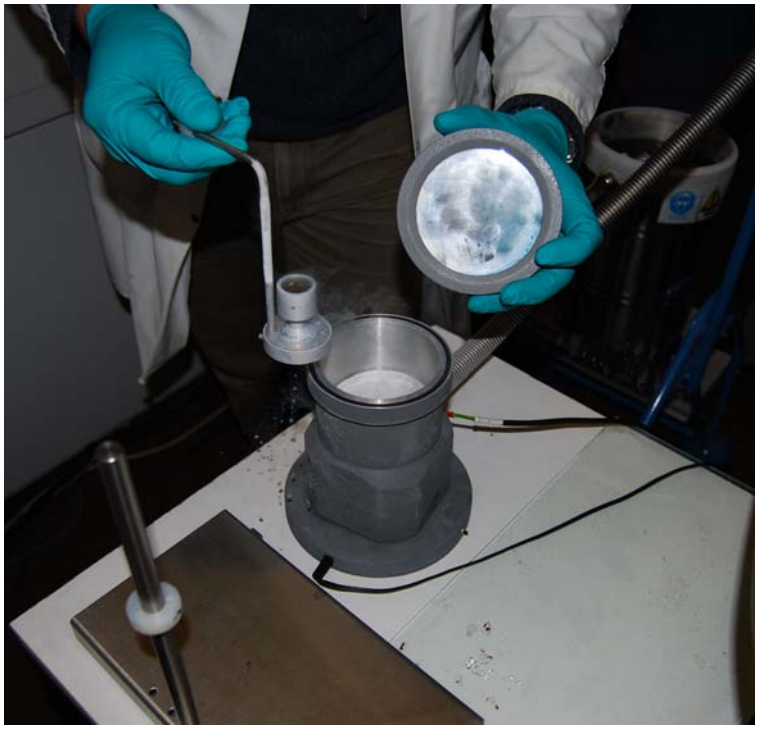

Plate 5 Liquid nitrogen pre-freezing slushing unit, with aluminium cup used for immersing BIOTRAN samples into liquid nitrogen-solid nitrogen slush for pre-freezing for cryoSEM.

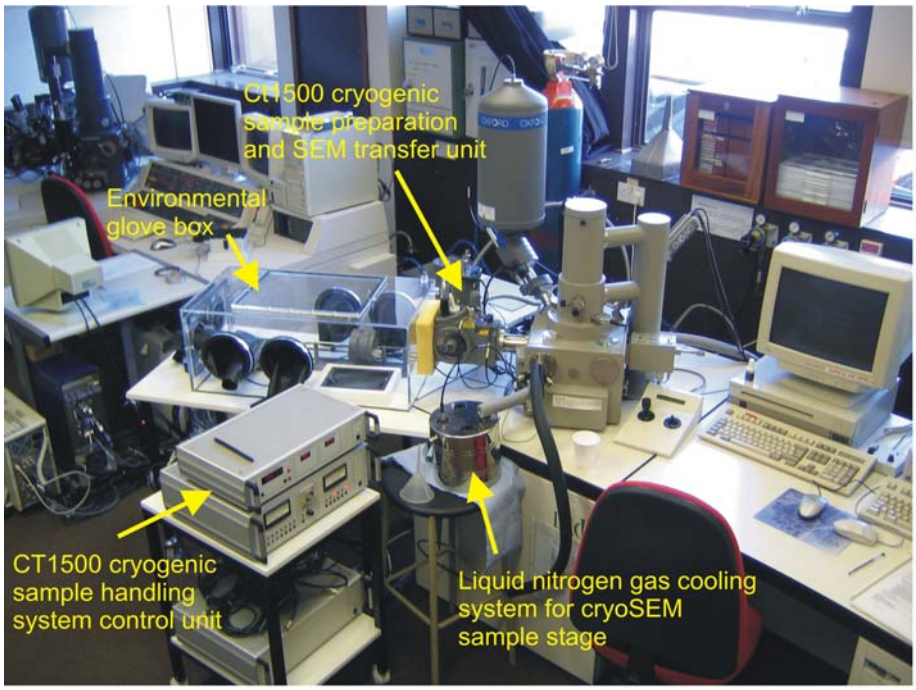

Plate 6 LEO 435VP SEM instrument fitted with an Oxford Instruments CT1500 cryogenic sample preparation and SEM sample-transfer unit. The purpose-built Perspex environmental glove box fits to the CT1500 sample transfer unit allowing frozen samples to be handled and fractured in a moisture-free environment.

Higher-resolution observations were made on selected samples under high-vacuum SEM (<1 x 10^{-4} torr). To do this the frozen sample was then withdrawn from the SEM chamber into the CT1500 cryogenic SEM preparation chamber (on-line with the SEM) and coated with a thin layer of gold using the units 'inbuilt' vacuum sputter coater. The gold coated sample was then

replaced on the cryogenically-cooled sample stage in the SEM and observed under high vacuum, whilst maintaining the sample at -170 °C.

SEM observations were made under variable beam voltage conditions between ~2-20 kV, with probe currents between 50-300 pA, as required.

2.10.2 SEM of freeze-dried samples

Samples for SEM analysis were also prepared as freeze dried material from the columns ("B" samples). Preparation involved initially pre-freezing sub-samples of wet material, as described in Section 2.10.1. The frozen samples were then placed in an Edwards Modulyo freeze-dryer for ~72 hrs and then left under vacuum until required for SEM sample preparation and analysis.

On examination after freeze-drying, it was found that each sample had completely collapsed and disaggregated into separate grains. Samples were prepared for SEM analysis by firstly taking a representative "grab" sample of disaggregated material and then "dipping" an SEM stub coated with an adhesive carbon tab, into the material to give an even covering of grains on the surface. Each stub was then placed into an Emitech K950 carbon evaporation coater, equipped with a planetary stage, and then carbon coated to a thickness of approximately 250 Å. This provided a conductive layer on the grains in order to enable the material to be analysed under high vacuum in the SEM.

2.10.3 SEM of solvent-dried and polystyrene-impregnated samples

Samples were also examined in the SEM after being prepared from the wet state by solvent replacement and drying, followed by impregnation with polystyrene cement. Samples prepared in this way were selected from the column experiments ("C" samples).

Aluminium foil cups were made (~10 mm diameter). These were then mounted onto SEM stubs using "Leit C" carbon adhesive and the stubs placed into a holder to keep them upright. A small sub-sample of "wet" column material was added to each cup, ensuring that there was sufficient space within the cup to give access to the sample base. Acetone was then dropped by pipette into each cup in order to permeate the samples to dehydrate them. This was removed, again by pipette after a few minutes and the operation repeated a further 2 or 3 times to ensure that the sample was as moisture free as possible. The samples needed to be as dehydrated as possible in order to carry out the next stage of preparation which utilised a 15 % (v/v) solution of polystyrene cement dissolved in amyl acetate, which is immiscible with water. Approximately 2-3 drops of this solution were then carefully added by syringe, into the base of each cup and surrounding the sample. The solvent carrying the polystyrene cement was then allowed to impregnate the sample via capillary action. The polystyrene-impregnated samples were left overnight in a fume cupboard, allowing the solvent to evaporate and the cement to set. This served to bind the friable granular material with the polystyrene cement producing a robust intact sample that could be handled in the SEM instrument. The quantity of solvent based cement used was deliberately insufficient to impregnate the entire sample, leaving undisturbed grains at the top of the sample which could then be analysed and observed in the SEM without being occluded by polystyrene cement.

Prior to placing them in the SEM, the samples were carefully carbon coated in an Emitech K950 carbon evaporation coater in order for them to be analysed under the SEM at high vacuum.

3 Development of methodologies to grow and observe biofilms in flow-through cells and columns

3.1 EXPERIMENTAL APPROACH

Experimental work at the start of the BioTran project focussed on developing methodologies to grow biofilms reliably in the laboratory and observe their development. This was accomplished by means of a closed system of PTFE tubing connecting reservoirs of sterile synthetic Äspö groundwater to either a column or a flow cell. Circulation of the groundwater was by means of a peristaltic pump. A diagram of the system is shown in

Figure 3. An inlet in the top of the groundwater reservoir was used to inoculate the medium; this inoculation port was kept sterile by attachment of a small diameter 25µm Sartorius filter as shown in Plate 7. Peristaltic tubing (1.52 mm ID) was used and the flow rate was estimated to be in the region of 3.0 to 3.5 ml min^{-1}, although there was some back-pressure in the system which was not accounted for. A photograph of this setup is shown in Plate 7. The groundwater was circulated through the flowcell and column for at least 24 hours to allow the system to stabilise before inoculation of the *P. aeruginosa* culture.

Growth of the biofilm was monitored using a digital microscope suspended over the flowcell. The magnification of the microscope was set at 10X throughout the experiment. The design of the microscope did not allow for higher magnification as the image could not be focussed due to the depth of the flowcell window. Two combined flowcell/column experiments were carried out; both were terminated 360 hours after inoculation of the groundwater with the bacterial culture.

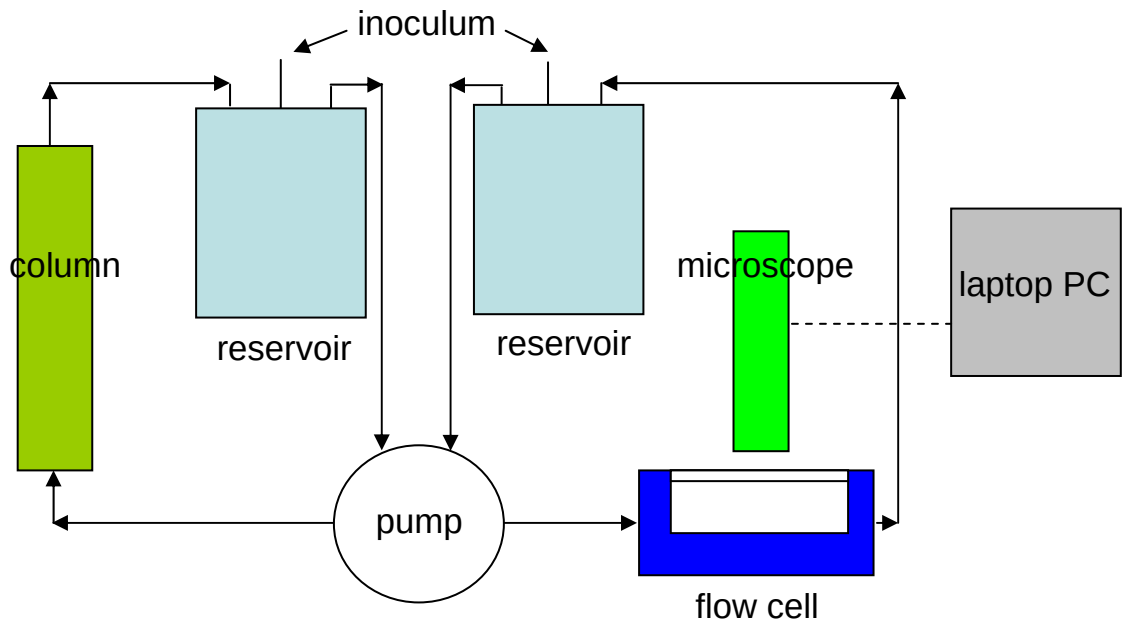

Figure 3 Schematic of the flowcell and column experimental setup

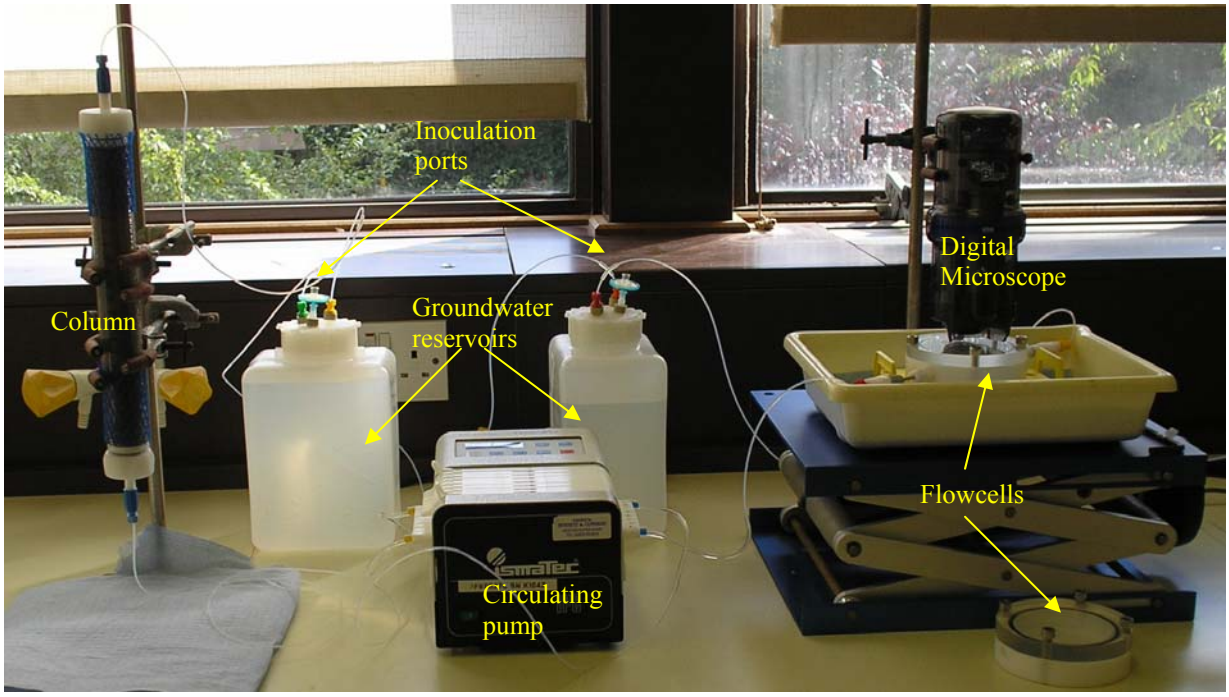

Plate 7 Experimental setup of flowcell and column

3.2 RESULTS

At the end of the first experiment, a digital microscope image of the flowcell was captured using visible light. The material in the flowcell was then stained *in-situ* by replacing the synthetic groundwater feed with a solution of Acridine Orange and restarting the peristaltic pump. When the flowcell was completely saturated with the stain, images of the flowcell were captured under long UV light (366 nm) in a darkened room. The column was not stained as the borosilicate glass would have prevented the penetration of UV light and the Acridine Orange stain would not fluoresce sufficiently for photography. Attempts to remove the material from the column without perturbing the biofilm were unsuccessful. However, a significant biofilm growth near to the base of the column was visible; this appeared to extend upwards into the bulk of the material.

In the second experiment, biofilm formation was monitored by time-lapse photography; images were captured using the digital microscope at 5 minute intervals to produce video footage of the developing biofilm. At the end of this experiment instead of staining the entire contents of the flowcell, small portions of diorite and associated biofilm were carefully removed from the flowcell using a spatula and transferred to microscope slides. This material was stained using Congo Red and photographed under a visible light source, again using the digital microscope.

3.2.1 Digital imaging

The image in Plate 8 was taken during the first flowcell/column experiment and shows the flowcell 196 hours after inoculation. This image was captured using the digital microscope at 10X magnification under visible light. During biofilm growth, small air pockets became visible at the surface of the flowcell and it is possible that this also occurred within the bulk material. As the biofilm developed further, these air pockets appeared to ‘dry out’ at the surface of the flowcell and were replaced with crystalline material, most likely deposits of salt from the synthetic groundwater, gelatinous strands of biofilm are also clearly visible.

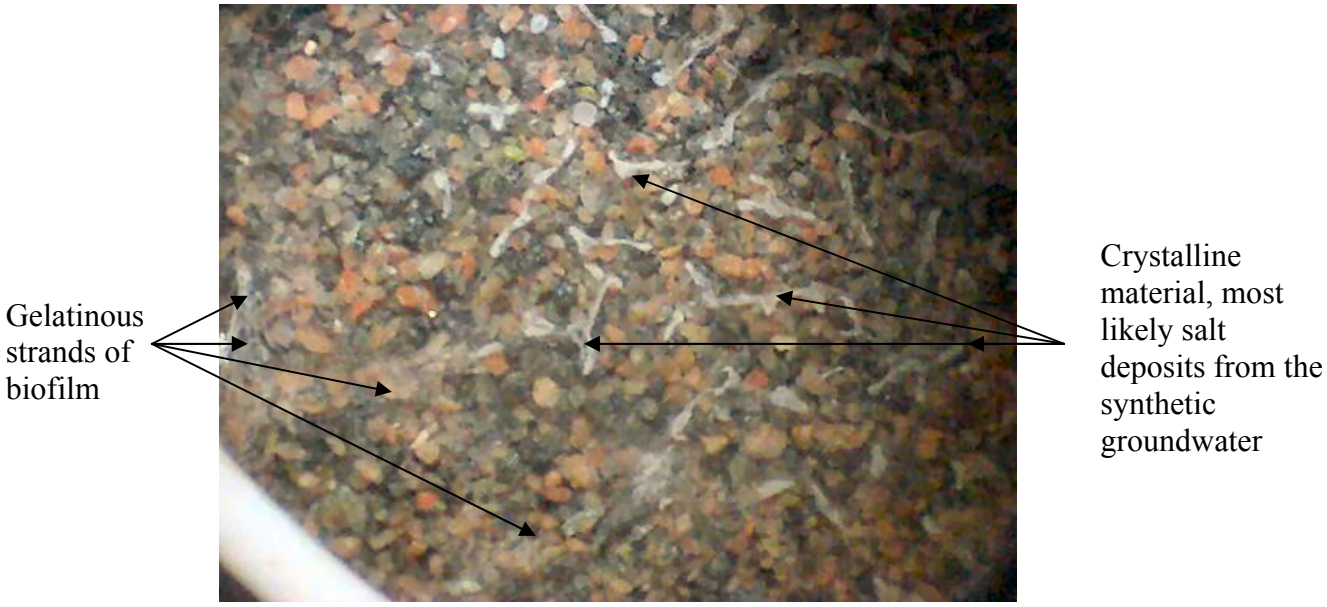

Plate 8 Flowcell image captured using the digital microscope at 10X magnification, 196 hours after inoculation

Using time-lapse photography, the growth of the biofilm within the flowcell was monitored visually. The most rapid period of growth of the biofilm occurred between 168 and 240 hours. Plate 9(a) was taken at the start of the second experiment, the flowcell is fully saturated with artificial groundwater and no air pockets are seen. Plate 9(b) was taken 168 hours after inoculation and shows the diorite grain surfaces coated with the gelatinous biofilm. Plate 9(c)

9(a) Flowcell at inoculation, the surface of the packed diorite is saturated with synthetic groundwater

9(b) Flowcell 168 hours after inoculation. The surfaces of the diorite grains still appear to be saturated with groundwater but they are now covered with gelatinous biofilm.

9(c) Flowcell 360 hours after inoculation. The surface of the packed diorite has partially dried and pockets of air have been replaced with salt deposits from the groundwater.

Plate 9 Images of the flowcell taken using the digital microscope at 10X magnification. 9(a) shows the flowcell at the time of inoculation. 9(b) shows the flowcell 168 hours after inoculation, the surface of the grains are covered with a glutinous biofilm. 9(c) shows the flowcell 360 hours after inoculation. The surface material has partially dried and salt deposits have filled former air pockets

shows the diorite surface 360 hours after inoculation. In this image the surface appears to have dried out, the biofilm is not as visible and areas of salt deposition are clearly seen in former air pockets.

Plate 10 shows the flowcell at the conclusion of the first flowcell/column experiment after staining with Acridine Orange. The replacement of the synthetic groundwater by the fluorescent stain has enabled a picture to be taken of the flowcell under long UV light (360 nm). This unmagnified image taken in low light conditions shows the large inlet area of the flowcell on the right, fluorescent staining around the inner rim of the flowcell and a slightly smaller area of staining at the outlet on the left. Under dark room conditions, (Plate 11) the staining of the flowcell was more distinct. Fluorescent material was seen throughout the body of the flowcell and appeared to follow a track through the centre of the flowcell from inlet to outlet.

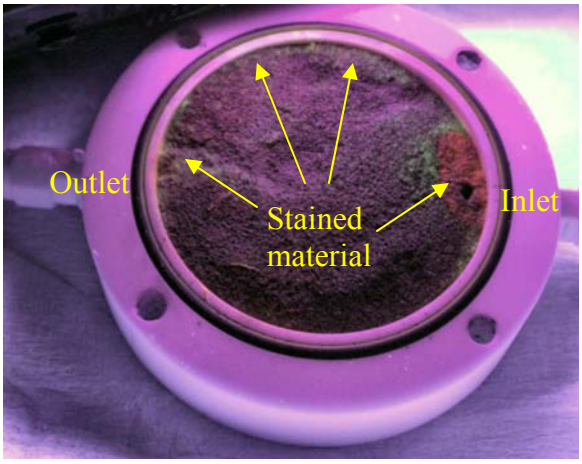

Plate 10 Image of the flowcell stained with Acridine Orange under long UV (360nm) illumination in low light conditions

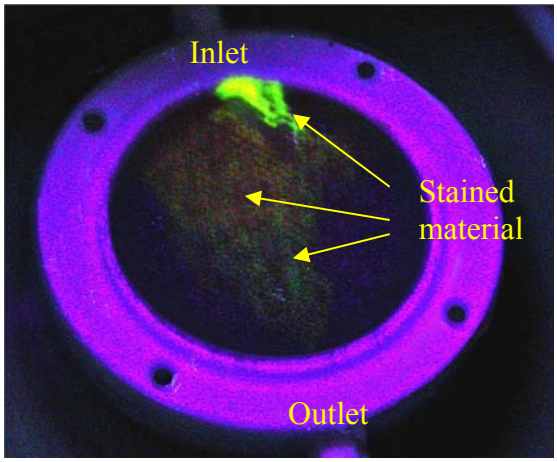

Plate 11 Darkroom image of the flowcell stained with Acridine Orange under long UV (360nm) illumination (NB different orientation to Plate 10)

3.2.2 Visible light microscopy

At the conclusion of the second flowcell/column experiment, granodiorite material was carefully removed from the flowcell and transferred to microscope slides with the minimum of disturbance. Plate 12 shows five microscope slides part-way through the Congo Red staining procedure, the slides have been suspended over a drip tray. The flowcell material and its

associated biofilm was fixed on the slides, stained with Congo Red/Tween solution and are shown during the Ziehl carbol fushin staining stage prior to final rinsing and drying.

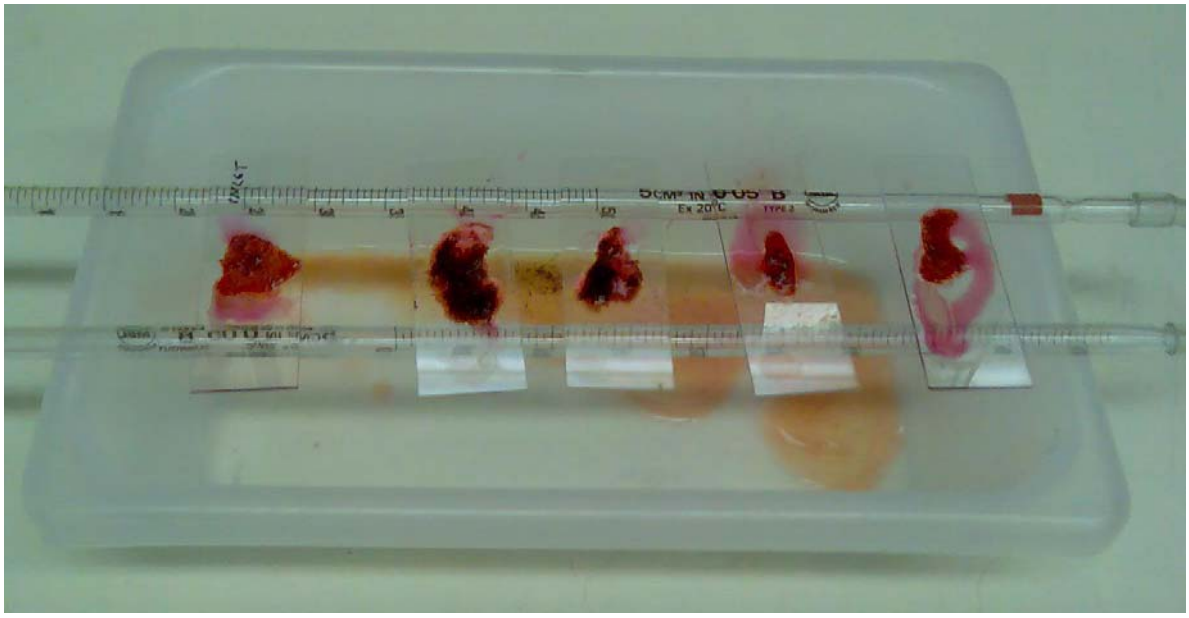

Plate 12 Five microscope slides of the granodiorite material during the Congo Red staining procedure. The slides were suspended over a drip tray and flooded with Ziehl carbol fushin stain prior to final rinsing.

The Congo Red staining technique successfully differentiated between bacterial cells (dark red) and EPS (orange-pink) formed by the biofilm. The image shown in Plate 13 is of the Congo Red stained diorite under 10X magnification. The bacterial cells appear to be surrounded by EPS except in the right-hand side of this image where the density of the bacterial clusters obscures the EPS. The dark spots are the individual grains of diorite.

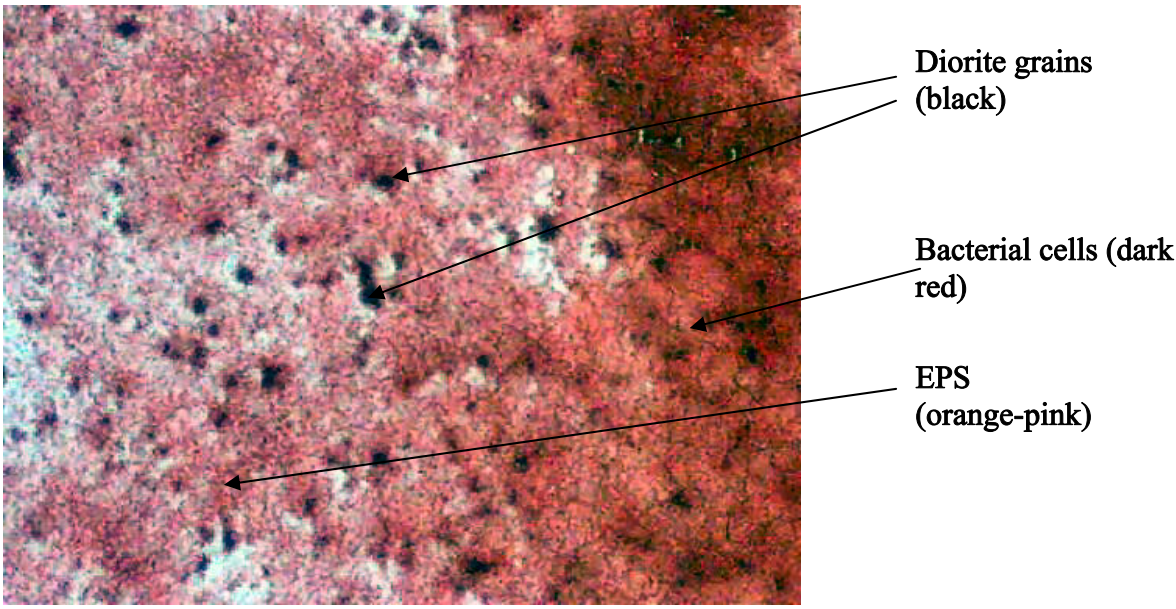

Plate 13 Diorite material taken from the flowcell, stained using Congo Red. Image was captured by the digital microscope at 10X magnification.

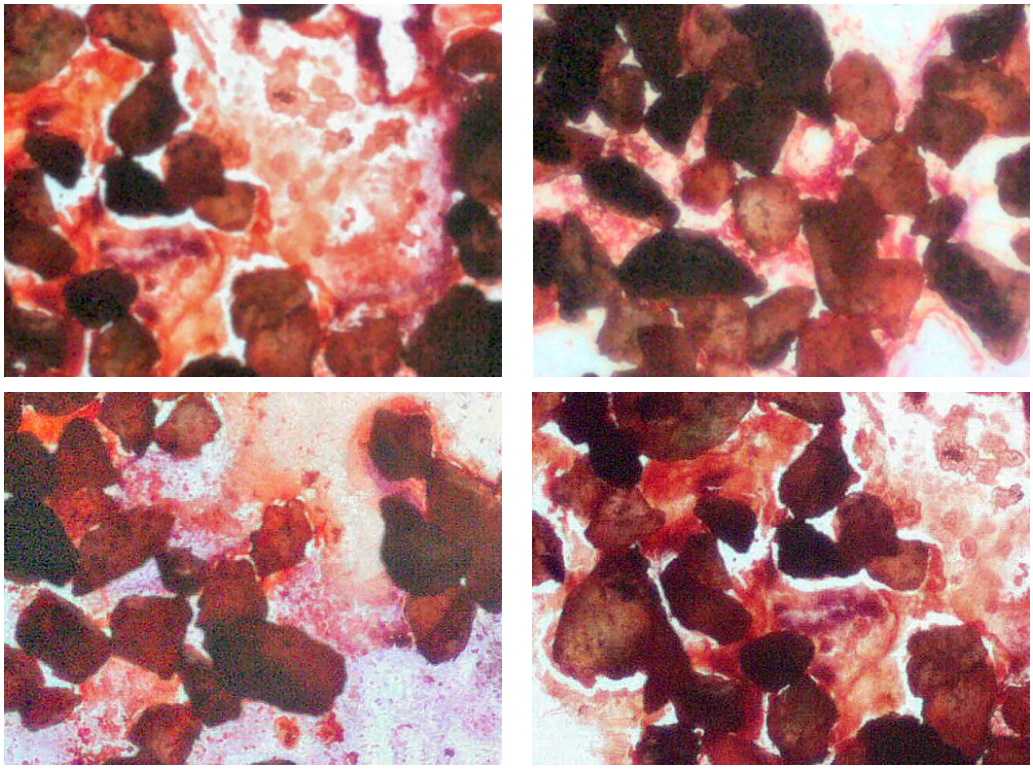

Plate 14 Images of Congo Red stained diorite after biofilm growth at 60X magnification. The dark grains of diorite appear to be surrounded by bacterial cells (stained red) and EPS (stained orange-pink)

Plate 14 shows images taken from four of the five microscope slides stained using the Congo Red procedure. Under this higher magnification (60X), the individual grains of diorite appear to be surrounded by EPS (stained orange-pink in colour). Clusters of bacterial cells (stained red) are clearly visible and are closely associated with both the EPS and the diorite grains.

3.3 SUMMARY OF RESULTS

The apparatus and methodologies described in this section have been used to show that:

- *P. aeruginosa* biofilms can be grown reliably using Äspö diorite and synthetic groundwater as a growth medium;
- *P. aeruginosa* biofilms can be grown in laboratory flowing systems.
- Biofilm growth and development can be imaged using a variety of techniques;

The following section describes pilot experiments using the same geological materials to ascertain the quantitative effects of *P. aeruginosa* biofilms on transport properties

4 Pilot study to quantitatively evaluate the effects of biofilms on fluid flow through crushed Äspö diorite.

The main aim of this pilot study was to study the effect of *P. aeruginosa* biofilm growth on fluid flow in columns packed with crushed Äspö diorite over a period of 2,141 hours. The impacts of a change in pH and bacteriophage on the biofilm (and hence on flow) were also examined.

4.1 EXPERIMENTAL APPROACH

4.1.1 Effect of *P. aeruginosa* biofilm on fluid flow

In this experiment, a flow-through system was setup using two columns. Column 1 acted as a control while conditions in the second column were changed. During the course of the experiment, the pH of Column 2 was lowered from pH 7.2 to pH 5.52 to determine the effect on flow, and in the latter part of the experiment, the pH of Column 2 was raised back to pH 7.2 before the introduction of phage to simulate starting conditions. Flow rates through the columns were measured by mass balance and samples of the groundwater taken at regular intervals for chemical analysis. A concise diary was kept to log times of fluid chemistry and microbiological sampling and to note any important observations in the status of the experiment. A diagram of 'Configuration A', illustrating the setup of the columns at the start of the experiments, is shown in Figure 4; with a photograph of actual laboratory setup in Plate 15. Unlike the earlier experiments, a peristaltic pump was used to maintain the level of groundwater in the header vessel. This arrangement provided a fixed pressure head, so changes in flow rate were proportional to permeability.

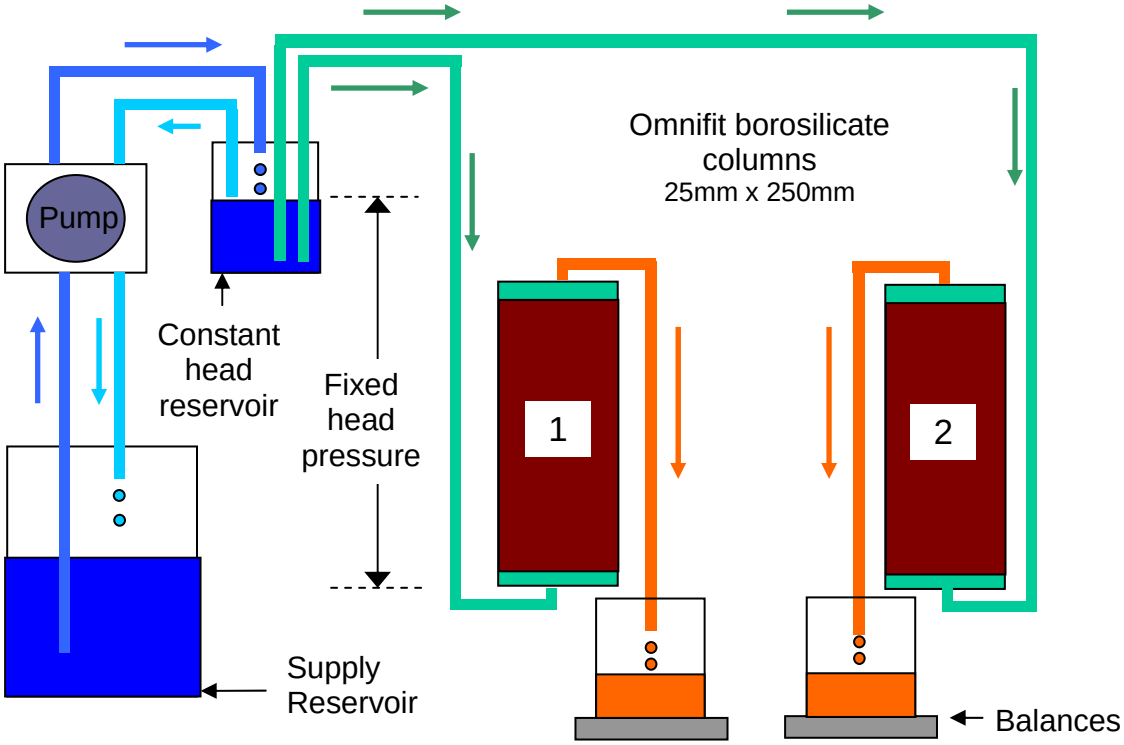

Figure 4 Diagram of the experimental setup of the dual columns, Configuration A

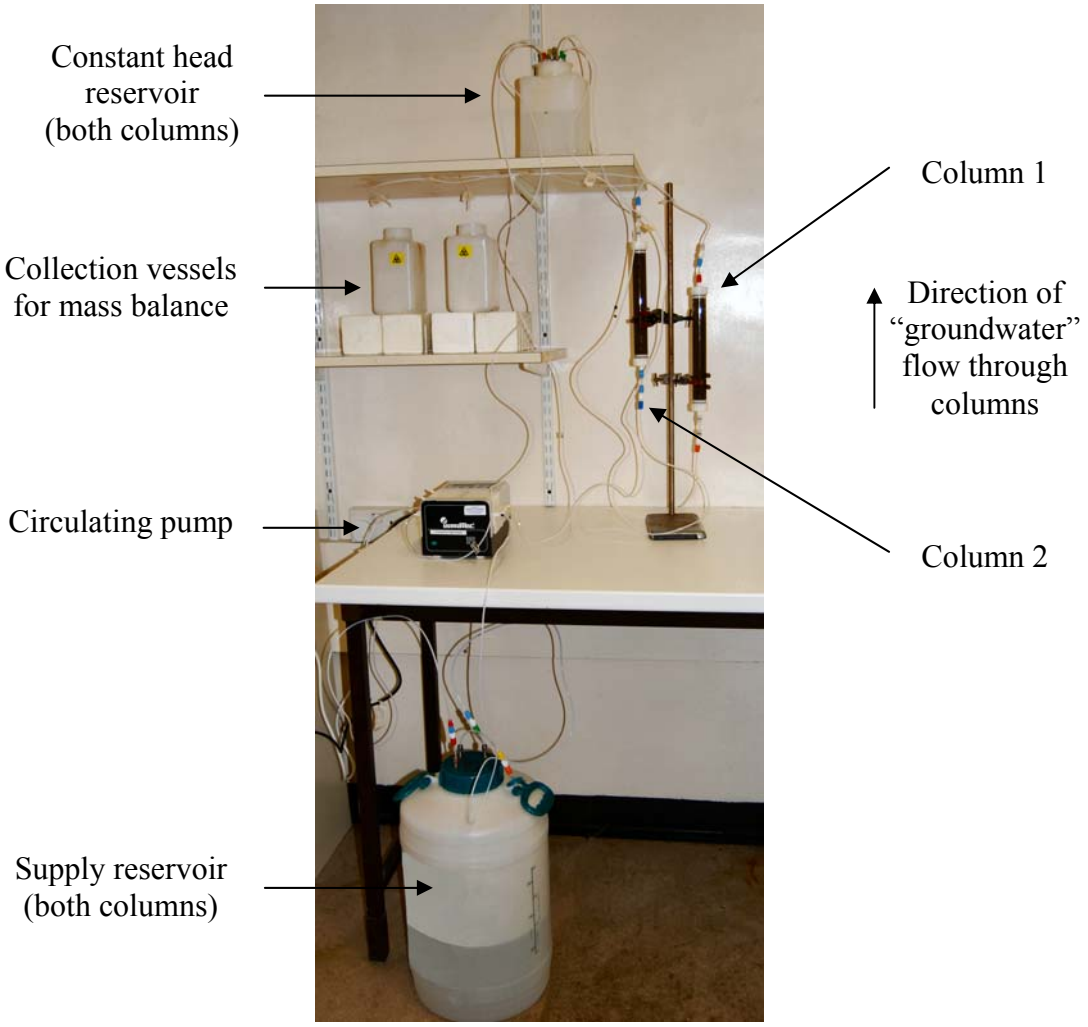

Plate 15 Laboratory setup, Configuration A

At the start of the experiment a sample of the *P. aeruginosa* culture was taken to determine the bacterial population injected into the groundwater reservoir. This starting culture was determined to be 6.99 x 10^8 bacteria ml^{-1}. Ten ml of this culture was then injected into each reservoir, each containing 23 l of synthetic groundwater. This gave a starting culture in each of the reservoirs of 3.04 x 10^4 ml^{-1} bacteria (Time 0). Throughout the experiment, 1 ml liquid samples were then taken at intervals from the collection vessels. These samples were preserved in gluteraldehyde fixative until the total counts of bacterial numbers could be determined.

4.1.2 Effect of change in pH on *P. aeruginosa* biofilm and fluid flow

At the start of the experiment, the pH of the Äspö synthetic groundwater was pH 7.05. This fluid was pumped to a single header vessel from the supply reservoir. After 726 hours, a second supply reservoir and header vessel was introduced into the system to supply Column 2, Column 1 remained connected to supply reservoir 1. This is shown as 'Configuration B' in Figure 5 and Plate 16. The pH of the groundwater in supply reservoir 2 was adjusted to pH 5.52 by addition of sterile dilute hydrochloric acid to assess whether this influenced flow characteristics through alteration of biofilm and bacterial attachment properties. The flow rate continued to be monitored. After 966 hours, sterile sodium hydroxide solution was added to supply vessel 2 to return the pH close to its original value, the pH achieved was 7.22.

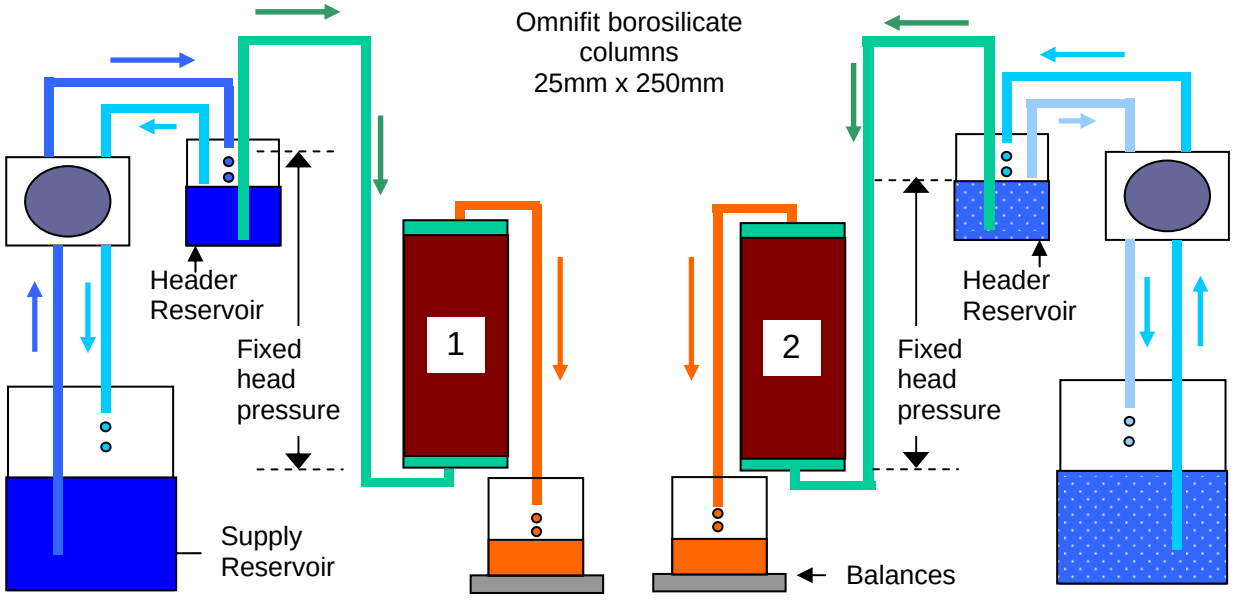

Figure 5 Diagram of the experimental setup of the dual columns, Configuration B

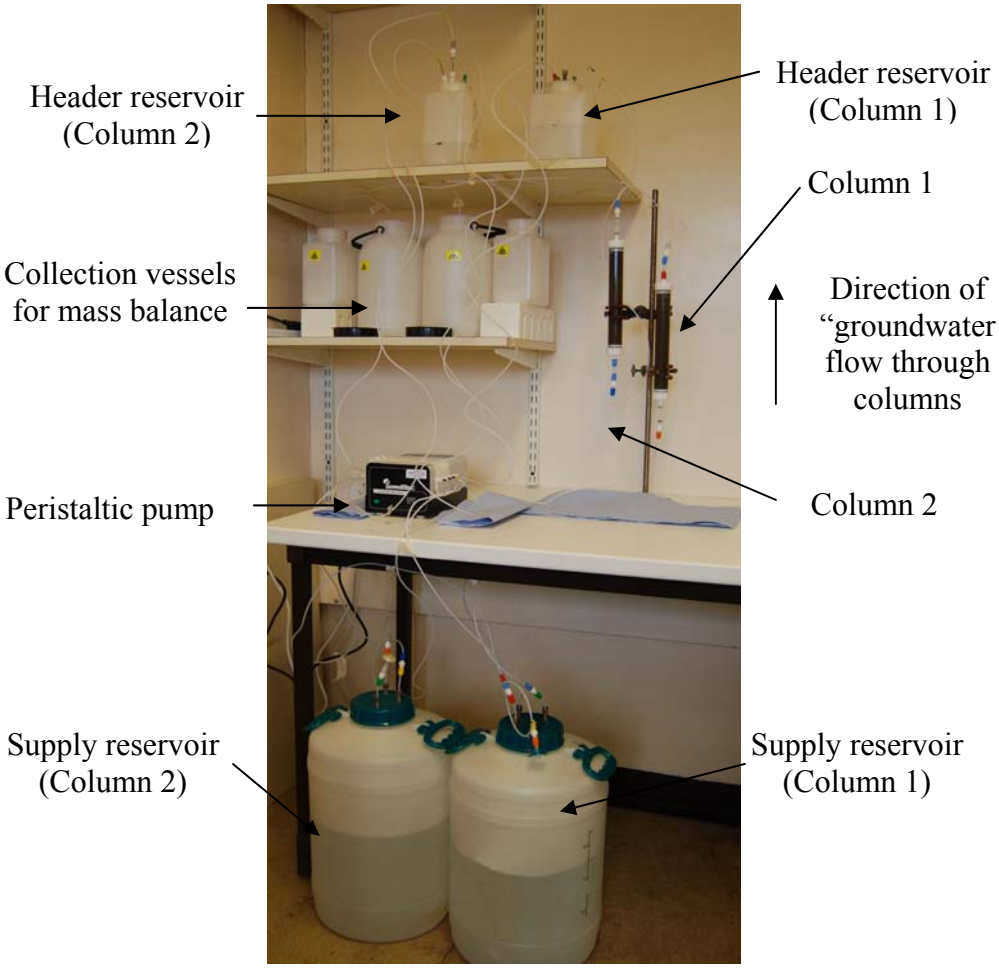

Plate 16 Laboratory setup, Configuration B

4.1.3 Effect of injection of bacteriophage E79 on *P. aeruginosa* biofilm and fluid flow

The column experiments culminated with the addition of the bacteriophage E79. After 1,156 hours from inoculation, 0.5 ml of the phage solution was introduced into the small groundwater reservoir of Column 2 using a sterile syringe. A phage assay sample was taken from Column 2 supply reservoir 48 hours later and a second assay was performed 1,560 hours after inoculation of the bacterium. As no effects were apparent, at 1,971 hours) the inlet tubing was disconnected from the reservoir of Column 2 and a further 0.1ml of the phage solution was injected into the tubing before reconnecting. The experiment was concluded at 2,141 hours.

4.1.4 Chemical and microbiological analysis

Samples were taken for fluid chemistry and for total microbial numbers (epifluorescence microscopy) at regular intervals during the experiment; the flow rate at each sampling time was recorded. Analytical techniques are described in section 2.

4.2 MEASUREMENT OF POROSITY AND FLOW RATES

4.2.1 Porosity determination

At the start of the experiment the porosity of each column was determined by weight using the following equations. Equation 1 calculates the volume of the solid material within the packed column giving a value for the volume of solids by assuming the minerals have the same density as quartz (2.64 g ml^{-1}). Equation 2 calculates the volume of fluid equivalent to the pore volume in ml, assuming the density of the synthetic groundwater is 1.0 g ml^{-1} and the column is fully water saturated. Equation 3 calculates the porosity of the columns as a percentage of the total volume.

$$\text{Volume of solid (ml)} = \frac{\text{mass of dry packed column (g)} - \text{mass of empty column (g)}}{2.64}$$

Equation 1 Calculation of the volume of solid material in the columns

$$\text{Volume of fluid (ml)} = \frac{\text{mass of wet packed column (g)} - \text{mass of dry packed column (g)}}{1.0}$$

Equation 2 Calculation of the volume of fluid within the columns

$$\text{Porosity (\%)} = \frac{\text{volume of fluid (ml)}}{\text{volume of fluid (ml)} + \text{volume of solid (ml)}} \times 100$$

Equation 3 Calculation of column porosity as a percentage of the total volume

To calculate porosity, the columns were weighed empty, after packing with dry diorite sand and weighed again after saturation with synthetic groundwater. Using the equations given above, the porosity of columns was calculated.

4.2.2 Measurement of flowrates

The flow rates were measured by mass balance over a given time period. At the start of the experiment, the columns were allowed to stabilise and a steady flow rate achieved before inoculation of the supply reservoir by *P. aeruginosa*.

4.2.3 Calculation of hydraulic conductivity

Darcy's law states that the flow rate per unit area is proportional to the gradient of hydraulic head, the constant of proportionality being the hydraulic conductivity. For flow in a column this is expressed by equation 4, where Q is the flow rate ($m^3 s^{-1}$), A is the cross-sectional area (m^2), K is the hydraulic conductivity ($m s^{-1}$), Δh is the head difference across the column (m), and L is the length of the column (m).

$$\frac{Q}{A} = K\frac{\Delta h}{L}$$

Equation 4 Darcy's law for 1D flow in a column

The columns had cross-sectional areas of 4.91×10^{-4} m^2. The head difference across Column 1 was 0.184 m and that across column 2 was 0.128 m. Column lengths are given in Appendix 2. A simple re-arrangement of equation 4 allows the effective hydraulic conductivity of the column to be calculated from the flow rates.

4.3 RESULTS

4.3.1 Porosity

Initial calculations showed Column 1 to be significantly more porous than Column 2 and as a result, Column 1 was emptied and repacked. The agreement between the columns was better with Column 1 having a porosity of 45.4% and Column 2 a porosity of 43.6%. The porosity calculations appear in full in Appendix 2.

4.3.2 Flow rates and hydraulic conductivity

Figure 6 shows the flow rates through the columns from the time of inoculation to the cessation of the dual column experiments at 2208 hours. It also shows the time when the pH was changed in the synthetic groundwater in Column 2 (from 726 hours to 926 hours – a 240 hour exposure). Figure 7 shows the flow rate data converted to hydraulic conductivity for both columns. The phage were added at 1,156 hours to Column 2.

Both figures show how flow rate and hydraulic conductivity change in each column throughout the duration of the experiment. These changes are complex with Column 1 appearing to have several fluctuations during the first 250 hours. These are not observed in Column 2. However, in both columns flow rate reaches a maximum of ~4.5 ml min^{-1} during the experiment at a period of between 500 hours (Column 1) and 250 hours (Column 2). Similarly, hydraulic conductivity is between 2×10^{-4} m s^{-1} (Column1) and 3×10^{-4} m s^{-1} (Column 2) at this time. However, in both columns hydraulic conductivity appears to decrease at a similar rate from about 500 hours to a point at about 1000 hours where no flow is occurring (0.003 ml min^{-1} to 0.01 ml min^{-1}). Changes in pH in Column 2 make no difference to flow rate, neither does introduction of the phage.

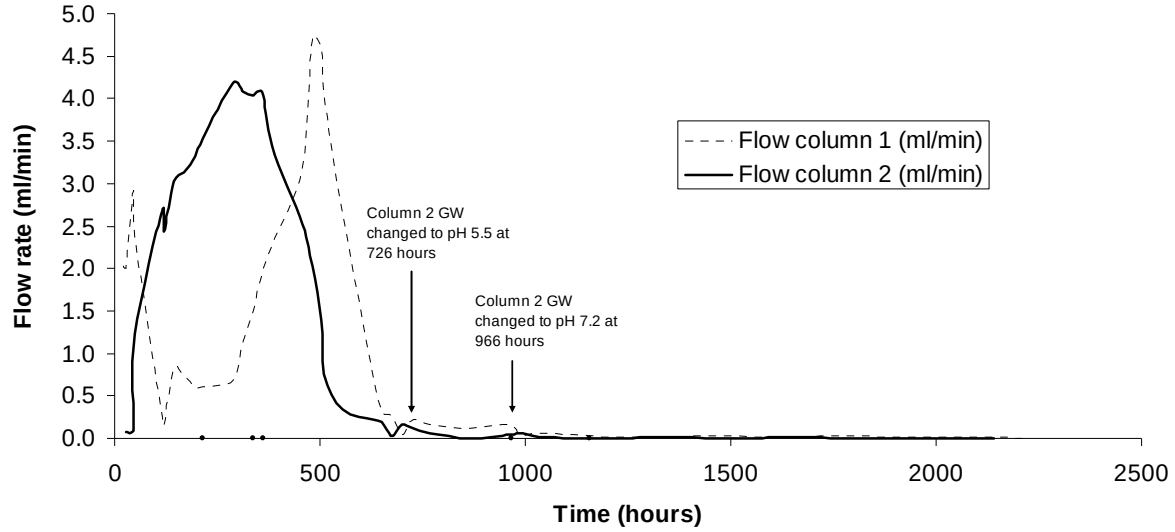

Figure 6 Flow rate of groundwater through Column 1 and Column 2 after injection of bacteria at time 0 hours

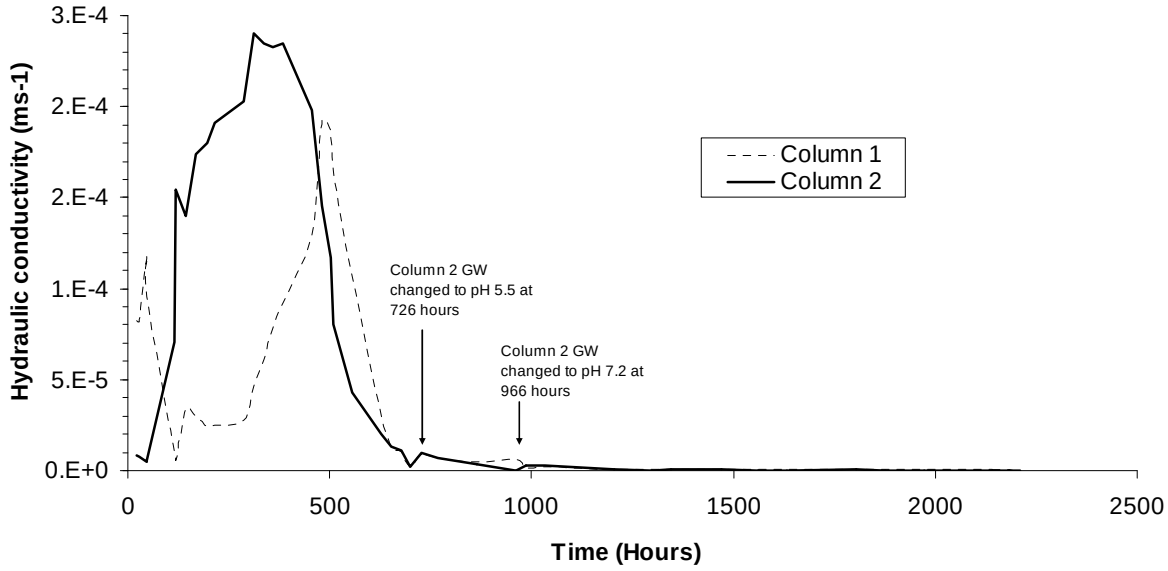

Figure 7 Hydraulic conductivity for Column 1 and Column 2

4.3.3 Epifluorescence Microscopy

The results for total bacterial counts using epifluorescence microscopy are given in Table 2 and shown graphically in Figure 8. Although numbers fluctuate in the first 500 hours, there is a drop in mean bacterial numbers in both columns of about one order of magnitude from the inoculation of 3.04×10^4 ml^{-1} bacteria . At around 700 hours, the mean number of bacteria of ~ 3×10^5 to bacteria ml^{-1} were present in the waters sampled from both columns. The number of bacteria in Column 2 groundwater then dropped to 1.34×10^4 bacteria ml^{-1} when sampled at ~800 hours. The mean number of bacteria in the waters collected from both columns then increased towards the end of the experiment; in Column 1 from 1.26×10^5 to 1.41×10^6 bacteria ml^{-1} between ~1350 and ~1500 hours and in Column 2 from 4.17×10^5 to 2.59×10^6 bacteria ml^{-1} between ~1500 and ~1550 hours. At the end of the experiment the total numbers of bacteria in waters from both columns were similar, 9.42×10^4 bacteria ml^{-1} in Column 1 and 2.36×10^4 bacteria ml^{-1} in Column 2.

Table 2 Mean total bacterial counts by epifluorescence microscopy of water samples collected after flowing through Column 1 and Column 2

Time since injection (h)	Column 1 Bacteria ml^{-1}	Standard error	Column 2 Bacteria ml^{-1}	Standard error
0	3.04×10^5	2.60×10^4	3.04×10^5	2.60×10^4
117	1.88×10^6	3.72×10^5	1.12×10^6	3.96 x 104
312	9.50×10^5	5.36×10^4	9.90×10^5	6.27×10^4
336	1.85×10^6	5.34×10^5	2.05×10^6	1.76×10^5
456	1.34×10^6	7.50×10^4	3.38×10^5	5.10×10^4
530	9.66×10^5	5.79×10^4	1.11×10^6	3.87×10^5
675	1.30×10^6	5.06×10^5	8.33×10^5	2.90×10^4
794	6.36×10^5	4.41×10^4	1.34×10^4	1.15×10^5
866	8.80×10^5	4.30×10^4	8.64×10^5	3.85×10^4
986	2.28×10^5	2.89×10^4	6.68×10^4	5.56×10^3
1156	6.13×10^5	1.73×10^4	6.28×10^4	1.01×10^4
1345	1.26×10^5	1.66×10^4	2.98×10^5	5.36×10^4
1469	1.41×10^6	1.56×10^5	4.17×10^5	3.23×10^4
1561	4.63×10^6	4.89×10^5	2.59×10^6	8.11×10^5
1805	2.20×10^5	3.91×10^4	2.38×10^6	1.01×10^5
1971	9.42×10^4	1.69×10^4	2.36×10^4	4.97×10^3

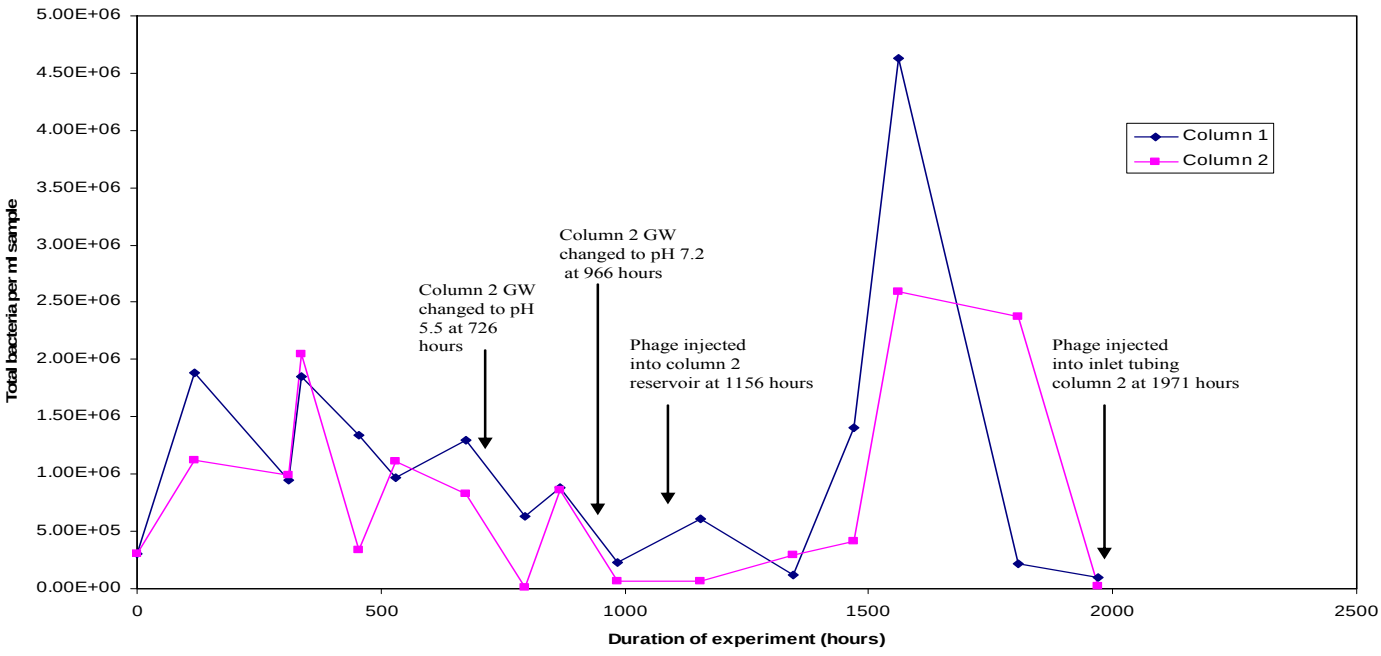

Figure 8 Mean total bacterial mean counts by epifluorescence Microscopy from the water samples collected after flowing through Column 1 and Column 2.

On completion of the column experiments, samples were taken from along the length of both columns to determine the bacterial distribution. These samples were removed from the exposed diorite following the longitudinal slicing of the columns detailed in Section 4.3.5. Samples were taken from the centre and edge of the exposed surface, along the length of the column using a sterile spatula and preserved in fixative. The weight of the preserved sample was calculated in order to determine an accurate number of bacteria per gram of sample once the count had been made. The results are shown in Table 3. Figure 9 shows the total counts from Column 1 at the end of the experiment and Figure 10 shows the total counts from Column 2. Plate 17 shows an epifluorescence image of bacteria from the diorite sample taken from the inlet end of Column 1.

Table 3 Results of the total count of bacteria by epifluorescence microscopy of Column 1 and Column 2 at the end of the flow experiment

Column 1				Column 2			
mm from inlet	Sample position in column	Bacteria g^{-1}	Standard error	mm from inlet	Sample position in column	Bacteria g^{-1}	Standard error
0-10	Centre	1.65×10^{6}	1.07×10^{5}	0 -10	Centre	1.59×10^{6}	9.22×10^{4}
0-10	Edge	3.06×10^{5}	2.52×10^{4}	0 -10	Edge	2.75×10^{5}	4.61×10^{4}
20-30	Centre	1.05×10^{6}	5.40×10^{4}	20-30	Centre	4.09×10^{5}	3.07×10^{4}
20-30	Edge	5.44×10^{5}	2.96×10^{4}	20-30	Edge	1.43×10^{6}	7.96×10^{4}
50-60	Centre	1.94×10^{5}	1.81×10^{4}	50-60	Centre	1.44×10^{5}	3.62×10^{4}
50-60	Edge	2.35×10^{5}	2.16×10^{4}	50-60	Edge	3.40×10^{5}	4.24×10^{4}
70-80	Centre	3.79×10^{5}	2.93×10^{4}	70-80	Centre	8.99×10^{4}	3.04×10^{4}
70-80	Edge	5.40×10^{5}	4.79×10^{4}	70-80	Edge	5.30×10^{5}	2.81×10^{4}
100-110	Centre	6.61×10^{4}	1.37×10^{4}	100-110	Centre	6.06×10^{5}	2.75×10^{4}
100-110	Edge	1.04×10^{5}	1.50×10^{4}	100-110	Edge	3.94×10^{5}	2.29×10^{4}
140-150	Centre	4.10×10^{4}	1.00×10^{4}	140-150	Centre	6.36×10^{5}	4.44×10^{4}
140-150	Edge	4.52×10^{4}	9.91×10^{3}	140-150	Edge	2.13×10^{5}	2.30×10^{4}
180-190	Centre	1.38×10^{4}	5.34×10^{3}	180-190	Centre	6.36×10^{5}	5.92×10^{4}
180-190	Edge	7.54×10^{4}	1.18×10^{4}	180-190	Edge	5.75×10^{5}	3.46×10^{4}
210-220	Centre	8.95×10^{3}	3.65×10^{3}	210-220	Centre	8.96×10^{4}	1.20×10^{4}
210-220	Edge	1.18×10^{4}	4.37×10^{3}	210-220	Edge	1.13×10^{5}	1.21×10^{4}

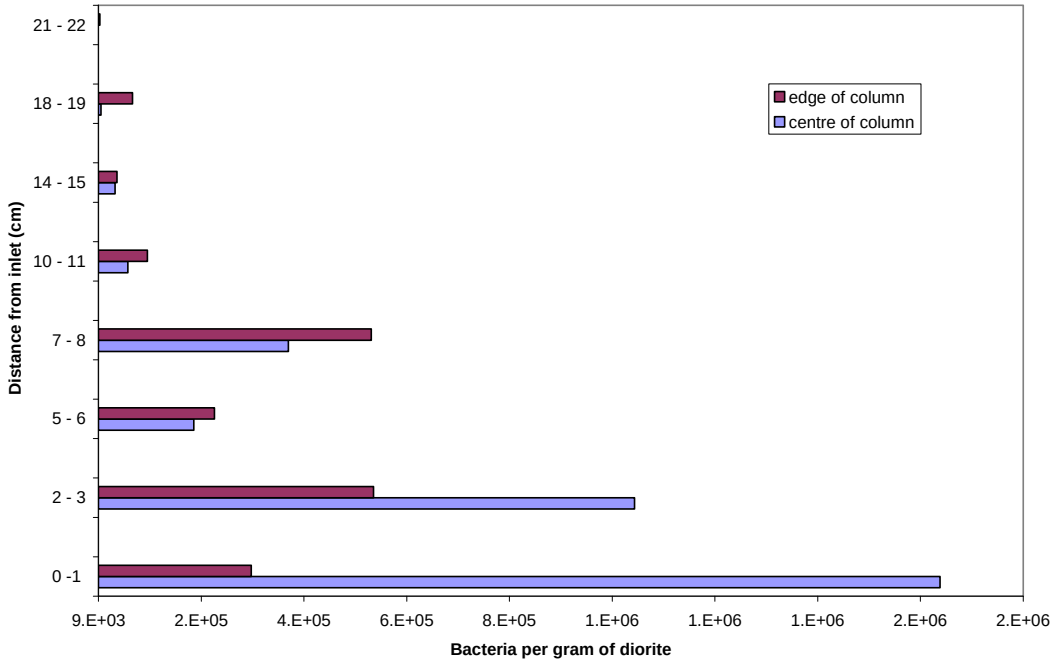

Figure 9 Total bacterial mean counts from Column 1 at end of the experiment

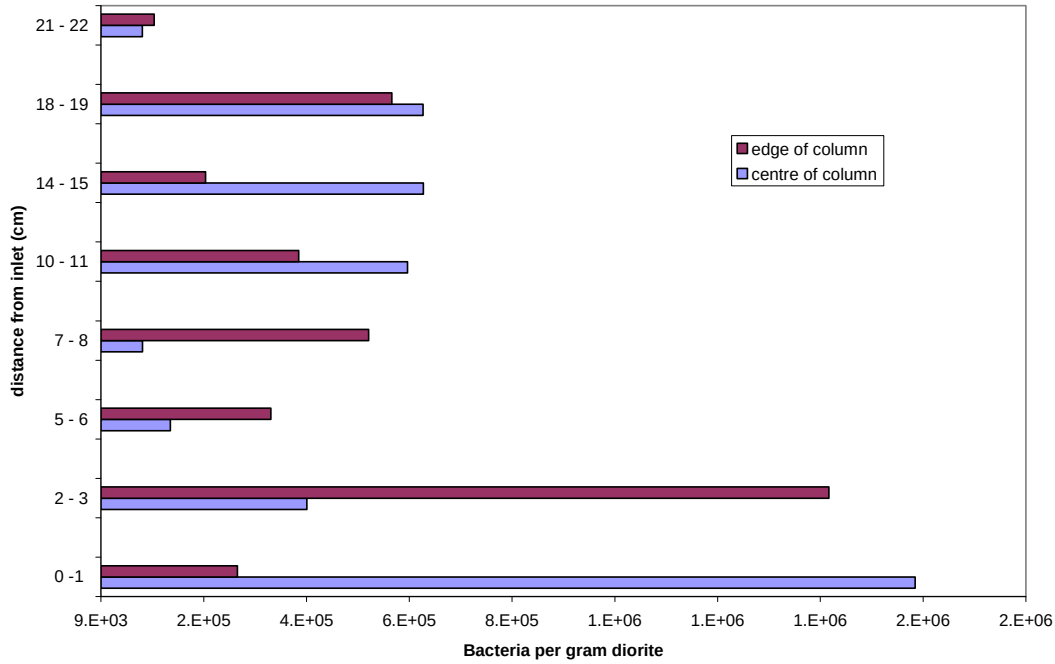

Figure 10 Total bacterial mean counts from Column 2 at end of the experiment

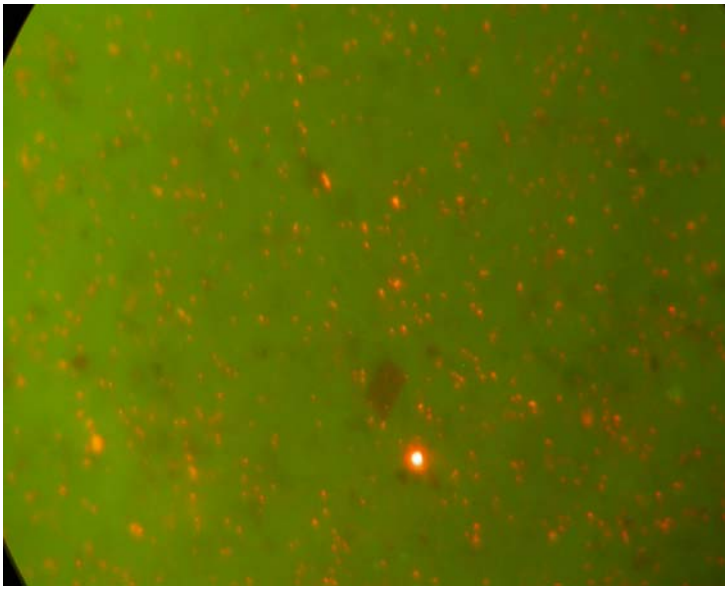

Plate 17 Epifluorescence Microscopy image of *P. aeruginosa* bacteria taken from a diorite sample from Column 1 at the 0 – 1cm inlet position (400x magnification) Image shows bacterial cells stained with Acridine Orange.

In Column 1 the distribution of bacteria determined by epifluorescence microscopy shows the greatest mean number of bacteria, 1.65 x 10^6 bacteria g^{-1}, to be present at the centre of the column at the inlet position between 0-10 mm. This number decreases to a mean of 1.94 x 10^5 bacteria g^{-1} at 50 mm before a slight increase to 3.79 x 10^6 bacteria g^{-1} at 70-80 mm. The number then steadily decreases to a mean of 8.95 x 10^3 bacteria g^{-1} at the outlet position of 210-220mm. In the samples taken from the edge of the column the greatest mean number, 5.44 x 10^5 bacteria g^{-1}, occurs at 20-30 mm with a similar number at 70-80 mm. Numbers then decrease to a mean of 1.18 x 10^4 bacteria g^{-1} at 200-220 mm.

In Column 2, the distribution of bacteria is similar to that in Column 1 in that the greatest mean number, 1.59 x 10^6 bacteria g^{-1}, were present at the centre of the column at the inlet position of 0-10 mm. This mean number reduces to 4.09 x 10^5 bacteria g^{-1} at 20-30 mm before increasing to 6.06 x 10^5 bacteria g^{-1} at 100 -110 mm. From 100-190 mm, numbers remain fairly constant before reducing to 8.96 x 10^4 bacteria g^{-1} at the outlet. In the samples taken from the edge of Column 2 the greatest number, 1.42 x 10^6 bacteria g^{-1}, occurs at 20-30 mm. Between 50 mm and 210 mm, numbers remain at ~10^5 bacteria g^{-1} with the lowest number, 1.13 x 10^5 bacteria g^{-1}, occurring at the outlet position of 210-220 mm.

The distribution profiles of bacteria show differences between the columns (Figure 9 and Figure 10). In Column 1 the maximum number of bacteria occurs at the position closest to the inlet between 0 and 30 mm. In Column 2 the maximum number of bacteria also occurs between 0 and 30 mm. However, higher numbers are found at the edge at 20-30 mm than in the central position. In Column 1, bacteria appear to be concentrated in the first 80 mm of the column with a gradual reduction in numbers towards the outlet.

The image shown in Plate 18 was captured using a microscope-mounted digital camera at 400X magnification (10X eye, 40X lens) without oil immersion. The bacterial cells shown were isolated from inoculated groundwater and stained using the Acridine Orange epifluorescence staining method.

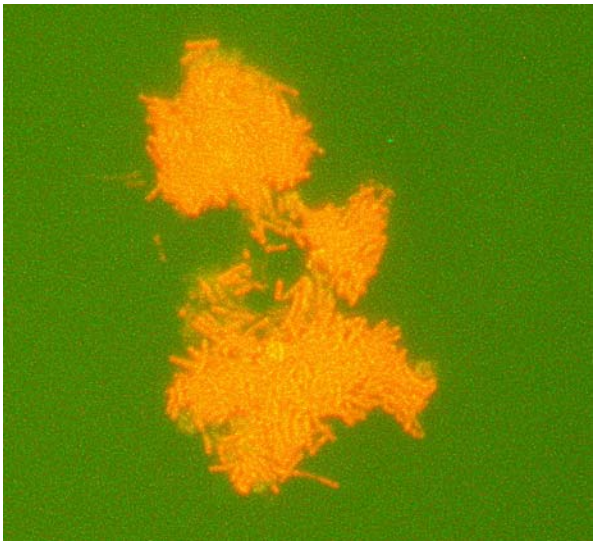

Plate 18 Isolate of clumps of *P. aeruginosa* bacteria from the groundwater reservoir stained with Acridine Orange under 400X magnification

4.3.4 Fluid chemistry

Appendix 2 lists the fluid analytical data for both columns. On initial inspection of the data there appeared to be some changes with time for both columns but only minor differences between the data for the 2 columns in terms of the chemistry of the reacted fluids. However, examination of the data for chloride, which was expected to be a conservative element, shows an apparent increase in concentration approximately 700 hours after the experiment started. This corresponds with the flow rates in both columns dropping to below 0.1 ml min^{-1} and it is thought likely that the increase is due to evaporation of the fluid sample during collection (typical sample interval was around 100 hours). If the data is normalised with respect to [Cl^-] then the chemistry of the reacted fluids (within analytical error) are almost identical to that of the starting fluids with no observed significant changes in concentrations. No significant changes in outflow fluid chemistry were observed with the change in input fluid pH (from pH = 7.20 to 5.52), nor were any changes noted during the addition of phage to the columns.

4.3.5 Mineralogical analysis

Following cessation of the column experiments, the columns were flushed with Acridine Orange solution to stain for the presence of any biofilm and bacteria in the columns.

4.3.5.1 VISUAL OBSERVATION AND SAMPLING THE COLUMN EXPERIMENTS

The columns were longitudinally sliced open by cutting lengthwise through the glass wall of the column using a small hand-held diamond modelling saw (Plate 19). The column was sliced in half by drawing a bronze cheese wire along the length of the column, through the cut glass walls (Plate 20).

The cut surfaces of Column 1 and Column 2 were photographed in normal visible light and under ultraviolet (UV) illumination (Plate 21 and Plate 22). Sub-samples for petrographical analysis by scanning electron microscopy (SEM) were cut by scalpel from one half of the moist crushed granodiorite filling the column, and were prepared as described in Section 2.10. The positions of "A" (cryogenic SEM) and "B" (freeze dried) samples are shown in Plate 21 and Plate 22. Details of the sub-samples are given in Table 4.

Plate 19 Cutting the glass BioTran Column 1 longitudinally using diamond saw, with dust controlled via a portable dust extraction unit.

Plate 20 Crushed diorite fill within Column 1 was sliced longitudinally by drawing a bronze cheese wire though the cut walls of the column to produce two halves.

Column 1

Under UV light Column 1 displayed the distribution of red-fluorescent Acridine Orange within the crushed granodiorite fill, extending from the inlet of the column to 75mm from the inlet. There was a transition region ("interface region") about 10mm wide beyond which no Acridine Orange stain was observed (Plate 21). Staining by Acridine Orange could also be seen in visible light but was less obvious than under UV light. The Acridine Orange stain distribution would suggest that the biofilm development and bacterial presence is limited to within the 75-85mm of the inlet of the column. Samples were taken for SEM analysis along the length of column as shown in Plate 21.

Table 4 Summary of SEM sample information from BioTran Column 1 and Column 2.

Sample number	Distance from inlet (mm)	Sample designation		
		cryoSEM	Freeze dried	Solvent dried
Column 1				
1A	0-15	●		
2A	15-30	●		
3A	60-75	●		
4A	75-90	●		
5A	90-105	●		
6A	135-150	●		
7A	200-215	●		
1B	0-15		●	
2B	15-30		●	
3B	60-75		●	
4B	75-90		●	
5B	90-105		●	
6B	135-150		●	
7B	200-215		●	
1C	40-50			●
2C	90-100			●
3C	160-170			●
Column 2				
1A	0-15	●		
2A	15-30	●		
3A	60-90	●		
4A	195-210	●		
1B	0-15		●	
2B	15-30		●	
3B	60-90		●	
4B	195-210		●	
1C	35-40			●
2C	40-50			●
3C	65-80			●
4C	110-120			●
5C	170-180			●

Column 2

Under UV light Column 2 displayed the distribution of red-fluorescent Acridine Orange within the crushed granodiorite fill, extending from the inlet of the column up to 90 mm from the inlet. However, unlike Column 1, the interface between the unstained granodiorite and the Acridine Orange stained material was uneven in distribution, with preferential fingering of Acridine Orange along one side of the column (Plate 22). The Acridine Orange stain fluoresce largely red

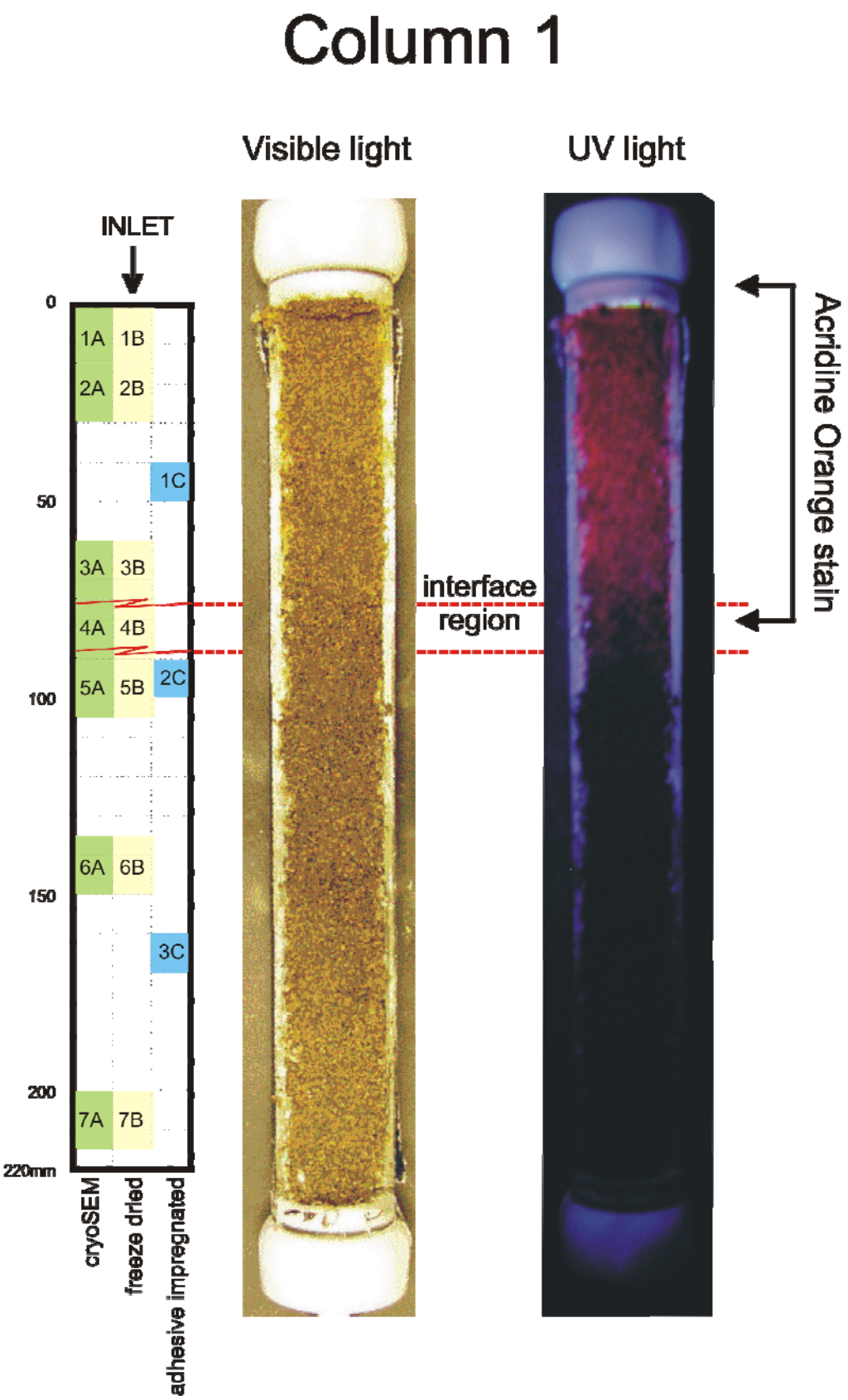

Plate 21 Summary schematic of Column 1 showing the location of samples examined for petrographical analysis, and comparative photographs of the opened column under visible and UV light

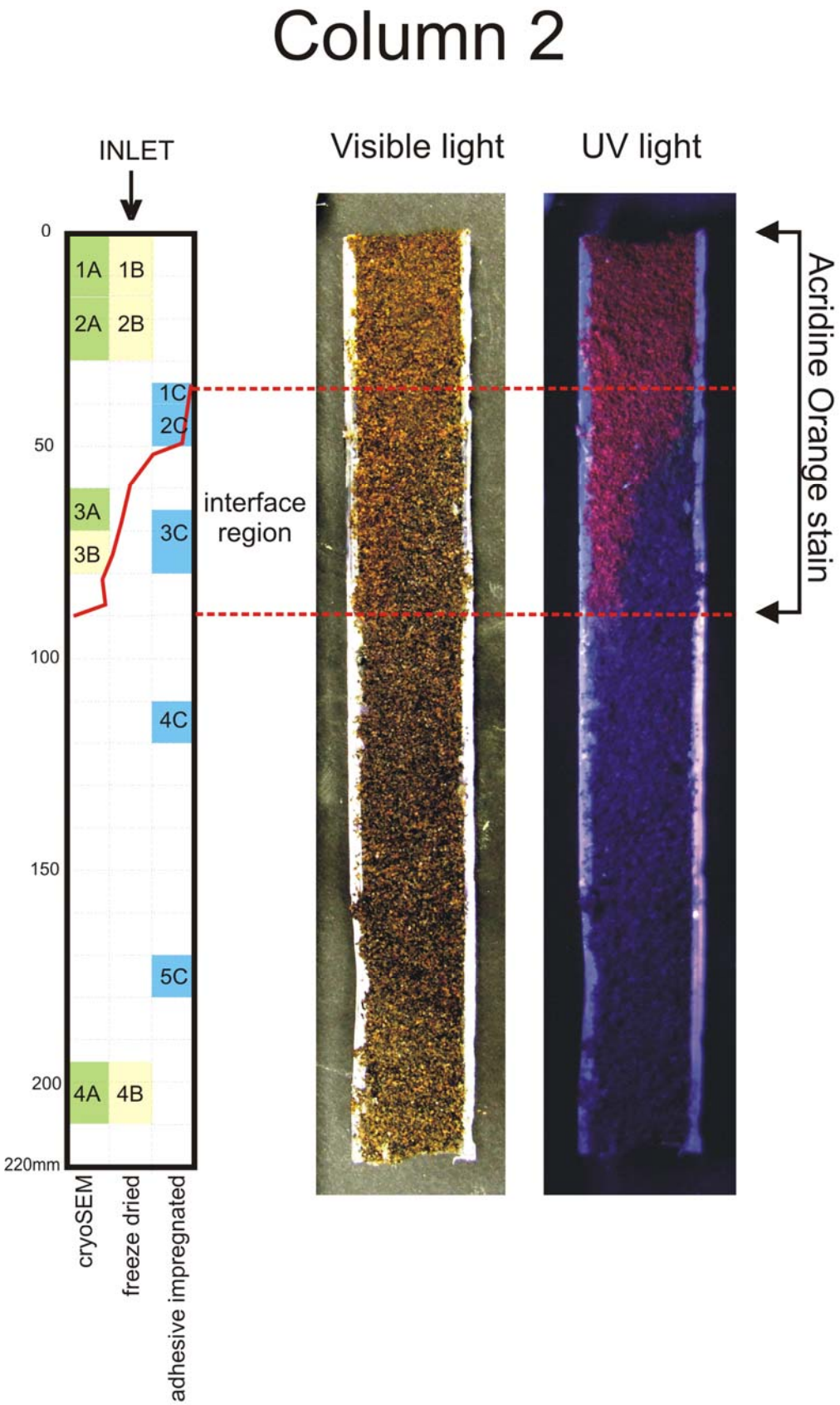

Plate 22 Summary schematic of Column 2 showing the location of samples examined for petrographical analysis, and comparative photographs of the opened column under visible and UV light

over this region but at the leading edge of the stain a thin, discontinuous, green fluorescent "front" up to 1 mm wide was observed under UV light.

As in Column 1, the Acridine Orange stain distribution would suggest that the biofilm development and bacterial presence is limited to within 90 mm of the inlet of the column. Samples were taken for SEM analysis along the length of column as shown in Plate 22.

4.3.5.2 OBSERVATIONS

Column 1 experiment

CryoSEM samples

Column 1 material was initially examined by cryoSEM. Although seven sub-samples were collected and preserved for cryoSEM (samples 1A to 7A, (Plate 21) only samples 1A and 2A from within the region of the column (close to the inlet) stained by the UV-fluorescent Acridine Orange were observed, because of the limited time available for analysis.

Despite attempted rapid pre-freezing of small sub-samples in a melting mixture of liquid nitrogen and solid nitrogen slush, it was apparent that cooling was still too slow within the "core region" of each sample, such that relatively large ice crystals had still formed which caused microstructural distortion of fabric. The effect of ice crystal growth within the intergranular pore spaces was to "push" any dispersed material within the pores towards the edges of the growing ice crystals, effectively "squeezing" and concentrating this material along the grain boundaries between adjacent ice crystals (Plate 23). The reason for this is that the sample size used was probably too large to facilitate rapid cooling of the interior of the samples. We believe that in future, smaller (i.e. <5mm) samples would probably give faster freezing behaviour and better sample preparation results.

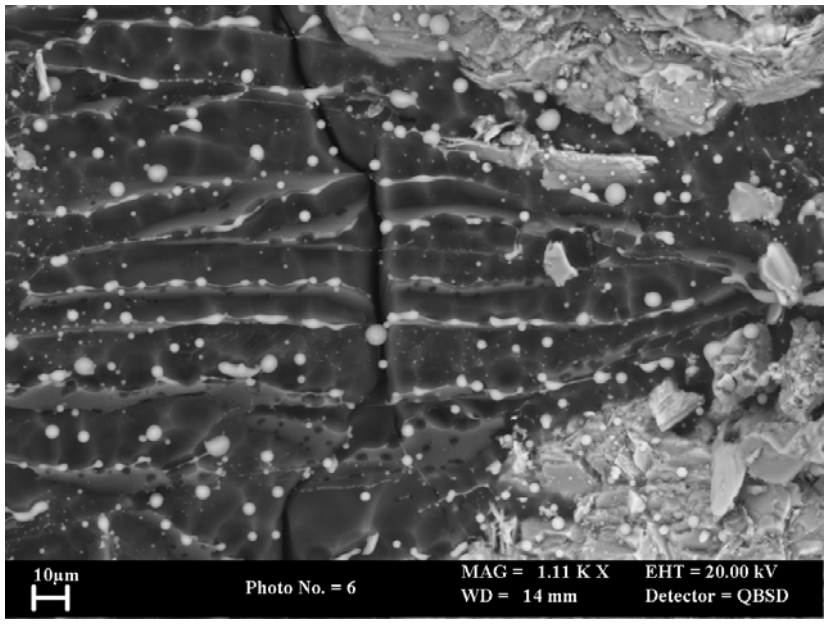

Plate 23 CryoSEM image (SEI) showing concentrations of droplets of organic emulsion (bright) along the grain boundaries of elongated ice crystals (dark) formed within an intergranular region in crushed granodiorite. The ice crystals have forced the grains apart as they grew during freezing. Column 1, sample 1A.

Although freezing of the samples was problematic, the cryoSEM observations revealed the presence of abundant fine 'liquid droplets' distributed throughout the intergranular regions (filled by frozen porewater. The droplets were concentrated along the ice crystal boundaries as a result of displacive ice crystal growth (Plate 23 and Plate 24). The droplets were revealed as ice was ablated (sublimed) from the surface during warming the sample to -80 °C, and were observed to be readily vaporised under the electron beam. EDXA indicates that the droplets are organic (only C and O detected) and clearly were immiscible with the porewater in the sample. These appear to represent emulsion droplets of a non-aqueous organic phase that are closely associated with organic biofilaments and meshworks that bridge the intergranular pore region (Plate 24, Plate 25, Plate 26 and Plate 27). The emulsion droplets appear to adhere to, or nucleate on, the biofilaments (Plate 24, Plate 25, Plate 26 and Plate 27).

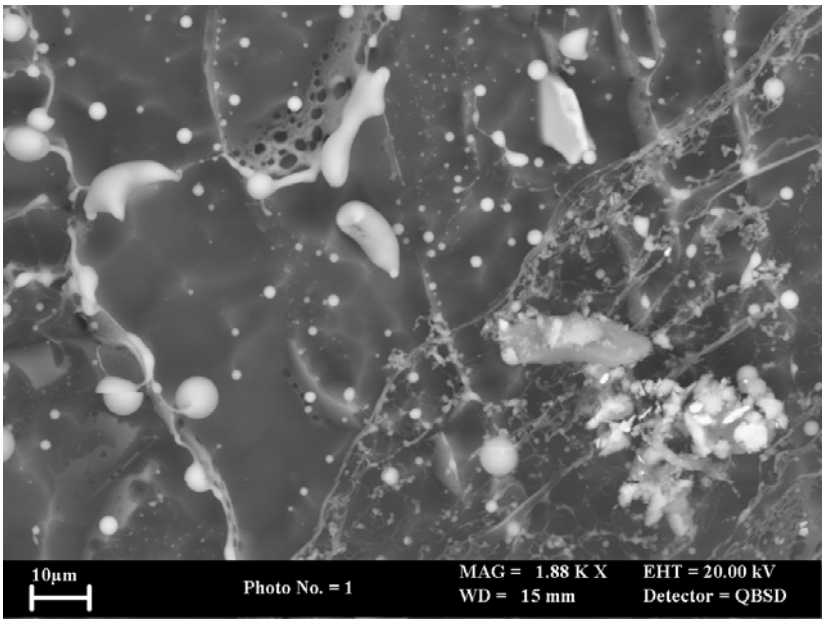

Plate 24 CryoSEM image (SEI) showing detail of the organic emulsion droplets (water-immiscible liquid) distributed throughout the porewater (ice) but concentrated along the grain boundaries of ice crystals (dark background). The droplets are closely associated with filaments and meshworks of organic (?biofilm) material that have also been displaced to the ice crystal grain boundaries in the frozen sample. Column 1, sample 1A.

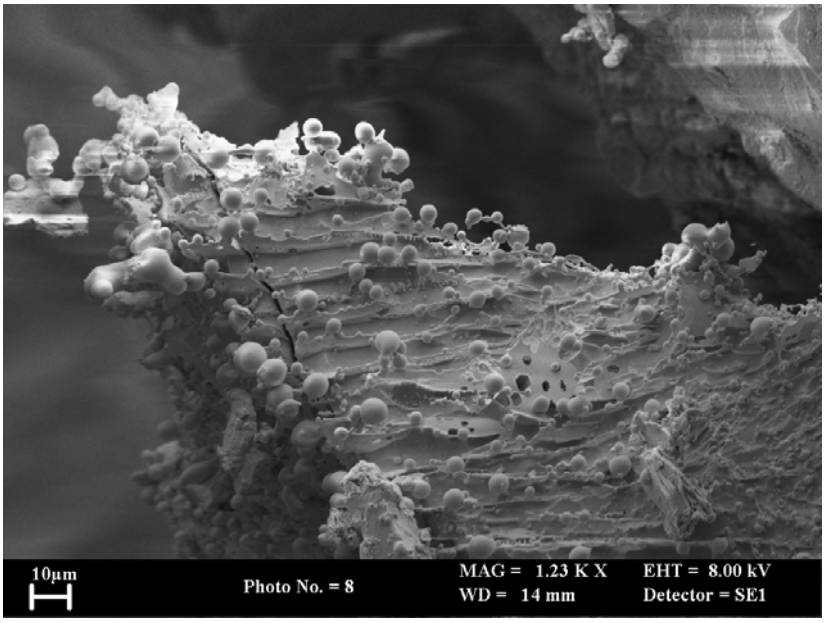

Plate 25 CryoSEM image (SEI) showing detail of the organic emulsion droplets attached to the biofilaments and organic meshwork (?biofilm) material that have also been displaced to the ice crystal grain boundaries in the frozen sample. Column 1, sample 1A.

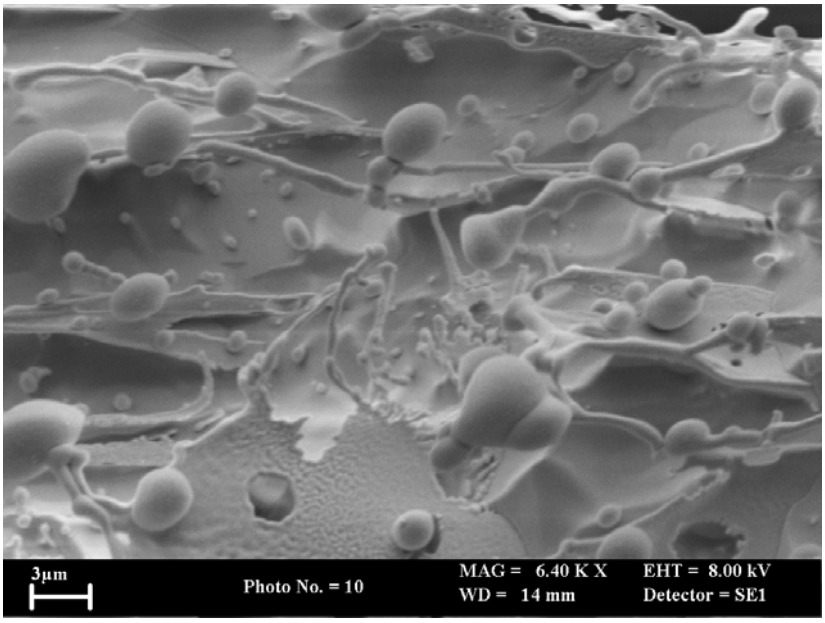

Plate 26 CryoSEM image (SEI) showing detail of the organic emulsion droplets attached to, or nucleated on, the biofilaments. Column 1, sample 1A.

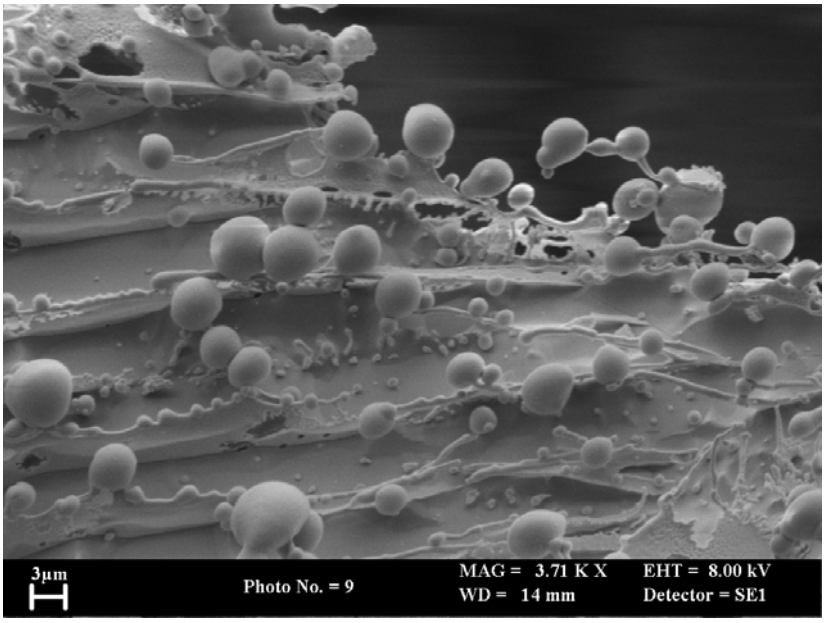

Plate 27 CryoSEM image (SEI) showing detail of the organic emulsion droplets attached to, or nucleated on, the biofilaments. Column 1, sample 1A.

Close examination showed that mineral grain surfaces were coated with a very thin film of organic material (Plate 28). Impressions in the surface of the film appear to indicate that emulsion droplets may be trapped beneath this film (Plate 28). This may represent biofilm that has collapsed onto the grain surface as a result of sample preparation and drying during cryoSEM.. Organic filaments were also occasionally observed to be preserved as pore-bridging structures (Plate 29). Unfortunately, these are rare and it would appear that the sample freezing preparation for cryoSEM may have disrupted and destroyed most of these structures. Locally fine mineral particles were seen to have been concentrated within constricted pore throats, where they were trapped on biofilaments and meshworks bridging the pore throats (Plate 30). Both the organic film and the filaments were very sensitive to damage from the electron beam during SEM analysis.

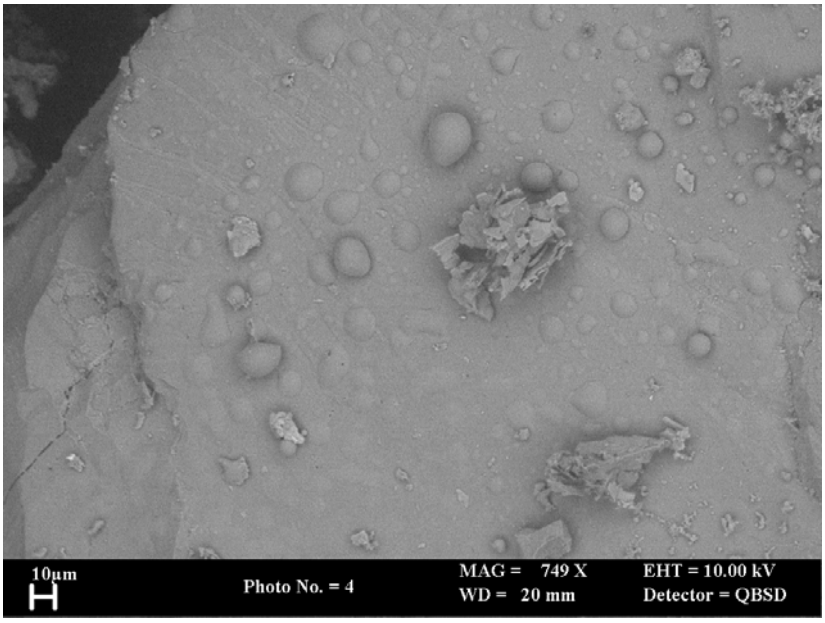

Plate 28 CryoSEM image (SEI) showing quartz grain surface after complete ablation of ice during cryoSEM analysis. The surface of the grain is coated with a thin organic film beneath which droplets of emulsion appear to be trapped. Column 1, sample 2A.

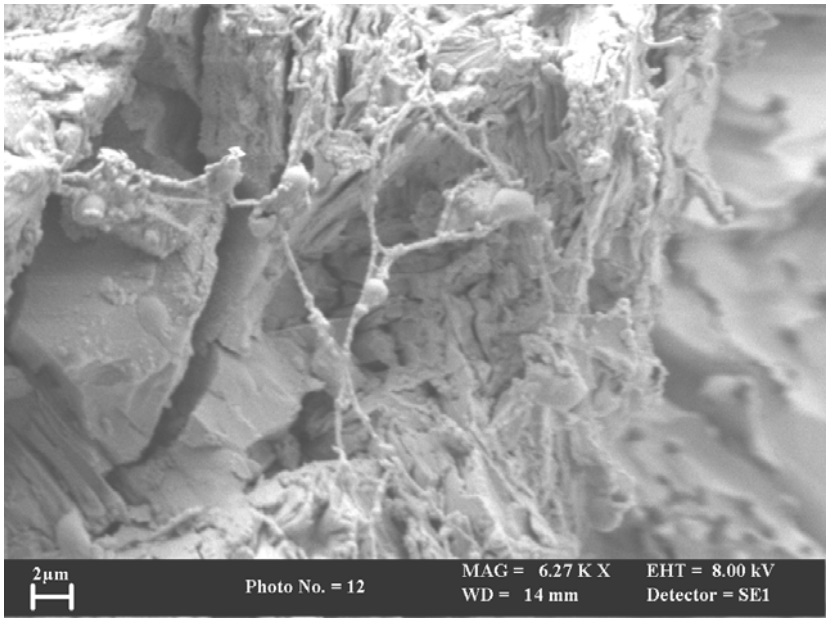

Plate 29 CryoSEM image (SEI) of intergranular pore after complete removal of ice during cryoSEM analysis. Strands of organic filaments (with rare attached oily droplets) cross the pore throat. Column 1, sample 2A.

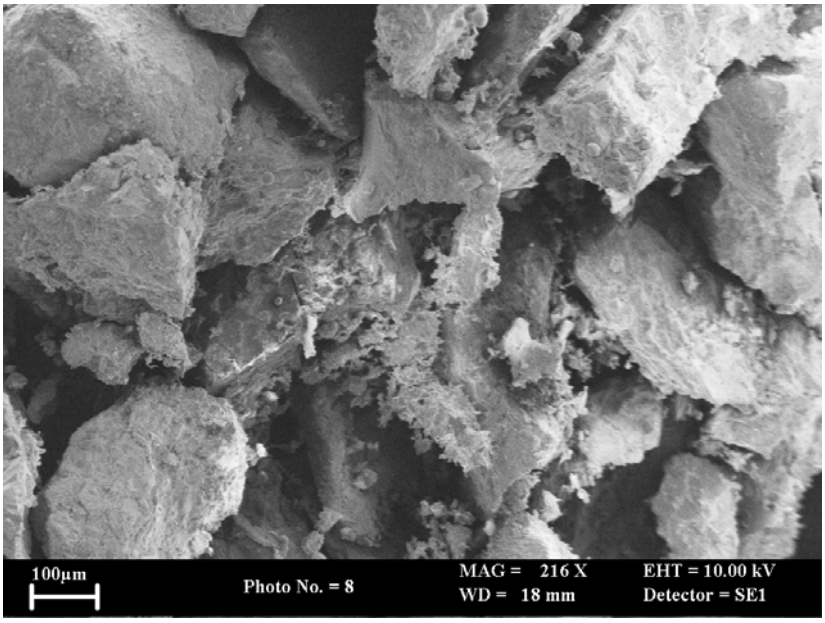

Plate 30 CryoSEM image (SEI) of intergranular pore after complete removal of ice during cryoSEM analysis. Fine mineral debris is trapped on pore-bridging biofilm, blocking or reducing the pore throat aperture. Column 1, sample 2A.

Freeze-dried samples

All freeze-dried samples from Column 1 (samples 1B to 7B, Plate 21) were examined by SEM. In contrast to cryoSEM, the samples completely disaggregated on freeze drying and consequently, intact material could not be examined. Very little evidence of biofilm was observed and would appear that most of the structure was destroyed by the sample preparation. Rare traces of single biofilaments were preserved locally on grain surfaces (Plate 31). Many of the filaments appear broken and have probably collapsed onto the grain surface during the drying

process (c.f. damage to filamentous fabrics caused by sample drying described by McHardy *et al.*, 1982). These were only observed within the Acridine Orange stained region.

Some mineral surfaces were found to be coated by a microcrystalline precipitate of potassium phosphate consisting of aggregates of platy crystallites (Plate 32). Although crystalline potassium phosphate was relatively uncommon, structureless films of this material were observed on mineral grains along the whole length of the column. Since very little phosphate was introduced in the experimental fluid and there is no evidence of alteration of the traces of primary apatite in the crushed diorite, it is unlikely that the potassium phosphate phase formed

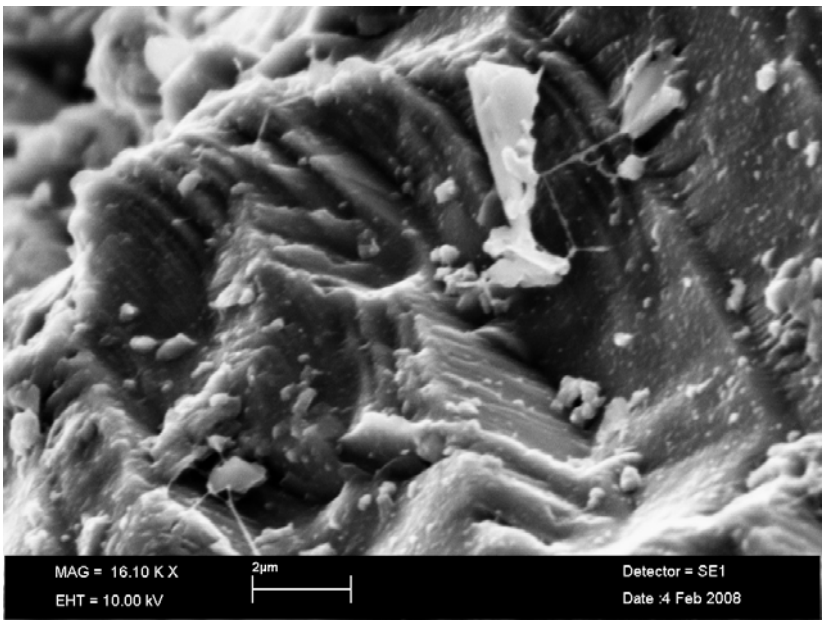

Plate 31 SEI photomicrograph showing poorly-preserved organic filaments resting on the surface of a plagioclase grain. Column 1, sample 3B.

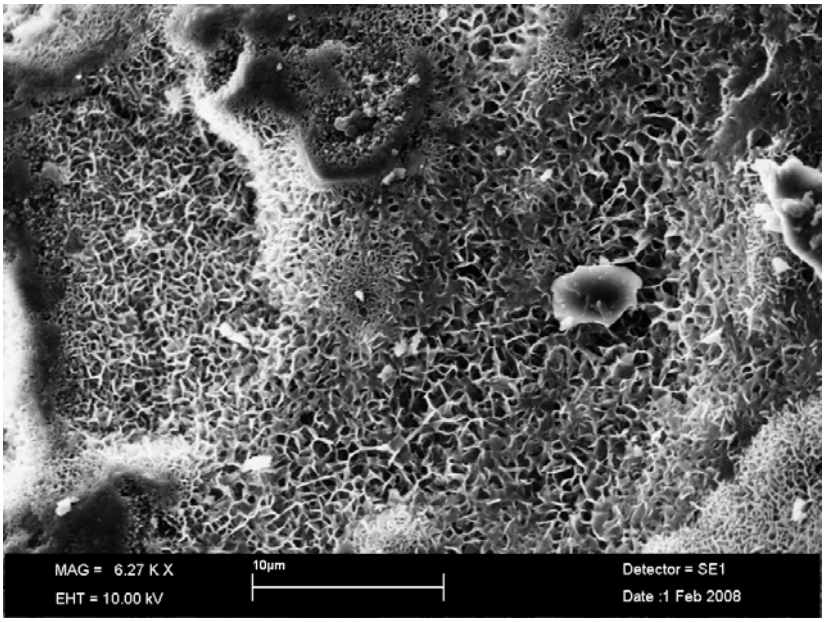

Plate 32 SEI photomicrograph showing potassium phosphate crystallites precipitated on plagioclase grain. Column 1, sample 1B.

during the experiment. It is most likely to be an artefact of the post-experimental treatment of the column with Acridine Orange staining solution, which included a significant concentration of potassium phosphate as a buffer. Drying of residual amounts of this staining solution during SEM sample preparation would account for the observed potassium phosphate precipitate.

Solvent-replacement – polystyrene-impregnated samples

This sample preparation technique produced a coherent sample that remained intact without disaggregation during analysis in the SEM instrument. The grains were bonded together by the polystyrene cement within the bulk of the sample while a sufficient area of the upper surface of the sample remained free of any contamination of polystyrene cement (Plate 33).

SEM analysis revealed within the samples close to the inlet the blocking of pores by fine grain mineral debris (Plate 34). The particles appear to be bonded together by a very fine structureless organic film (Plate 35), which may represent biofilm material. This pore blockage by organically-bound fine mineral particulate may partially account for the reduction in permeability that was observed during the course of the experiment.

Close examination of the grain surfaces revealed the occasional presence of patches of a gelatinous meshwork of organic material (Plate 36). These were observed in samples taken along the entire length of the column. EDXA revealed the presence of significant oxygen, potassium and phosphorus within this material (Figure 11), which implied that the organic material was stained by the Acridine Orange staining solution (which contained potassium phosphate). In contrast, only carbon was detected by EDXA in the polystyrene cement, showing that these "filaments" are not simply the result of contamination from the polystyrene adhesive solution used in sample preparation. Unlike the very fine and delicate biofilaments observed in cryoSEM or freeze-dried samples, the morphology of this "organic" material was different and was found in samples along the whole length of the column and not just near the "inlet" end of the column. It is possible that this gelatinous material represent residual Acridine Orange stain that has been remobilised and redistributed by the solvents (acetone and amyl acetate) used in the preparation of these particular SEM specimens.

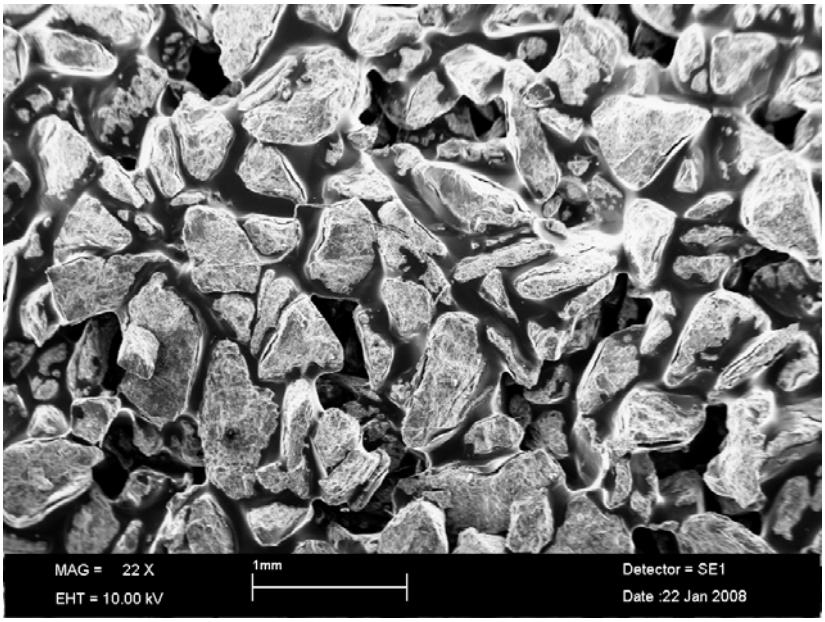

Plate 33 SEI photomicrograph showing an impregnation of intergranular porosity by polystyrene cement. Upper surfaces of the grains are uncontaminated by the glue. Column 1, sample 3C.

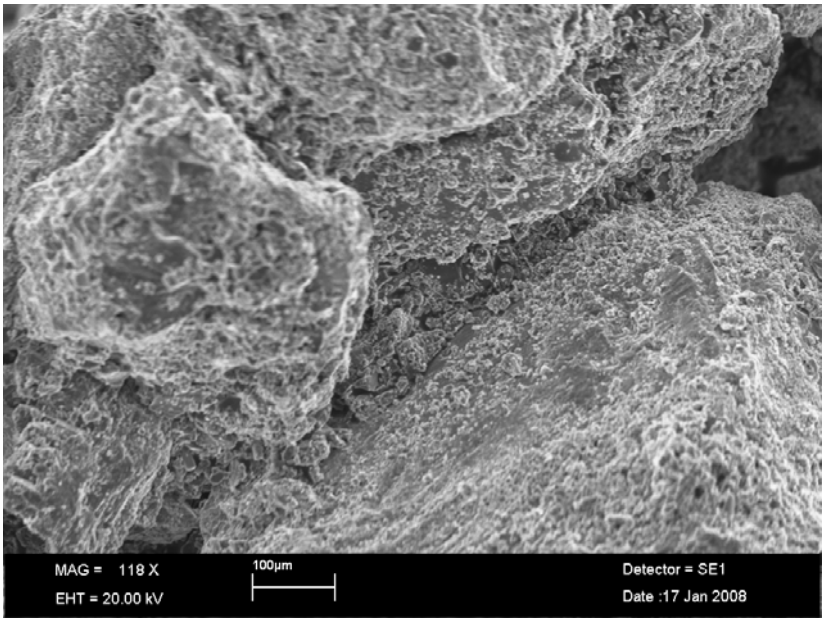

Plate 34 SEI photomicrograph showing the blocking of pore spaces by accumulated mineral fines. Column 1, sample 1C.

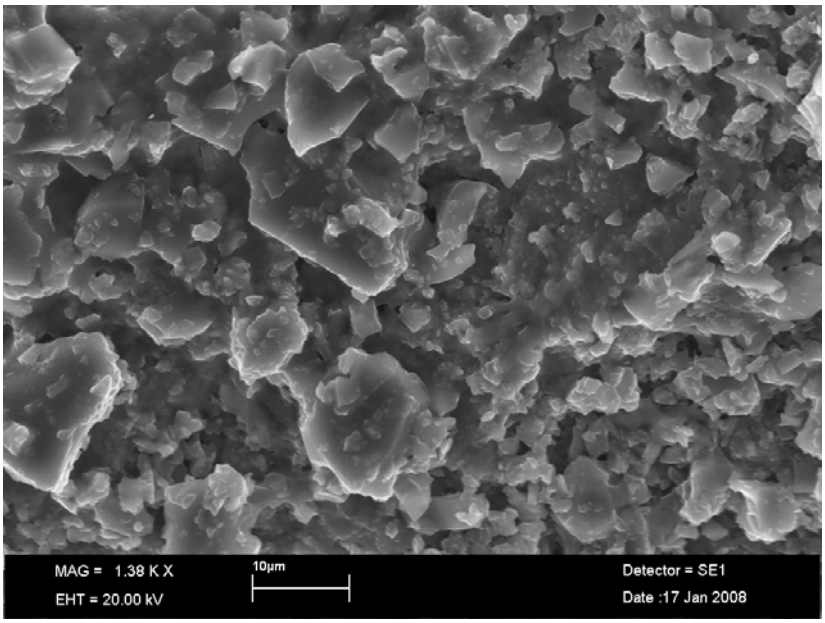

Plate 35 SEI photomicrograph showing mineral fines bonded by a gelatinous organic film.

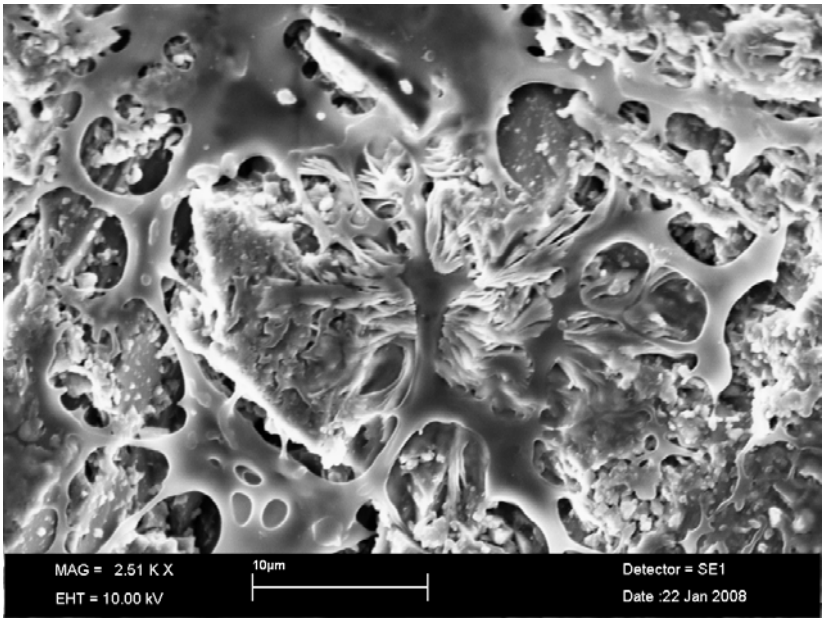

Plate 36 SEI photomicrograph showing a web of gelatinous organic filaments collapsed onto a mineral grain surface. In the centre of the image a dendritic precipitate of potassium phosphate can be seen. Column 1, sample 3C.

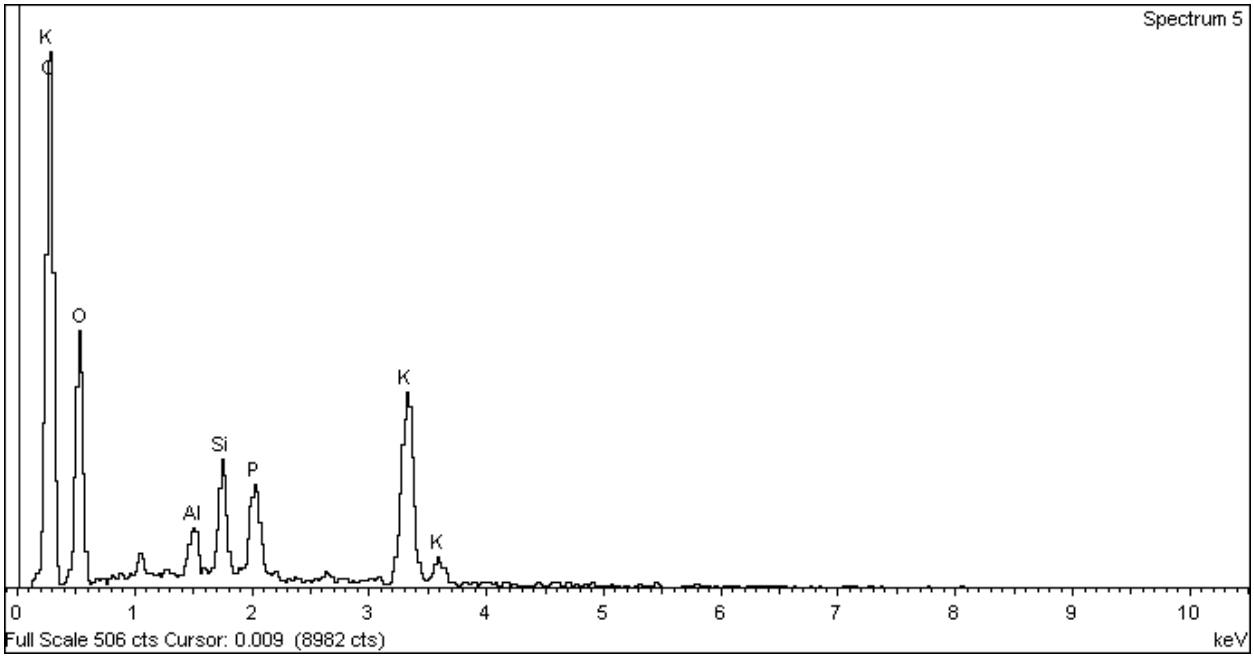

Figure 11 EDXA spectrum of gelatinous organic meshwork, showing it is carbon-rich but contains potassium phosphate (probably from the Acridine Orange staining solution). Column 1, sample 3C.

A potassium phosphate precipitate was also observed on the grain surfaces of all samples along the length of the column. Its morphology was distinctly different to the encrustations seen in the freeze-dried samples (Section 0), and in these samples the potassium phosphate occurred as radial-stellate or dendritic fibrous growths (Plate 37) that also contained a significant amount of carbon (Figure 12). Again, the source of this potassium phosphate is most probably from the Acridine Orange staining solution. However, the different growth morphology of the phosphate precipitate in these samples may be related to the different sample preparation technique used.

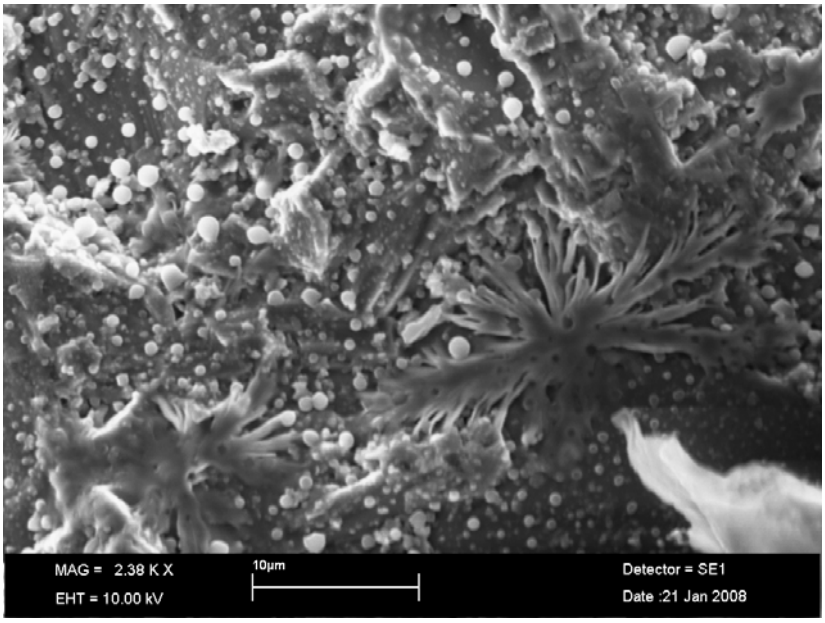

Plate 37 SEI photomicrograph showing the development of a dendritic precipitate of potassium phosphate and droplets of waxy or oily organic material on grain surfaces. Column 1, sample 2C.

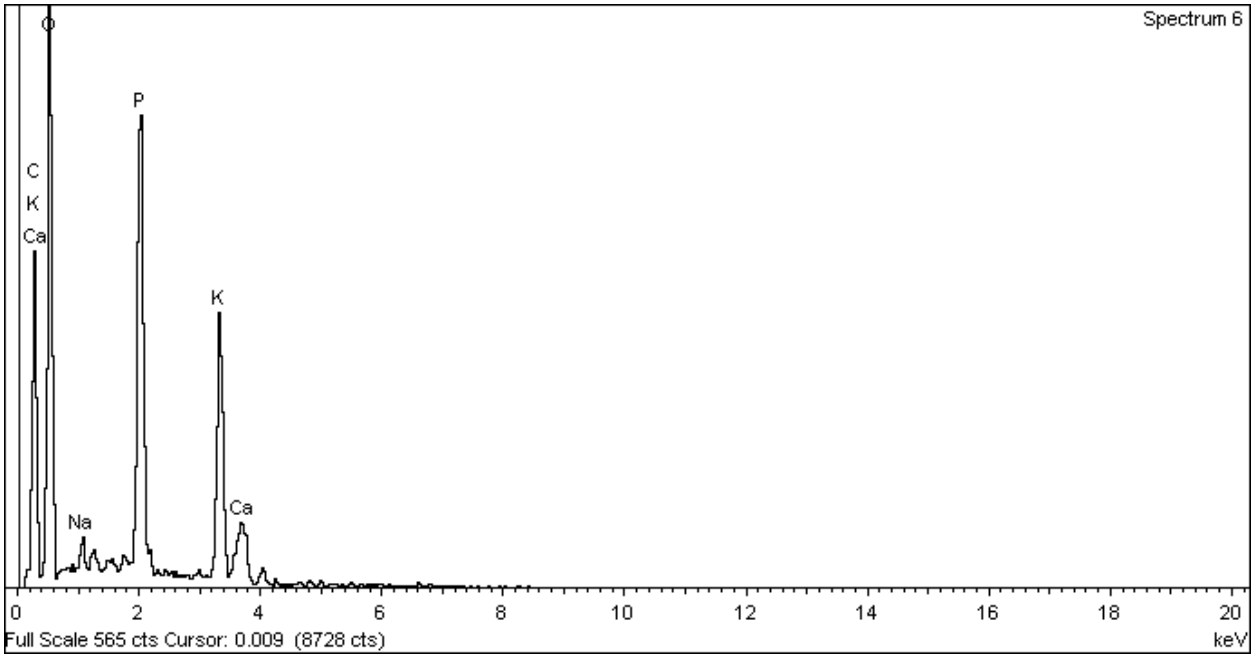

Figure 12 EDXA spectrum of dendritic potassium phosphate precipitate (albite substrate subtracted). Column 1, sample 3C.

As in the cryoSEM and freeze-dried samples, droplets of a waxy or oily material were observed on grain surfaces. However, in samples prepared by the use of solvent-replacement and polystyrene impregnation, droplets were observed in samples from along the whole length of the column. EDXA shows that these contain potassium phosphate from the Acridine Orange staining solution. It would appear that maybe this sample preparation technique, using organic solvents, has resulted in remobilisation of some of the biopolymer material, or that these droplets also represent remobilised and redistributed Acridine Orange stain material.

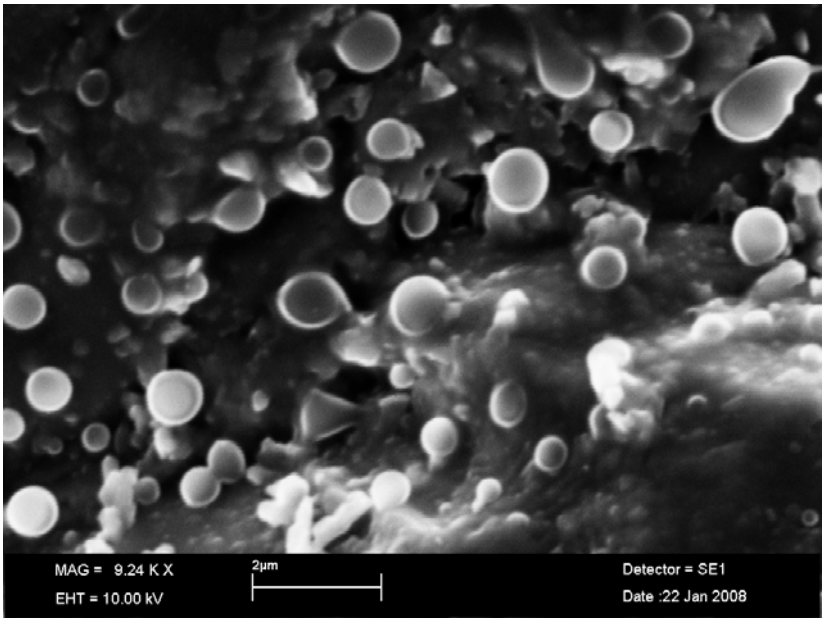

Plate 38 SEI photomicrograph showing detail of oily globules (?emulsion droplets) within a thin organic film on the surface of a quartz grain. Column 1, sample 3C.

Column 2 experiment

CryoSEM samples

Although samples were frozen and preserved from Column 2, no cryoSEM analyses were undertaken due to time and budget limitations. Consequently, all of the SEM observations from this experiment utilised samples prepared by freeze-drying and "solvent-replacement – polystyrene impregnation" techniques only.

Freeze-dried samples

SEM observations on freeze-dried samples from Column 2 appear to show some evidence of biofilm development (Plate 39, Plate 40, Plate 41 and Plate 42). However, preservation (or development) of the biofilm is restricted within the Acridine Orange-stained region of the column close to the interface with the unstained region (Sample 3B, Plate 39). There may also be some correlation between the distribution of K-rich mineral surfaces (such as muscovite, biotite and K-feldspar) and the most extensive development of the biofilm. The biofilm forms thin, long characteristic filaments and webs which are attached to the mineral surface (Plate 39). Much of this biofilm appears to have collapsed, forming over the mineral grain surfaces (Plate 40 and Plate 41). However, meshworks and webs of biofilaments are locally preserved which show that they extended across the intergranular porosity between adjacent grains, and bound fine mineral material matter to constrict pore throats (Plate 42).

Throughout the column, there is evidence of dispersed fine grained potassium phosphate precipitate. As discussed earlier, this is considered to be an artefact that is most probably derived from the potassium phosphate used in the Acridine Orange staining solution.

There is evidence of biotite alteration to secondary chlorite (chloritisation). The chlorite was observed occasionally as a crust on the surface biotite flakes, occurring as platy crystal. However, this mineral could have been present originally within the experimental charge, and is known to have formed during hydrothermal alteration history of the granodiorite.

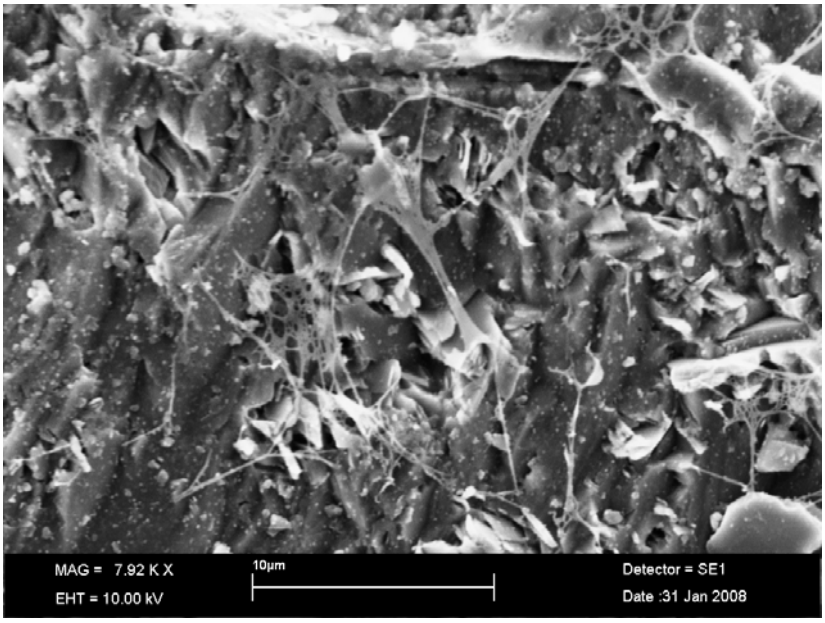

Plate 39 SEI photomicrograph showing delicate biofilaments "rooted" to the rough surface of a feldspar grain. Column 2, sample 3B.

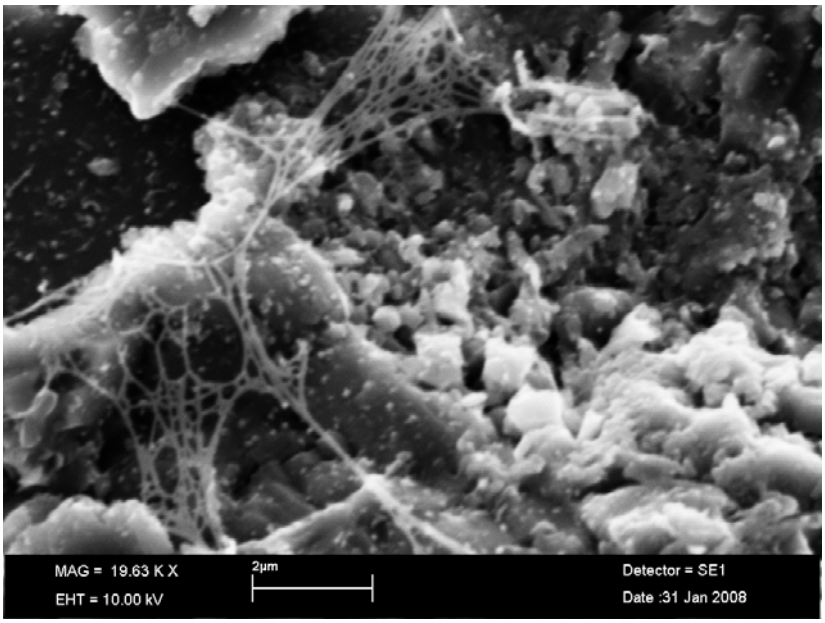

Plate 40 SEI photomicrograph showing a delicate "web-like" meshwork of biofilm draped over the surface a mineral grain. Column 2, sample 3B.

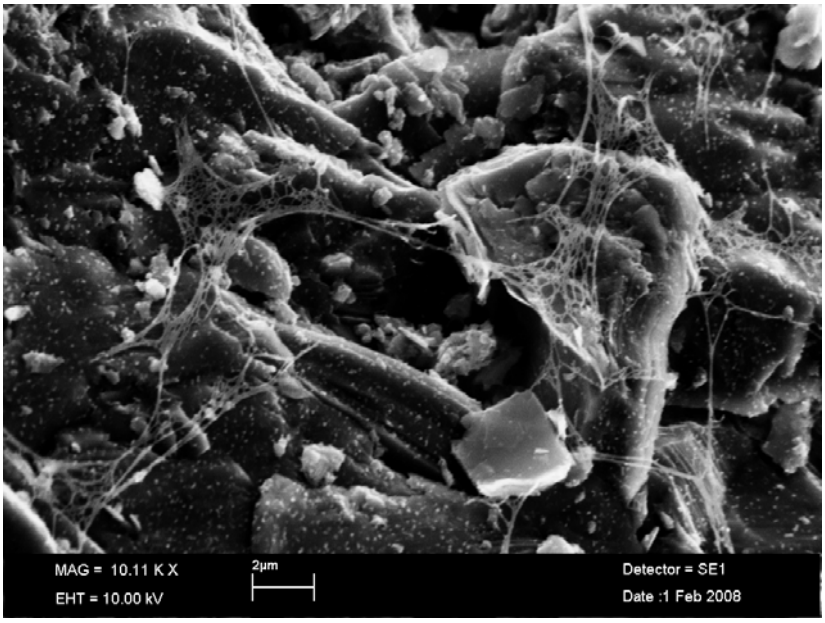

Plate 41 SEI photomicrograph showing a "web-like" biofilm and biofilaments draped over the surface of a plagioclase grain. Column 2, sample 3B.

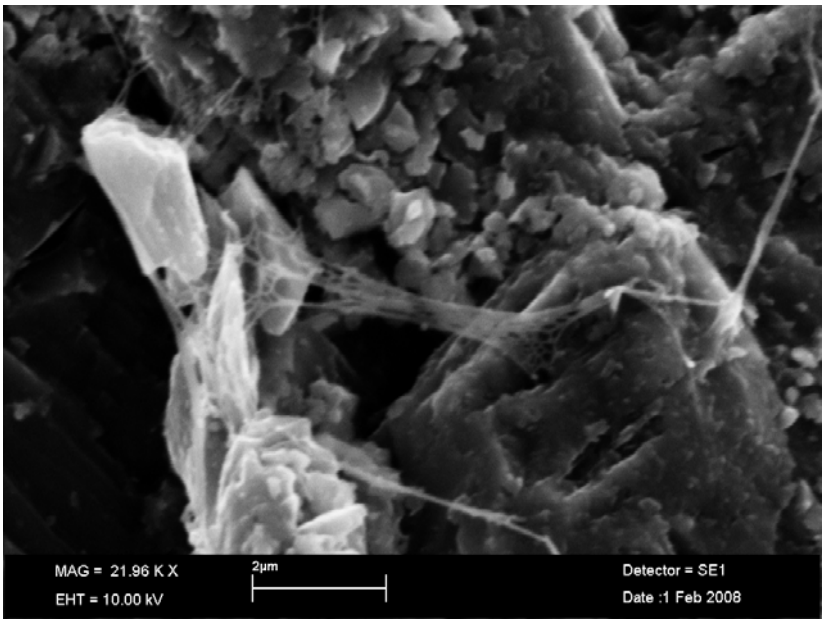

Plate 42 SEI photomicrograph showing "web-like" biofilm binding together the loose fine mineral debris within pore throats. Column 2, sample 3B.

Solvent-replacement – polystyrene-impregnated samples

Very little evidence of biofilm development or preservation was seen in samples prepared by the solvent-replacement and polystyrene impregnation technique. Gelatinous films, trails of strand-like deposits and globules of organic matter enriched in potassium phosphate, similar to that observed in Column 1 were seen on mineral surfaces in samples towards the outlet end of the column (Plate 43). In addition, dendritic precipitates of potassium phosphate, similar to those described from samples from Column 1 (cf. Plate 37) that were prepared the same way, were also seen. These features may be artefacts of the sample preparation technique, as discussed previously.

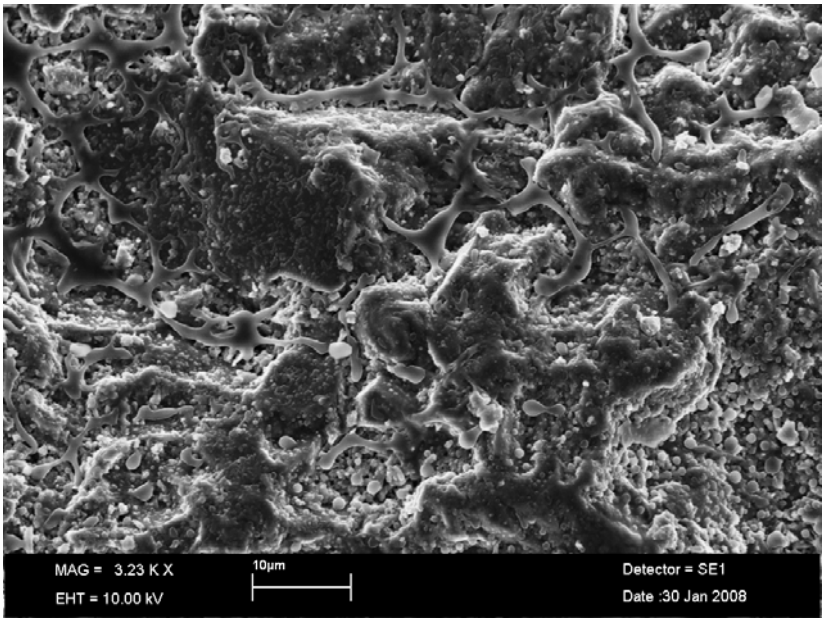

Plate 43 SEI photomicrograph showing "trails" of potassium phosphate-enriched gelatinous organic matter coating the surface of a mineral grain. Column 2, sample 14.

4.4 DISCUSSION

4.4.1 Flow rates and hydraulic conductivity

The changes in flow rates and, hence in hydraulic conductivity in both columns are complex during the first 500 hours after injection of the bacteria. Fluctuations are evident in Column 1 but these are not reflected in Column 2 in this initial time period. This could be caused by non-uniform, incomplete saturation of Column 1 at the start of the experiment. However, in both columns there is an increase in flow rate to around 4.0-4.5 ml min^{-1} at some stage in this phase of the experiment (at 500 hours for Column 1 and 250 hours for Column 2). After this point, both flow and, consequently, hydraulic conductivity, fall quickly to reach 0.003 ml min^{-1} to 0.01 ml min^{-1} at around 1000 hours. This remains unchanged for the rest of the experiment. Changes in pH did not appear to alter the flow characteristics in Column 2 for this particular experimental duration. This may have been due to the low flow rates which meant that the bulk of the contents of column were not exposed to these changes.

The fluctuations in transport properties during the experiments demonstrate the complexity of systems which include a biological component. However, use of these data in existing microbial transport models is limited because few of them provide the option of coupling the flow to the microbial growth (Bateman *et al.,* 2006). General reactive transport codes could also be considered e.g. PHREEQC (Parkhurst and Appelo, 1999) and the BGS in-house code PRECIP (Noy, 1998). However, PHREEQC requires a steady flow field – clearly not obtained in this study. Alternatively, PRECIP supports coupling between flow and transport so could, in principle, be developed to take into account changing transport properties as illustrated in this experiment.

4.4.2 Total bacterial counts

In general, bacterial populations fluctuate during the first 500 hours of the experiment but there is a decrease in mean bacterial numbers in both columns of about one order of magnitude from the initial inoculation of 3.04×10^4 ml^{-1} bacteria. The mean number of bacteria in the waters collected from both columns then increased towards the end of the experiment and by the end of

the experiment the total numbers of bacteria in waters from both columns were similar (9.42 x 10^4 bacteria ml^{-1} in Column 1 and 2.36 x 10^4 bacteria ml^{-1} in Column 2).

These results suggest that in the first 550-700 hours of the experiment, the bacteria were either not surviving in the columns or that they were being sorbed onto the grain surfaces. This could have been a passive or active process (West *et al.,* 1991) and would be the precursor to any subsequent biofilm formation (Coombs *et al.*, 2008). The reduction in flow rate and hydraulic conductivity after 500 hours in both columns indicates a profound alteration of the characteristics of both columns and the formation of biofilm at this period is the most likely explanation. As the biofilm developed, it is likely that the numbers of bacteria within it increased. Some of these bacteria were probably released into the flowing water which would account for the rising numbers observed in sampled waters from both columns observed at the end of the experiments. Changes in pH in Column 2 over a 240 hour period did not appear to have any effect on bacterial numbers. This suggests that pH does not influence *P. aeruginosa* behaviour over this time period or that the exposure period was insufficient to generate observable changes in populations.

4.4.3 Effect of introduction of phage E79

After injection of the phage at 1156 hours the flow rate through Column 2 remained low, 0.003 ml min^{-1} to 0.01 ml min^{-1} over the following 800 hours. Due to the low flow rate the phage in the reservoir may have not reached as far as the column and therefore not come into direct contact with the bacteria within the column. A further injection of the phage into the inlet tubing of Column 2 was made at 1971 hours in an attempt to see if any change could be observed as a result of the proximity of the phage to the column inlet. However due to the pressure within the column it was difficult to ensure that the flow was sufficient to allow contact of the phage with the bacteria within the column. No change in flow rate was observed as a result of introduction of the phage.

Additionally, it is possible that the phage were not active in the columns. A phage assay sample of the supply reservoir taken two days after introducing phage E79 into the header reservoir of Column 2 proved negative thus suggesting that the phage had either become inactive or had not survived in the groundwater.

4.4.4 Fluid Chemistry

Fluid chemistry of the reacted fluids (within analytical error) are almost identical to that of the starting fluids with no significant changes in concentrations. No significant changes in outflow fluid chemistry were observed with the change in input fluid pH (from pH = 7.2 to 5.5) in Column 2, nor were any changes noted during the addition of phage to the columns. These results show that no observable fluid/solid interactions took place in either column during the experiment.

4.4.5 Mineralogical observations

Petrographical analysis of the residues from Column 1 and Column 2 demonstrated that biofilm had formed in both experiments. However, the different SEM preparation and analysis techniques produced markedly different preservations of the fabrics. CryoSEM preparation (Column 1 experiment only) resulted in significant disruption of the pore fabrics as a result of the growth of coarse ice crystals. This is believed to have occurred because the sample size used was too large to allow rapid (instantaneous) freezing, which have formed ice glass instead of coarse crystals. Nevertheless, the observations showed that biofilm and biofilaments grew across the fluid-saturated intergranular pore spaces and trapped and bound mineral fines within pore throats, resulting in pore constriction and blockage. This could at least partially account for the reduced permeability observed during the course of the experiment.

CryoSEM observations also revealed that a non-aqueous, non-wetting organic liquid was also present within the biofilm. It occurred as fine "oily" or "waxy" droplets that appear to represent a dispersed emulsion in the aqueous pore fluid, or were trapped by or attached to biofilm. Similar emulsion droplets were observed in samples prepared by freeze-drying and solvent-replacement techniques. It is possible that this material represents an immiscible organic liquid produced by the *P. aeruginosa*. This bacterium is known to produce alginate, which is an organic liquid that is immiscible with water.

The development of biofilm appears to have been largely limited to within the first third of the Column length (i.e. close to the inlet zone, where biological activity was indicated by staining with Acridine Orange). There was little evidence of development or preservation of biofilm further along the columns.

The cryoSEM observations also found that the mineral surfaces were heavy contaminated with potassium phosphate deposits. Films of organic material, also containing potassium phosphate were observed throughout the length of both columns. This material is considered to be an artefact deposited (on sample preparation and drying) from residual Acridine Orange staining solution (which contained a significant amount of potassium phosphate uffer). It would appear that the use of acetone and amyl acetate during the solvent-replacement drying technique may have remobilised and redistributed deposits from the Acridine Orange staining solution. Unfortunately, deposits from the staining solution obscured much of the mineral surfaces and complicated interpretation.

Comparison of the three different sample preparation methods used showed that they gave different preservations of biofilm material:

- The limited amount of cryoSEM undertaken on Column 1 material only demonstrated the preservation of emulsion within pore spaces, and showed that biofilaments grew across intergranular pore spaces. However, because freezing was too slow during sample preparation, ice crystal growth caused significant fabric damage. Future cryoSEM, using small sample sizes would probably result in more rapid freezing and better sample preservation;
- Samples prepared by freeze drying were found to completely disaggregate on drying. As a result, there was little or no preservation of pore-bridging biofilm fabrics although, vestiges of collapsed biofilaments and their roots of attachment were preserved on grain surfaces.
- Samples prepared by solvent-replacement drying, followed by impregnation with polystyrene solution produced a coherent sample that could be readily handled in the SEM. However, the polystyrene cement almost completely filled the intergranular pore spaces thereby limiting the observations that could be made. However, it was possible to make observations on the upper surfaces of the grains without any glue contamination. This technique would appear to have some promise for future work and would probably work better if a more viscous (i.e. more concentrated) solution of polystyrene was to be used. This would slow and limited the capillary uptake and saturation of polystyrene solution in the pore spaces.

5 Conclusions

The work described in this report has shown that:

- *P. aeruginosa* biofilms can be grown reliably using Äspö diorite and synthetic groundwater as a growth medium;
- *P. aeruginosa* biofilms can be grown in a variety of laboratory flowing systems;

- Biofilm growth and development can be imaged using a variety of techniques.

The pilot quantitative study evaluated the effects of biofilms on fluid flow through crushed Äspö diorite over a period of 1971 hours. It showed that:

- Numbers of *P. aeruginosa* gradually increased suggesting that the bacteria were not only surviving, but were also growing in the flow systems;
- Biofilms did develop in both columns as evidenced by direct observations and by petrographic analysis of both columns at the end of the experiment;
- Quantitative results could be obtained using the methodologies described in this report, allowing calculation of hydraulic conductivity. The fluctuations in transport properties during the experiments demonstrate the complexity of systems which include a biological component. The results also show, indirectly, the effect of biofilm on transport properties which is particularly evident after 500 hours when flow in both columns dropped to very low rates. However, use of these data in existing and microbial transport and clogging models is limited because few of them provide the option of coupling flow to microbial growth;
- Changes in pH do not appear to influence transport properties in the described flowing systems containing *P. aeruginosa* biofilms over the experimental exposure period. It is possible that column material and the biofilms may not have been exposed to the pH change because of the low flow rates which will need to be further investigated in future experiments;
- Introduction of phage E79 does not appear to influence transport properties in these flowing systems containing *P. aeruginosa* biofilms. However, it is possible that the phage were not active in these experiments;
- No observable fluid/solid interactions took place in either column.

Future work will concentrate on developing the quantitative methodologies further so that studies can be undertaken under anaerobic conditions. Further development work is also required to directly observe biofilm growth in columns, particularly for petrographic analysis. Consideration is also needed on how best to utilise the quantitative transport measurements as existing transport models are very limited in their ability to couple biological processes with flow calculations. Development of the BGS in-house model PRECIP model may be most appropriate.

Appendix 1

BIOFILMS

A biofilm is an agglomeration of microbial cells and their excreted organic and inorganic products that is attached to, or coats, mineral surfaces or other substrates (Taylor and Jaffe 1990a). Biofilms are very common in the geosphere and biosphere, forming in diverse environments including the surfaces of human teeth (Marsh, 2004), wall murals and stone monuments (Dornieden *et al.*, 2000), stream sediments (Konhauser *et al.*, 1998), cave and mine walls and the subsurface (Tuck *et al.*, 2006). In such natural systems, they often comprise a mixture of interacting microbial species forming complex ecosystems. Biofilm thickness is extremely variable ranging from a single cell monolayer, to thick mucous microcolonies of microbes held together by Extracellular Polymeric Substances (EPS) (Beyenal *et al.*, 2004;

Bishop *et al.*, 1995; Fletcher, 1991; Paulsen *et al.*, 1997; Wimpenny *et al.*, 2000). In all environments, including the subsurface, biofilm formation is initiated by the attachment of a microbe to a solid surface. Attachment may be a reversible transitory physicochemical attraction or may become permanent if the EPS forms a strong chemical bridge to the solid surface (Dowd *et al.*, 2000). The EPS provides a matrix for the attachment of microbial cells and influences the functioning and survival of biofilms in hostile environments by providing a microenvironment for viable microbial activity that may be very different to the ambient surroundings. Biofilm structure appears to be of three main types: planar structures; stacks of microcolonies of microbes held together by EPS; or mushroom or tulip shaped formations (Wimpenny *et al.*, 2000; Beyenal *et al.*, 2004). However, laboratory grown biofilms often comprise interwoven filamentous biomass with micropores of 20-200µm diameter (Okabe *et al.*, 1998).

The formation and development of biofilms in the subsurface environment will depend on the presence of the microbes themselves; plus the availability of nutrients, energy sources and water necessary for life processes (West and Chilton, 1997). In a very low nutrient/energy environment with low groundwater flow, biofilms may not form and organisms may be dormant or maintain a very low metabolic rate. In this situation, it is unlikely that biofilm formation will influence the transport properties of the surrounding rock. However, in environments where nutrients and energy are more available, and where groundwater flow may be higher, biofilm formation will take place. As a result, the transport properties of the host rock will be altered to a greater or lesser degree depending on the characteristics and thickness of the biofilm and the nature of the rock itself. Such alteration in rock transport properties will be important to contaminant movement, as illustrated by some recent studies.

MICROBIAL TRANSPORT STUDIES ASSOCIATED WITH THE ÄSPÖ HARD ROCK LABORATORY, SWEDEN

The Äspö Underground Research Laboratory (URL) has been used for many studies and experiments evaluating aspects of the geological disposal of radioactive waste in hard rock (granodiorite) environments (SKB, Annual Reports, 2003; 2004). The significance of microbiological processes in the containment of radioactive waste has long been recognised (West *et al.*, 1982; West, 1995, West and McKinley, 2002) and, consequently, detailed evaluations of the biofilms present on the walls of the URL and on the significance of indigenous microbial populations has been a key area of work (see Pedersen, 1999 and references therein).

A recent in-situ study at the URL examined the redox buffering of groundwater in vertical fractures zones penetrated by recent, oxidising, shallow-recharged meteoric water, simulating processes that might occur in repository construction, and which could alter the geochemical experiment. This showed that indigenous bacteria were capable of maintaining reducing conditions in the deep groundwaters (Banwart, 1995). As a result, a further laboratory experimental study was undertaken to simulate the interactions of microbes with mineralogical surfaces associated with groundwater flow systems at Äspö (Hama *et al.*, 2001). Indigenous iron-reducing bacteria and sulphate-reducing bacteria were introduced in Äspö groundwater flowing through either columns or continuously stirred tank reactors (CSTR) packed with crushed Äspö diorite rock. The columns containing the organisms became blocked within a few days and no flow was possible. Petrographic analyses of the column residues inoculated with the bacteria indicated that the reduction in permeability in the columns was associated with (1) mobilisation of ‘fines’ from grain surfaces and their accumulation in intergranular pore throats; (2) development of filamentous organic biofilaments; and (3) formation of secondary mixed-layer chlorite-smectite. The observed change in permeability, in the biotic experiments, was surprising because of the low concentration of available nutrients (C, S, N, P) and because any mineralogical changes involved (and hence changes in porosity) were volumetrically small. Although only a small amount of biofilament was produced, it formed a filamentous mesh that acted as a sieve, trapping any ‘fines’ migrating within pore throats, and also significantly

decreased pore throat size whilst simultaneously increasing pore tortuosity. The liberation of 'fines' was not observed in the abiotic experiment and their appearance seemed to be related to the presence of the bacteria – possibly influenced by surfactant properties of biocrobial exudates. The formation of the secondary chlorite-smectite during the biotic experiment may have also had an influence and this again appeared to be related to the presence of the organisms. The same formation of secondary clay was also observed in the 3 month long CSTR experiments although smectite, rather than the mixed-layer chlorite-smectite, was detected. Once again, the amount of smectite formed was greater in the biotic CSTR experiments demonstrating that the bacteria were having a significant influence on clay mineral formation in the experiments. More details of these studies are described elsewhere (West *et al.*, 1998; Hama *et al.*, 2001).

Other studies at the Äspö URL examined radionuclide sorption processes which compared the adsorption capacity of granitic rock to biofilms grown in situ on glass and rock surfaces (Anderson *et al.*, 2006). After immersing the surfaces for 42 days in anaerobic synthetic groundwater containing a number of radioactive tracers the adsorption and distribution of the radionuclides was investigated using 2D autoradiography. Results showed that the rock absorbed more ^{60}Co, ^{99}Mo, ^{241}Am, ^{237}Np and ^{234}Th per unit area when compared to the biofilm grown on the glass slides whilst the biofilm absorbed more ^{147}Pm than the rock. Biofilms can form a barrier between the rock and groundwater and may slow down radionuclide diffusion to the rock. These results suggested that differences in adsorption were dependant upon the chemical properties of the individual radionuclides and the availability of different surface functional groups modified by the presence or absence of biofilms.

Further experiments by Tuck *et al.* (2006) used packed columns and stirred batch reactors to simulate microbial-geochemical interactions in deep subsurface low nutrient granitic environments. The columns, containing crushed Äspö grandodiorite and a single or mixed culture of chomolithotrophic bacteria became impermeable to synthetic Äspö groundwater after 5 days. Analysis revealed copious filamentous biofilm, encrusted with finer-grained material, across pore spaces with limited attachment sites on large grains in those columns. The work also suggested that the indigenous bacteria were capable of surviving in relatively low nutrient conditions and that bacteria can either concentrate relevant chemical species for mineral formation in localised microenvironments or may accelerate clay formation. This study implies that the localised hydrological regime of a granitic environment can be changed, particularly if new nutrient sources are introduced e.g. via links to surface water; or via links to the repository components. Biogenic mineral precipitates and trapped mineral matter are much more chemically and physically stable than the biofilm, and can persist in the pore system long after the biofilm has decayed or been removed (Brydie *et al.*, 2005).

Studies by Ferris *et al.* (1999) with iron oxides and groundwater samples collected from the Äspö site looked at the extent to which dissolved metals sorbed into bacteriogenic iron oxides in a deep, hard rock groundwater environment. Results of metal distribution coefficients (Kd values) showed Kd values decreased with increasing iron oxide content which appeared to be influenced by the bacterial organic matter in the solids. This has implications for the transport and fate of dissolved metals in groundwater systems where there is contact between iron oxides and bacterial organic matter.

Work by West *et al.* (1991) looked at radionuclide sorption onto a host rock, calcium montmorillonite (Fuller's Earth) as an important retarding mechanism. These studies used a batch sorption method (West *et al.*, 1986) of groundwater spiked with ^{137}Cs and pure rock and microorganisms under a variety of conditions. In anaerobic conditions Cs and microbes were sorbed onto the rock material. A reduction in Cs was observed suggesting that the varying amounts of biofilm produced were able to bind metals from solution thus lowering the amount of Cs in the groundwater. Their results showed that the presence of microbes decreased the amount of retardation of ^{137}Cs by the solid phase.

Experiments to better understand the physicochemical processes occurring at the biofilm-mineral interface were designed by Vaughan *et al.*,. (2001). These experiments used miniature flow cells to grow single species biofilms within a simulated rock fracture environment. The structure of the resulting biofilms and the bacterial distribution was determined using confocal scanning laser microscopy. Results indicated a greater permeability of the biofilm in the centre compared to the surrounding matrix areas surrounding it. This suggested that biofilms might have the effect of producing localised flow gradients and may have an important impact on hydraulic properties when modelling a flowing system.

Experiments have shown that fluid movement is influenced by the presence of microorganisms in the system, in particular the presence of biofilms. Where conditions are suitable there is potential for biofilaments to establish (in a matter of days) causing pore blockages resulting in a decrease in permeability of the porous media and a change in the local fluid flow patterns. Extensive formation of biofilm reduces pore space, which can lead to eventual blocking of the pore system (Taylor and Jaffé 1990 a;b) referred to as 'bioclogging' (Brydie *et al.*,. 2005). Brydie *et al.*, (2005) observed a 70 % reduction in the permeability of sand due to bioclogging. Even greater permeability reductions (three orders of magnitude) were observed in earlier studies by Taylor and Jaffé (1990a).

MODELLING OF BIOFILMS

There have been numerous attempts to model microbial growth in sub-surface environments and its effects on contaminant transport in groundwater. These models may be grouped into a number of categories depending upon sophistication and the nature of the processes that they try to represent: 'microbe mass balance' models, 'coupled microbe growth and mass transport' models and 'microbial transport and clogging' models.

The microbe mass balance model is perhaps the simplest in concept since it just attempts to calculate the limits to growth from the available supplies of nutrients and energy provided by the flow of groundwater and the leaching of the solid phase. This style of model was first proposed by Grogan and McKinley (1990) and similar models were used by Baker *et al.* (1998) and Jolley *et al.* (2003).

There are numerous models of 'coupled microbe growth and mass transport' reported in the literature over the past 30 or more years. A review of these models by Baveye and Valocchi (1989) divided them into three groups according to the treatment of the attached bacteria. The first group (I) consisted of those models that neglected pore scale processes and assumed that the bacteria respond directly to the macroscopic bulk fluid composition. The other two groups were based upon the assumptions of the bacteria forming microcolonies (II) or biofilms (III). Examples of the first group of models may be found in Corapcioglu and Haridas (1984), Corapcioglu and Haridas (1985), and Kindred and Celia (1989). Examples of the microcolonies approach are found in Molz *et al.* (1986) and Widdowson *et al.* (1988) whilst the biofilm approach was used, for example, in Rittmann *et al.* (1980) and Bouwer and McCarty (1984). Baveye and Valocchi noted the formal similarities in all the mathematical models with the differences arising in the detailed implementation of particular terms.

Widdowson (1991), in commenting on this review, noted the particularly close association of model types I and II, but demonstrated that the differences in detail could result in noticeable differences in the calculated concentrations. Widdowson also questioned the applicability of the biofilm concept to subsurface environments.

Microbial transport and clogging models are really a sub-set of those described in the previous section. They are distinguished by the fact that they attempt to model the changes in the hydraulic properties of the medium as well as the microbial growth and consequent changes of porewater chemistry. Examples of such models may be found in Corapcioglu and Haridas

(1984), Corapcioglu and Haridas (1985), Vandevivere et al. (1995), Clement et al. (1996), and Thullner et al. (2004).

Appendix 2 Data from fluid chemistry and Porosity calculations

Sample disc	Hours (since injection)	pH	Na^+	Ca^{2+}	Mg^{2+}	K^+	SiO_2	Al	Li	Ba	Sr	Mn	Reduced Fe	Oxidised Fe	Total Fe	Cl^-	SO_4^{2-}	Total S	NO_3^-	HPO_4^{2-}	Total P	Balance
			mg l^{-1}	mg l^{-1}	mg l^{-1}	mg l^{-1}	mg l^{-1}	mg l^{-1}	mg l^{-1}	mg l^{-1}	mg l^{-1}	mg l^{-1}	mg l^{-1}	mg l^{-1}	mg l^{-1}	mg l^{-1}	mg l^{-1}	mg l^{-1}	mg l^{-1}	mg l^{-1}	mg l^{-1}	%
Starting fluid	0.0	6.04	3478	5665	58.6	21.4	3.21	<0.20	<0.50	0.12	52.9	<0.04	<0.05	<0.20	<0.20	12971	479	243	<4.00	<20.0	<0.20	7.92
Starting fluid	0.0	6.38	3019	4839	51.5	18.7	3.21	<0.20	<0.50	0.22	46.3	0.06	<0.05	<0.20	<0.20	12705	448	209	<4.00	<20.0	<0.20	1.45
Starting fluid	216.0		3171	4851	51.9	19.6	3.21	<0.20	<0.50	<0.04	68.7	<0.04	n.d.	n.d.	<0.20	13719	487	212	<4.00	<20.0	<0.20	-1.38
Starting fluid (pH 5.52)	792.0	5.52	3087	4712	50.2	18.3	3.21	<0.20	<0.50	<0.04	70.5	<0.04	n.d.	n.d.	<0.20	12908	432	202	<4.00	<20.0	<0.20	0.33
Starting fluid	2200.0	6.33	3856	6219	63.5	21.5	3.21	<0.20	<0.50	<0.04	89.5	<0.04	<0.05	<0.20	<0.20	24734	654	258	<8.00	<40.0	<0.20	-18.83
Starting fluid	2200.0	6.50	3182	4966	52.9	19.0	3.21	<0.20	<0.50	<0.04	89.2	<0.04	<0.05	<0.20	<0.20	14668	646	258	<4.00	<20.0	<0.20	-4.17
Starting fluid	216.0		3212	5135	54.1	30.7	3.21	<0.20	<0.50	<0.04	53.9	<0.04	n.d.	n.d.	<0.20	13983	470	220	<4.00	<20.0	<0.20	-0.22
Column 1/1	144.0	6.41	3460	5660	58.4	19.9	3.21	<0.20	<0.50	0.13	52.7	<0.04	<0.05	<0.20	<0.20	13561	474	240	<4.00	<20.0	<0.20	5.66
Column 1/2	27.5		2990	4777	50.7	16.4	3.21	<0.20	<0.50	0.09	45.5	<0.04	<0.05	<0.20	<0.20	13365	466	209	<4.00	<20.0	<0.20	-1.66
Column 1/3	48.0		3213	5200	53.9	18.9	3.21	<0.20	<0.50	0.10	48.8	<0.04	<0.05	<0.20	<0.20	13366	470	221	<4.00	<20.0	<0.20	2.32
Column 1/4	117.0		3418	5557	57.4	20.9	3.21	<0.20	<0.50	0.11	52.0	<0.04	<0.05	<0.20	<0.20	13859	492	236	<4.00	<20.0	<0.20	3.75
Column 1/5	168.0	6.57	3447	5702	58.3	21.5	3.21	<0.20	<0.50	0.13	53.0	<0.04	<0.05	<0.20	<0.20	13635	471	239	<4.00	<20.0	<0.20	5.58
Column 1/6	216.0	6.56	3045	4851	51.5	20.2	3.21	<0.20	<0.50	0.12	46.3	<0.04	<0.05	<0.20	<0.20	13609	483	210	<4.00	<20.0	<0.20	-1.76
Column 1/7	312.0	6.44	3200	5025	53.6	19.0	3.21	<0.20	<0.50	0.10	52.9	<0.04	n.d.	n.d.	<0.20	13324	472	221	<4.00	<20.0	<0.20	1.32
Column 1/8	336.0	6.56	3092	4779	51.9	19.0	3.21	<0.20	<0.50	0.08	51.0	<0.04	n.d.	n.d.	<0.20	13753	524	209	<4.00	<20.0	<0.20	-2.57
Column 1/9	359.0	6.55	3253	5214	53.7	18.8	3.21	<0.20	<0.50	0.08	56.3	<0.04	n.d.	n.d.	<0.20	13391	477	222	<4.00	<20.0	<0.20	2.53
Column 1/10	384.0		3840	6085	63.3	22.3	3.21	<0.20	<0.50	0.08	72.3	<0.04	n.d.	n.d.	<0.20	14026	515	264	66.1	<20.0	<0.20	7.98
Column 1/11	456.0	5.84	3040	4795	50.0	18.0	3.21	<0.20	<0.50	0.05	60.2	<0.04	n.d.	n.d.	<0.20	13972	522	210	<4.00	<20.0	<0.20	-3.52
Column 1/12	482.0	5.68	3201	4918	52.1	19.0	3.21	<0.20	<0.50	<0.04	63.4	<0.04	n.d.	n.d.	<0.20	13692	478	214	16.1	<20.0	<0.20	-0.71
Column 1/13	503.0	6.06	3538	5643	57.8	20.5	3.21	<0.20	<0.50	0.04	73.1	<0.04	n.d.	n.d.	<0.20	13970	499	241	8.69	<20.0	<0.20	4.46
Column 1/14	530.0	6.12	3051	4687	49.7	19.3	3.21	<0.20	<0.50	<0.04	63.3	<0.04	n.d.	n.d.	<0.20	13489	474	207	<4.00	<20.0	<0.20	-2.33
Column 1/15	555.0		3689	5857	60.0	25.0	3.21	<0.20	<0.50	0.05	77.5	<0.04	n.d.	n.d.	<0.20	14142	526	251	53.3	<20.0	<0.20	5.66
Column 1/16	675.0	5.69	3658	5659	60.3	29.4	3.21	<0.20	<0.50	0.11	84.1	<0.04	<0.05	<0.20	<0.20	14773	504	239	<4.00	<20.0	<0.20	2.50
Column 1/17	700.0	6.03	3785	6043	61.2	29.4	3.21	<0.20	<0.50	0.13	86.9	<0.04	n.d.	n.d.	<0.20	15347	533	247	<4.00	<20.0	<0.20	3.26
Column 1/18	794.0	6.20	4108	6541	66.8	32.8	3.22	<0.20	<0.50	0.15	94.3	<0.04	n.d.	n.d.	<0.20	16042	550	266	<4.00	<20.0	<0.20	5.07
Column 1/19	866.0	6.25	4568	7342	73.7	37.0	3.43	<0.20	<0.50	0.16	73.5	<0.04	n.d.	n.d.	<0.20	17556	584	294	<8.00	<40.0	<0.20	6.14
Column 1/20	986.5	6.43	4087	6228	66.6	32.5	3.82	<0.20	<0.50	0.15	93.0	<0.04	<0.05	<0.20	<0.20	17790	595	263	<8.00	<40.0	<0.20	-1.71
Column 1/21	1033.5	6.43	4909	8342	80.5	41.0	5.20	<0.20	<0.50	0.18	75.9	<0.04	<0.05	<0.20	<0.20	19062	659	326	<8.00	<40.0	<0.20	7.37
Column 1/22	1156.0	6.2	4062	6829	66.7	30.4	3.59	<0.20	<0.50	0.15	91.8	<0.04	n.d.	n.d.	<0.20	21760	397	262	<8.00	<40.0	<0.20	-8.39
Column 1/23	1205.0	6.32	4188	6660	67.1	33.2	4.23	<0.20	<0.50	0.15	96.1	<0.04	n.d.	n.d.	<0.20	17817	636	272	<4.00	<20.0	<0.20	0.69
Column 1/24	1345.0	6.27	4831	8014	78.0	38.3	4.62	<0.20	<0.50	0.17	84.4	<0.04	<0.05	<0.20	<0.20	20393	653	316	<8.00	<40.0	<0.20	2.52
Column 1/25	1469.0	6.50	5143	8631	83.0	40.8	4.85	<0.20	<0.50	0.18	85.8	<0.04	<0.05	<0.20	<0.20	20209	665	332	<8.00	<40.0	<0.20	6.43
Column 1/26	1561.0	6.50	5228	9300	85.7	38.4	5.48	<0.20	<0.50	0.19	85.0	<0.04	<0.05	<0.20	<0.20	19600	645	343	<8.00	<40.0	<0.20	10.66
Column 1/27	1805.0		4910	8151	78.6	37.6	4.11	<0.20	<0.50	0.17	109	<0.04	<0.05	<0.20	<0.20	n.d.	n.d.	313	n.d.	n.d.	<0.20	n.d.
Column 1/28	2141.5	6.41	5775	6486	92.9	43.9	5.06	<0.20	<0.50	0.21	92.1	<0.04	<0.05	<0.20	<0.20	22742	763	379	<8.00	<40.0	<0.20	-5.77

Sample disc	Hours (since injection)	pH	Na^+	Ca^{2+}	Mg^{2+}	K^+	SiO_2	Al	Li	Ba	Sr	Mn	Reduced Fe	Oxidised Fe	Total Fe	Cl^-	SO_4^{2-}	Total S	NO_3^-	HPO_4^{2-}	Total P	Balance
			mg l^{-1}	mg l^{-1}	mg l^{-1}	mg l^{-1}	mg l^{-1}	mg l^{-1}	mg l^{-1}	mg l^{-1}	mg l^{-1}	mg l^{-1}	mg l^{-1}	mg l^{-1}	mg l^{-1}	mg l^{-1}	mg l^{-1}	mg l^{-1}	mg l^{-1}	mg l^{-1}	mg l^{-1}	%
Column 2/1	144.0		3615	5998	60.5	20.2	3.21	<0.20	<0.50	0.10	54.7	<0.04	<0.05	<0.20	<0.20	13318	124	251	<4.00	<20.0	<0.20	10.11
Column 2/2	27.5		3519	5621	59.1	22.4	3.21	<0.20	<0.50	0.13	52.7	<0.04	<0.05	<0.20	<0.20	13664	500	243	12.4	<20.0	<0.20	5.28
Column 2/3	48.0		3084	4840	52.1	23.4	3.21	<0.20	<0.50	0.14	46.2	<0.04	<0.05	<0.20	<0.20	13577	483	210	<4.00	<20.0	<0.20	-1.48
Column 2/4	117.0		3070	4822	52.2	20.0	3.21	<0.20	<0.50	0.11	46.5	<0.04	<0.05	<0.20	<0.20	13929	505	211	<4.00	<20.0	<0.20	-2.99
Column 2/5	168.0	6.50	3057	4831	51.9	17.6	3.21	<0.20	<0.50	0.08	46.3	<0.04	<0.05	<0.20	<0.20	14066	509	211	<4.00	<20.0	<0.20	-3.50
Column 2/6	216.0	6.45	3667	5944	61.4	19.0	3.21	<0.20	<0.50	0.09	55.3	<0.04	<0.05	<0.20	<0.20	13421	479	254	<4.00	<20.0	<0.20	8.73
Column 2/7	312.0	6.45	3201	5000	53.3	17.7	3.21	<0.20	<0.50	0.05	53.4	<0.04	n.d.	n.d.	<0.20	13621	509	218	<4.00	<20.0	<0.20	0.00
Column 2/8	336.0	6.50	3259	5314	54.5	17.4	3.21	<0.20	<0.50	0.05	54.6	<0.04	n.d.	n.d.	<0.20	13535	480	225	<4.00	<20.0	<0.20	2.65
Column 2/9	360.0	6.50	3146	5016	52.1	16.4	3.21	<0.20	<0.50	0.05	54.4	<0.04	n.d.	n.d.	<0.20	13660	491	214	7.14	<20.0	<0.20	-0.33
Column 2/10	384.0		3487	5568	57.7	18.9	3.21	<0.20	<0.50	0.05	65.9	<0.04	n.d.	n.d.	<0.20	14054	501	239	37.4	<20.0	<0.20	3.41
Column 2/11	456.0	5.89	3938	6129	64.0	21.3	3.21	<0.20	<0.50	0.05	77.4	<0.04	n.d.	n.d.	<0.20	13536	468	269	10.4	<20.0	<0.20	10.61
Column 2/12	482.0	6.01	3822	6536	62.9	22.0	3.21	<0.20	<0.50	0.06	75.6	<0.04	n.d.	n.d.	<0.20	13891	501	262	<4.00	<20.0	<0.20	10.81
Column 2/13	503.0	6.15	3385	5223	55.3	21.7	3.21	<0.20	<0.50	0.05	68.5	<0.04	n.d.	n.d.	<0.20	13923	523	232	<4.00	<20.0	<0.20	1.33
Column 2/14	530.0	6.18	3971	6287	64.2	26.7	3.21	<0.20	<0.50	0.06	82.5	<0.04	n.d.	n.d.	<0.20	14116	515	269	<4.00	<20.0	<0.20	9.45
Column 2/15	555.0		3604	5797	58.7	24.3	3.21	<0.20	<0.50	0.07	76.4	<0.04	n.d.	n.d.	<0.20	13772	502	244	301	<20.0	<0.20	5.77
Column 2/16	675.0	5.90	3887	6104	63.1	30.1	3.21	<0.20	<0.50	0.12	88.9	<0.04	<0.05	<0.20	<0.20	15035	521	254	<4.00	<20.0	<0.20	5.09
Column 2/17	700.0	6.08	4354	6955	70.5	33.7	3.21	<0.20	<0.50	0.14	96.1	<0.04	n.d.	n.d.	<0.20	17271	611	284	<4.00	<20.0	<0.20	4.34
Column 2/18	794.0	6.19	4238	6793	68.9	33.6	3.22	<0.20	<0.50	0.15	87.9	<0.04	n.d.	n.d.	<0.20	23415	679	291	<8.00	<40.0	<0.20	-11.84
Column 2/19	866.0	6.33	5783	7476	92.4	47.1	4.40	<0.20	<0.50	0.20	126	0.05	n.d.	n.d.	<0.20	25249	950	421	<8.00	<40.0	<0.20	-7.00
Column 2/20	986.5	6.29	5421	9175	88.6	47.8	5.11	<0.20	<0.50	0.21	120	0.06	<0.05	<0.20	<0.20	22806	732	359	<8.00	<40.0	0.25	3.40
Column 2/21	1033.5		4595	7506	74.7	39.9	4.80	<0.20	<0.50	0.17	108	0.05	n.d.	n.d.	<0.20	19575	827	349	<4.00	<20.0	<0.20	1.27
Column 2/22	1156.0	6.26	6558	8720	105	57.1	5.23	<0.20	<0.50	0.27	148	0.09	n.d.	n.d.	<0.20	13547	463	342	<8.00	<40.0	<0.20	30.38
Column 2/23	1205.0		5034	8387	82.0	38.9	5.53	<0.20	<0.50	0.20	119	0.06	n.d.	n.d.	<0.20	22369	886	388	22.3	<40.0	<0.20	-0.14
Column 2/24	1345.0	6.53	4681	7579	76.0	38.8	5.05	<0.20	<0.50	0.18	111	0.06	<0.05	<0.20	<0.20	21886	732	319	<8.00	<40.0	<0.20	-3.35
Column 2/25	1469.0	6.55	7610	8726	123	60.3	8.53	<0.20	<0.50	0.28	143	0.09	<0.05	<0.20	<0.20	28311	1070	567	<8.00	<40.0	<0.20	-2.46
Column 2/26	1561.0	6.21	6731	9041	109	54.2	6.72	<0.20	<0.50	0.23	152	0.08	n.d.	n.d.	<0.20	32934	1091	436	32.3	<40.0	<0.20	-11.37
Column 2/27	1805.0		9645	12945	150	78.1	10.37	<0.20	<0.50	0.34	222	0.10	<0.20	<0.20	<0.20	40267	1293	566	<8.00	<40.0	<0.20	-3.46

Porosity calculations

	Column 1	Column 2	Unit
Column length	220	217	(mm)
Empty column weight, A	206.73	204.54	(g)
Dry packed weight, B	357.85	361.55	(g)
Wet weight packed, W	405.34	407.35	(g)
Wt of solid, (B-A)	151.12	157.01	(g)
Wt of fluid (≡ Pore Vol)	47.49	45.80	(g)
Wt of solids	57.03	59.25	(g)
Porosity	45.4	43.6	(%)

Glossary

CryoSEM	Cryogenic Scanning Electron Microscopy
BSEM	Backscattered Scanning Electron Microscopy
EDXA	Energy-Dispersive X-ray Microanalysis
SEI	Secondary Electron Imaging/image
SEM	Scanning Electron Microscopy
UV	UltraViolet
VP	Variable Pressure (cf. VPSEM)
VPSEM	Variable Pressure SEM. SEM using low vacuum operation.

References

The British Geological Survey holds most of the references listed below, and copies may be obtained via the library service subject to copyright legislation (contact libuser@bgs.ac.uk for details). The library catalogue is available at: http://geolib.bgs.ac.uk.

ALLISON, D G, AND SUTHERLAND, I W, 1984. A staining technique for attached bacteria and its correlation to extracellular carbohydrate production. *Journal of Microbiological Methods* Vol. 2, 93-99

ANDERSON, C, PEDERSEN, K.AND JAKOBSSON, A M, 2006. Autoradiographic comparisons of radionuclide adsorption between subsurface anaerobic biofilms and granitic host rocks. *Geomicrobiology Journal* Vol. 23, 15-19.

BAKER, S J, WEST, J M, METCALFE, R, NOY, D J, YOSHIDA, H, AND AOKI, K, 1998. A biogeochemical assessment of the Tono site, Japan. *Journal of Contaminant Hydrology* Vol. 35, 331-340.

BANWART, S, 1995. The Aspo redox investigations in block scale project summary and implications for repository assessment. *SKB Technical Report.*

BATEMAN, K, COOMBS, P, HARRISON, H, MILODOWSKI, AE, NOY, D, VANE, CH, WAGNER, D, AND WEST, J M, 2006. Bio Tran. Microbial transport and microbial indicators of mass transport through geological media – A literature survey. *British Geological Survey Internal Report* IR/06/029.

BAVEYE, P, AND VALOCCHI, A J, 1989. An evaluation of mathematical models of the transport of biologically reacting solutes in saturated soils and aquifers. *Water Resources Research* Vol. 25(6), 1413-1421.

ALLISON, D G, AND SUTHERLAND, I W, 1984. A staining technique for attached bacteria and its correlation to extracellular carbohydrate production. *Journal of Microbiological Methods* Vol. 2, 93–99.

BEVERIDGE, T. J, MAKIN, S A. KADURUGAMUWA, J L AND LI, Z, 1997 Interactions between biofilms and the environment. *FEMS Microbiology Reviews* Vol. 20, 291-303.

BEYENAL, H., DONOVAN, C, LEWANDOWSKI, Z, HARKIN, G. 2004. Three-dimensional biofilm structure quantification. *Journal Microbiological. Methods* Vol. 59, 395-413.

BISHOP, P L,TIAN, C.Z AND YUN-CHANG, F, 1995. Effects of biofilm structure, microbial distributions and mass transport on biodegradation processes. *Water Science and Technology* Vol. 31, 143-152.

BOUWER, E J, AND MCCARTY, P L, 1984. Modelling of trace organics biotransformation in the subsurface. *Ground Water* Vol. 22, 433-440.

BRYDIE, J R, WOGELIUS,R A, MERRIFIELD, C, BOULT, S, GILBERT, P, ALLISON, D, AND VAUGHAN, D J, 2005. The Micro to Macro project on quantifying the effects of biofilm growth on hydraulic properties of natural porous media and on sorption equilibria: An overview. *Geological Society London Special Publications.*

CHAPELLE, F.H, 2000. *Ground-water microbiology and geochemistry.* (New York, John Wiley and Sons.), 468 p.

CLEMENT, T P, HOOKER, B S, AND SKEEN, R S, 1996. Macroscopic models for predicting changes in saturated porous media properties caused by microbial growth. *Ground Water* Vol. 34(5), 934-942.

COOMBS, P, WAGNER, D, BATEMAN, K, HARRISON, H, MILODOWSKI, A E, NOY, D, AND WEST, J M. (in preparation). The role of biofilms in subsurface transport processes. *Submitted to Q. J. Engineering Geology.*

CORAPCIOGLU, M Y, AND HARIDAS, A. 1984. Transport and fate of microorganisms in porous media: A theoretical investigation. *Journal of Hydrology* Vol. 72, 142-169.

CORAPCIOGLU, M Y, AND HARIDAS, A. 1985. Microbial transport in soils and groundwater: A numerical model. *Advances in Water Resources* Vol. 8, 188-200.

CUNNINGHAM, A L, WARWOOD, B, STURMAN, P, HORRIGAN, K, JAMES, G, COSTERTON, J W, AND HIEBERT, R, 1997. Biofilm processes in porous media – practical applications. 325-344 in *The Microbiology of the Terrestrial Deep Subsurface:* AMY, P A, HALDEMAN, D L, (editors). (CRC :Lewis)

DOOLITTLE, M M, COONEY, J J, AND CALDWELL, D E, 1996. Tracing the interaction of bacteriophages with bacterial biofilms using fluorescent and chromogenic probes. *Journal of Industrial Microbiology* Vol. 16, 331-341

DORNIEDEN, T, GORBUSHINA, A A, & KRUMBEIN, W E, 2000. Biodecay of cultural heritage as a space/time-related ecological situation – an evaluation of a series of studies. *International Biodeterioration and Biodegradation* Vol. 46, 261-270.

DOWD, S E, HERMAN, D C, MAIER, R M, 2000. Aquatic and Extreme Environments. 123-146 in *Environmental Microbiology* MAIER, R M, PEPPER, I. L, AND GERBA C P. (editors). (London: Academic Press.)

EHRLICH, H. L. 1999. Microbes as geologic agents:their role in mineral formation. *Geomicrobiology Journal* Vol. 16, 135-153.

FERRIS, F.G, KONHAUSER, KO, LYVÉN, B. AND PEDERSEN, K, 1999. Accumulation of metals by bacteriogenic iron oxides in a subterranean environment. *Geomicrobiology Journal* Vol. 16, 181-192.

FLETCHER, M, 1991. The physiological activity of bacteria attached to solid surfaces. *Advances in Microbiological Physiology* Vol. 32, 53-85.

FREDERICKSON, J K, GARLAND, T R, HICKS, R J, THOMAS, J M, LI, S W, AND MCFADDEN, K M, 1989. Lithotrophic and heterotrophic bacteria in deep subsurface sediments and their relation to sediment properties. *Geomicrobiology Journal* Vol. 7, 53-66.

GROGAN, H A, AND MCKINLEY, I G. 1990. An approach to microbiological modelling: application to the near field of a Swiss low/intermediate-level waste repository. *NAGRA technical report* 89-06.

HAMA, K, BATEMAN, K, COOMBS, P, HARDS, V L, MILODOWSKI, A E, WEST, J M, WETTON, P D, YOSHIDA H, AND AOKI, K, 2001. Influence of bacteria on rock-water interaction and clay mineral formation in subsurface granitic environments. *Clay Minerals* Vol. 36(2001): 599-613.

HAMA, T, 1997. Primary productivity and photosynthetic products in the Northwest Pacific Ocean. In: *Biochemical Processes in the North Pacific, Proceedings of the International Marine Science Symposium* 187-191.

JASS, J, AND LAPPIN-SCOTT, H M, 1992. *Practical Course on Biofilm formation using the modified Robbins device* University of Exeter.

JOLLEY, D M, EHRHORN, T F, AND HORN, J, 2003. Microbial impacts to the near-field environment geochemistry: a model for estimating microbial communities in repository drifts at Yucca Mountain. *Journal of Contaminant Hydrology* Vol. 62-63, 553-575.

KEITH-ROACH, M. J. AND LIVENS, F. R. (editors) 2002. *Interactions of microorganisms with radionuclides.* (Oxford UK, Elsevier), 400pp.

KONHAUSER, K O, FISHER, Q J, FYFE, W S, LONGSTAFF, F J AND POWELL, M A, 1998 Authigenic mineralisation and detrital clay binding by freshwater biofilms: The Brahmani River, India. *Geomicrobiology Journal* Vol. 15, 209-222.

KINDRED, J S, AND CELIA, M A, 1989. Contaminant transport and biodegradation. 2. Conceptual model and test simulations. *Water Resources Research* Vol. 25(6), 1149-1159.

MARSH, P D, 2004. Dental plaque as a microbial biofilm. *Caries Research* Vol. 38, 204-211.

MCHARDY, W J, WILSON, M J, AND TAIT, J M, 1982. Electron microscope and X-ray diffraction studies of filamentous illitic clay from sandstones of the Magnus Field., *Clay Minerals* Vol. 17, 23-40.

MILODOWSKI. A E, WEST, J M, PEARCE, J M, HYSLOP, E K, BASHAM, I R, AND HOOKER, P J, 1990. Uranium-mineralised microorganisms associated with uraniferous hydrocarbons in southwest Scotland. *Nature* Vol. 347, 465-467.

MOLZ, F J, WIDDOWSON, M A, BENEFIELD, L D, 1986. Simulation of microbial growth dynamics coupled to nutrient and oxygen transport in porous media. *Water Resources Research* Vol. 22(8), 1207-1216.

NOY, D J, 1998.User guide to PRECIP, A program for coupled flow and reactive solute transport. . *British Geological Survey Technical Report* WE/98/13.

OKABE, S, KURODA, H, WATANABE, Y, 1998. Significance of biofilm structure on transport of inert participates into biofilms. *Water Science and Technology* Vol. 38(8), 163-170.

PARKHURST, D L, AND APPELO, C A J, 1999. User's Guide to PHREEQC (VERSION 2) – A computer program for speciation, batch-reaction, one-dimensional transport, and inverse geochemical calculations. U S Geological Survey Report WRI 99-4259.

PAULSEN, J E, OPPEN, E, BAKKE, R, 1997. Biofilm morphology in porous media, a study with microscopic and image techniques. *Water Science and Technology* Vol. 36, 1-9.

PEDERSEN, K, 1999. Subterranean microorganisms and radioactive waste disposal in Sweden. *Engineering Geology* Vol. 52, 163-172.

PEPPER, I L, GERBA, C P, AND BRENDECKE, J W, 1995. *Environmental Microbiology: A Laboratory Manual.* (San Diego: Academic Press).

RITTMANN, B E, MCCARTY, P L, AND ROBERTS, P V, 1980. Trace-organic biodegradation in aquifer recharge. *Ground Water* Vol. 18, 236-243.

SCHULZE-MAKUCH D, GUAN H, AND PILLAI SD, 2003. Effect of pH and geological medium on Bacteriophage MS-2 in a model aquifer. *Geomicrobiology Journal* Vol. 20, 73-84.

SKB, 2003. Äspö Hard Rock Laboratory. Annual Report 2002. *Swedish Nuclear Waste and Fuel Management Company (SKB) Technical Report* TR-03-10.

SKB, 2004. RD and D – Programme 2004. *Swedish Nuclear Waste and Fuel Management Company (SKB) Technical Report* TR-04-21.

STOODLEY, P, HALL-STOODLEY, L, AND LAPPIN-SCOTT, H M, 2001. Detachment, surface migration, and other dynamic behavior in bacterial biofilms revealed by digital time-lapse imaging. *Methods in Enzymology* Vol. 337, 306-319.

SUTHERLAND, I W. HUGHES, K A, SKILLMAN, L C, TAIT, K, 2004. The interaction of phage and biofilms. *FEMS Microbiology Letters* Vol. 232, 1-6.

TAYLOR, R, CRONIN, A, PEDLEY, S, BARKER, J, AND ATKINSON, T. 2004. The implications of groundwater velocity variations on microbial transport and wellhead protection-a review of evidence. *FEMS Microbiology Ecology Letters* Vol. 49, 17-26.

TAYLOR, S W, AND JAFFÉ, P R, 1990a. Biofilm growth and related changes in the physical properties of a porous medium 1. Experimental investigation. *Water Resources Research* Vol. 26, 2153-2159.

TAYLOR, S W, AND JAFFÉ, P R, 1990b. Biofilm growth and related changes in the physical properties of a porous medium 3. Diversity and model verification. *Water Resources Research* Vol. 26, 2171-2180.

Technical Procedure AGN 2.3.5 British Geological Survey Issue 7.0, July 2007.

Technical Procedure AGN 2.3.6 British Geological Survey Issue 10.0, September 2007.

Technical Procedure AGN 2.3.11 British Geological Survey Issue 4.0, September 2007.

THULLNER, M, SCHROTH, M H, ZEYER, J, AND KINZELBACH, W. 2004. Modelling of a microbial growth experiment with bioclogging in a two-dimensional saturated porous media flow field. *Journal of Contaminant Hydrology* Vol. 70, 37-62.

TODAR, K, Todar's Textbook of Bacteriology [online]. Accessed 10/05/2006. Available from http://www.textbookofbacteriology.net

TUCK, V A, EDYVEAN, R. G J, WEST, J M, BATEMAN, K, COOMBS, P, MILODOWSKI, A E AND MCKERVEY, J A, 2006. Biologically induced clay formation in subsurface granitic environments. *Journal of Geochemical Exploration* Vol. 90, 123-133.

VANDEVIVERE, P, BAVEYE, P, DE LOZADA, D S, AND DELEO, P, 1995. Microbial clogging of saturated soils and aquifer materials: Evaluation of mathemetical models. *Water Resources Research* Vol. 31(9), 2173-2180.

VAUGHAN, D J, WOGELIUS, R, BOULT, S, AND MERRIFIELD, C, 2001. Quantifying the effects of biofilm growth on hydraulic properties and on sorbtion equilibria; microscopic to macroscopic measurements. *Progress summary 02/01 – 11/01* Williamson Research Centre, University of Manchester.

WAGNER, D, BATEMAN, K, COOMBS, P, HARRISON, H, MILODOWSKI, A E , AND WEST, J M, 2007. Experimental growth of biofilms for studies on the impact of microbes on transport processes in groundwater systems. Goldschmidt Conference 2007 Abstract A1077, 1P.

WEST, J M, MCKINLEY, I G, AND CHAPMAN, N A, 1982. Microbes in deep geological systems and their possible influence on radioactive waste disposal. *Radioactive Waste Management and the Nuclear Fuel Cycle* Vol. 3, 1-15

WEST, J M, HAIGH, D G, HOOKER, P J, AND ROWE, E J, 1991. Microbial influence on the sorption of ^{137}Cs onto materials relevant to the geological disposal of radioactive waste. *Experimentia* Vol. 47, 549-552.

WEST, J M, 1995. A review of progress in the geomicrobiology of radioactive waste disposal. *Radioactive Waste Management and Environmental Restoration* Vol. 19, 263-283.

WEST, J M, AND CHILTON, P J, 1997. Aquifers as environments for microbiological activity. *Quarterly Journal of Engineering Geology* Vol. 30, 147-154.

WEST, J M, AOKI, K, BAKER, S J, BATEMAN, K, COOMBS, P, GILLESPIE, M R, HENNEY, P J, REEDER, S, MILODOWSKI, A E, YOSHIDA, H, 1998. Redox experiment in detailed scale (REX)-Complementary laboratory work to examine microbial effects on redox. *Swedish Nuclear Fuel and Waste Management Co. Report SKB-PR-HRL-98-14* Also published as *British Geological Survey Research Report,* WE/97/3C.

WEST, J M, AND MCKINLEY, I G, 2002. The geomicrobiology of radioactive waste disposal. In: *The Encyclopaedia of Environmental Microbiology.* BITTON, G. (editor) (New York: John Wiley) 2661-2674.

WIDDOWSON, M A, MOLZ, F J, AND BENEFIELD, L D, 1988. A numerical transport model for Oxygen and Nitrate based respiration linked to substrate and nutrient availability in porous media. *Water Resources Research* Vol. 24(9), 1553-1565.

WIDDOWSON, M A, 1991. Comment on "An evaluation of mathematical models of the transport of biologically reacting solutes in saturated soils and aquifers." BAVEYE, P., AND VALOCCHI, A. *Water Resources Research* Vol. 27(6), 1375-1378.

WIMPENNY, J, MANZ, W, AND SZEWZYK, U, 2000. Heterogeneity in biofilms. *FEMS Microbiology Reviews* Vol. 24, 661-671.